NeTIRail

Needs Tailored Interoperable Railway Infrastructure

Deliverable D2.5

Corrugation reduction strategies for NeTIRail-INFRA track types, with estimates of costs and benefits

Submission date : 26/08/2017

NeTIRail-INFRA is funded by the European Commission under the Horizon 2020 programme - Grant agreement n° 636237

Lead contractor

TU Delft

Contributors

USFD

SZ

AFER

INTADER

TCDD

Project Coordinator

University of Sheffield, USFD

Executive Summary

The deliverable D2.5 presents the research efforts of the NeTIRail-INFRA project in the understanding of the phenomenon of short pitch corrugation. In the Section 1 of this deliverable, the literature review is presented and main challenges in terms of the physical understanding the origin of the phenomenon are discussed. Section 2 describes how the use of axle box acceleration measurement can support the detection of already existing short pitch corrugation. In Section 3, due to the fastening system being believed to importantly contribute to the phenomenon, a parametric study is presented. In the railway industry so far, the only corrective measure for delaying the growth of corrugation is grinding; thus, in Section 4 a review of the effects of grinding operations is discussed. Finally in Sections 5 and 6, the current situation of corrugation in Turkey and Slovenia are discussed.

Contribution to the task T2.4, "life extension for plain line through preventing corrugation".

The main goal of T2.4 is to provide a better understanding of corrugation (rail surface irregularity and waviness) and what can be done to prevent it. One of the hypothesis in this task is that corrugation is influenced by the choice of fastenings and rail pads. In direction to prove the hypothesis, in this deliverable we present:

- An analysis based on 3D model that allows to understand how the changes in fastening and rail pads can affect the resonant frequencies of the line, see Section 3 of this deliverable based on M. Oregui, A. Núñez, R. Dollevoet, and Z. Li, "Sensitivity analysis of railpad parameters on vertical railway track dynamics". ASCE Journal of Engineering Mechanics, Volume 143, Issue 5, May 2017. DOI: 10.1061/(ASCE)EM.1943-7889.0001207.
- Link with T4.2 in which on-board instrumentation is developed, in Section 2 of this deliverable.
- A new modelling approach with the wheel-rail frictional rolling contact in continuum dynamics (Section 2.2 of this deliverable). Further findings and analysis of the modelling approach will be described in the next deliverable.

As real-life solutions require a better understanding of the current situation about corrugation, in this deliverable the following topics were additionally included:

- A review on grinding strategy, as it is the most common current strategy to solve the corrugation problem (see Section 4 of this deliverable).
- Measurement and analysis of the effect of corrugation for different track types in both Slovenia and Turkey (Section 5 for the case in Turkey and Section 6 for the case in Slovenia).

Deviations from original deliverable plan:

- In the next deliverable D2.6, a further analysis of the 3D FE modelling approach and new insights about short pitch corrugation will be further detailed. The global explanation of the dynamic conditions (the wavelength fixing mechanisms) and the resulting corrugation damage will be described. The results are available in the paper: S. Li, Z. Li, A. Núñez, and R. Dollevoet, “New insights into the short pitch corrugation development enigma based on 3D-FE dynamic vehicle-track coupled modelling in frictional rolling contact”. Applied Sciences, 2017 7(8), 807, Aug. 2017. DOI: 10.3390/app7080807.
- It was not possible to obtain a link between certain clips and pads and corrugation, as the modelling approach is not able yet to develop corrugation from smooth rail condition. In view of this deviation, the experimental tests to be conducted for deliverable D2.5 will make use of the most usual clips and pads available from the industry. The consequence is that experiments conducted in Turkey will consider the following cases: 1) corrugated rail and old clips and pads; 2) corrugated rail and new clips and pads; 3) grinding effect on corrugated rail with new clips and pads.

Table of contents

Abbreviations and acronyms

Abbreviation / Acronym	Description
ABA	Axle box acceleration
BEL	Brown etching layer
CWT	Continuous wavelet transform
DMA	Dynamic mechanical analysis
EU	European Union
FE	Finite Element
FFT	Fast Fourier Transform
FT	Fourier transform
GPS	Geographical positioning system
IM	Infrastructure Manager
PSD	Power spectrum density
RCF	Rolling Contact Fatigue
SAWP	Scaled-averaged wavelet power
STFT	Short-time Fourier transform
SZ	Slovenske Železnice – Slovenian Railways
TCDD	Türkiye Cumhuriyeti Devlet Demiryolları – Turkish IM
TTS	Time-temperature superposition principle
TUD	Delft University of Technology
USFD	The University of Sheffield
WEL	White etching layer
WPS	Wavelet power spectrum

1 Literature survey about corrugation

1.1 Introduction

Rail corrugation is a periodic wave-like rail surface defect. The corrugation is to date explained by a damage mechanism and a wavelength-fixing mechanism [1.1]. According to these mechanisms, corrugation can be classified into six types: short pitch corrugation (Fig 1.1a), rutting (Fig 1.1b), other P2 resonance (Fig 1.1c), heavy haul (Fig 1.1d), light rail, and track form related corrugation (Fig 1.1e). Among them the development mechanisms of short pitch corrugation are still unknown. Short pitch corrugation (subsequently shortened as "the corrugation") refers to the corrugation with wavelength falling in the range of 20 – 80 mm, and with amplitudes (peak-to-trough distance) up to 100 µm. On Dutch railway network, the most commonly recorded corrugation has the wavelength of 20 – 40 mm [1.2], [1.3]. It mainly forms on straight tracks or at gentle curves under comparably light axle loads. It appears in different tracks, from traditional ballast tracks to modern slab tracks, from heavy rail to light rail and rapid transit, e.g. metro or tram lines, from discretely supported tracks to continuously embedded tracks [1.4]. On one hand, the corrugation increases the vibrations/dynamical interaction forces of the vehicle-track system, thus accelerates the degradation process of vehicle-track system key components, e.g. the deterioration in fastening system [1.1] and rail surface material structural damages in forms of WEL/BEL and cracks in late stage [1.5], [1.6]. On the other hand, the "roaring" noise due to the corrugation is a nuisance to residents nearby, especially in some densely inhabited areas. Due to the complexity of the problem, there has been no generally accepted explanation to the corrugation development process. The most effective solution so far is removal of the corrugation by grinding maintenance. Therefore, there is a necessity on one hand to:

1) understand the corrugation initiation and its growth;
2) analyse which track parameters are responsible for the corrugation and under which condition;
3) analyse the damaging process by the damage mechanisms of wear and plastic deformation;
4) propose guidance for optimal track structure/parameters and rail material design, and on the other hand to remove the corrugation by means of grinding maintenance.

Grinding increases the maintenance cost and reduces the network efficiency. From the IM's concern, a robust, efficient and economical inspection system, which records the damage status of the track, is necessary to help them optimize their maintenance interval and related grinding parameters and quality evaluations.

Over the past decades, there has been much research on the corrugation. The research can be by analytical and numerical simulations [1.7], [1.8], [1.9], [1.10], [1.11], [1.12], or from field and laboratory tests and monitoring [1.13], [1.15], or through metallographic characterizations of the material structural damages [1.5], [1.6]. The vehicle-track dynamic interaction system is a complex non-linear system, especially in the presence of corrugation between the wheel and rail contact. The

traditionally analytical method cannot take every aspect which might contribute to the problem into consideration, and hence numerical methods were developed. In comparison to the field and laboratory tests, the numerical approach has the advantages of low cost and high efficiency. With the development of high-computing-performance computers, it becomes more and more powerful. As a result, the numerical approach is widely used by researchers.

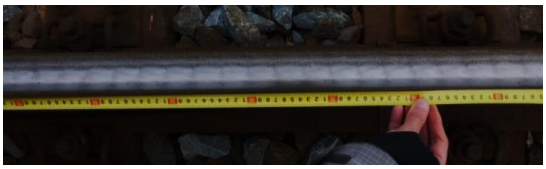

(a)

(b)

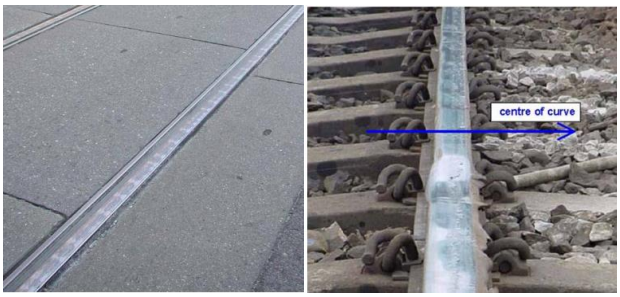

(c) (d)

(e)

Figure 1-1 Corrugation: (a) Short pitch corrugation in Dutch railway network. (b) Rutting, Source: [1.1]. (c) P2 resonance corrugation, Source: [1.1]. (d) Heavy haul corrugation, Source: [1.1]. (e) Corrugation from resonance of baseplate of rail pad, Source: [1.1].

The whole corrugation developing process is to date explained by a short term dynamical process and a long-term damage mechanism. The short-term dynamical process is believed to fix the wavelength

through structural dynamics [1.1], [1.16]. The interaction between the short- and long-term mechanisms is represented by a feedback loop. Thus, three aspects are needed to understand the corrugation development:

1) the structural dynamics excitation due to vehicle-track interaction. It determines the loading condition at the wheel-rail contact during each wheel passage.

2) the response to the loading at the wheel-rail interface with nonlinear contact mechanics. This determines the damage which accumulates over a long term.

3) the feedback from the contact and the damage to the structural dynamics, determined by the direct coupling between contact mechanics and structural dynamics.

Thus, besides a reliable treatment of the contact mechanics and an accurate representation of the vehicle-track interaction, it is essential to consider realistically the coupling between the structural dynamics and contact mechanics, as well as their interplay. However, the structural dynamics and contact mechanics are usually solved separately in different models/steps [1.12], [1.17]. It is unknown whether this way of treatment is a cause which leads to the current insufficiency in understanding the corrugation. It is therefore necessary to introduce a new modelling approach which includes such coupling and interplay.

As to the long-term damage mechanism, the corrugation is considered to be formed by differential wear, to some extent plastic deformation, or rolling contact fatigue [1.1]. In view of the damage mechanism of wear, the development process is explained as being consistently worn more at the corrugation trough than at the corrugation peak, with the supporting evidence that the surface at the corrugation troughs is dark and rougher than it at the corrugation peaks due to the adhesive wear [1.5]. The longitudinal creepage is the main contribution to the periodic wear. The input to the periodical longitudinal creepage, or wear should come from the dynamic wheel-rail contact forces either in the normal direction, or in the longitudinal direction or even combinations of the both. Most research on the corrugation initiation and growth processes is focused on the aspect of wear [1.9], [1.10], [1.11], and [1.12], there are limited number of numerical studies on the plastic deformation. Research on the material plastic deformation and degradations can be divided into two categories: metallurgical study and numerical analysis. Feller and Warf performed a metallurgical examination of corrugated rail samples [1.5]. They concluded that the rail material at the corrugation crest is broken down into finer cementite particles shown higher hardening property and wear resistance. Corrugation valleys experience less deformation, with a consequence of lower wear resistance, and worsened by corrosion. Higher hardness level at the crest than that at the trough was also revealed by Wild et al [1.18]. However, they found that rail material is severely plastic deformed at the corrugation trough. Hiensch et al. [1.2] performed a metallurgical study for a Dutch railway case, and found the corrugation peaks show a higher work hardening and wear resistance level. By using a numerical approach, Böhmer and Klimpel [1.19] analyzed the influence of plastic deformation on the corrugation growth, and explained the plastic deformation as a saturation mechanism. It seems not

appropriate to make the conclusion by neglecting the higher wear resistance at the corrugation crest due to the working hardening [1.2], [1.5]. Wen et al. [1.20] performed a numerical analysis of the corrugation induced by a scratch during curving. Models used for the normal and tangential solutions, and later for the material performance analysis are two dimensional (2D). Elastic-plastic material model is employed to study the ratcheting effect under multiple wheel passages. Based on the results, they concluded the corrugation is initiated from the plastic deformation induced by the scratch, develops at a decreasing rate, and tends to shift in the rolling direction. Admittedly, previous research, either in the metallurgical aspect, or from numerical viewpoint, has made great contributions to the understanding of the mechanisms of the corrugation. There is still a need of research for further understanding the initiation and growth for the reasons that: It is not yet clear about the role of plastic deformation during the evolution of the corrugation and its interaction with wear; analyses of wear, stress, strain and plastic flow of the rail material should be performed in three dimensional (3D) to explain metallurgical examinations.

When it comes to the contact model, a Hertzian solution is usually employed to study the normal contact problems due to its simplicity, while in the tangential direction, Carter's 2D theory, Kalker's linear, exact or simplified theories are generally used [1.21].

The Hertzian theory was built upon some assumptions:

1) the size of the contact is much smaller than radii of the contact bodies;
2) contact bodies are smooth and frictionless;
3) the strains are small and within the elastic limit;
4) each body can be considered as an elastic half-space.

The frictionless assumption is only applicable on normal contact problems. For the tangential solutions, other theories are necessary. The half space assumption puts geometrical limitations on the contact. For the corrugation with wavelength of 20-80 mm, the longitudinal contact dimension will be comparable to the radius of the rail in the longitudinal direction. In this situation, the half space assumption will not hold anymore. Hence, non-Hertz contact should be introduced. By employing a 2D non-Hertzian contact model in statics, Nielsen [1.9] found that the corrugation can only grow above a certain wave length and concluded the nonlinear contact mechanics is responsible for the growth. The Hertzian theory and Kalker's theory are based on statics. Because the contact patch is in the order of 2 cm, thus close to the corrugation wavelength, consideration of non-steady state process due to dynamical interaction becomes necessary [1.11], [1.22]. The non-steady contact mechanics is assumed being responsible for the wavelength-fixing mechanism [1.11]. Thus, non-Hertz and non-steady mechanics should be considered for rail corrugation in the short pitch study. Besides the contact mechanics, the corrugation "wavelength-fixing mechanism" is also explained structural dynamics which are determined by the vehicle-track system natural frequencies, e.g., anti-resonance at the pinned-pinned resonance of the discrete support track system [1.23], high lateral track resonance [1.24] and self-excited vibrations, which are governed by torsional modes of the driven wheels and longitudinal vibrations of the rails [1.25]. According to the explanation, the wavelength of the corrugation is expected to linearly increase with the increase of train speed, which is actually a

frequency-fixing mechanism. This obviously fails to comply with the field data that the corrugation wavelength changes minor with the increase of train speed [1.1]. In [1.4], it is reported that presence of the corrugation in a continuous support track also arouses; thus, a re-thinking about the pinned-pinned resonance based explanation is needed, which is inherently related to the discrete support track structure. In [1.24], Müller gave the explanation that the wavelength-fixing mechanism of the corrugation is governed by a mechanical contact filtering effect that only irregularities with wavelengths in the range of 2 to 8–10 cm can grow. When taking the structural dynamics effect into consideration, the wavelength-fixing mechanism was explained by certain structural dynamics that can cause the corrugation of wavelength falling into the amplification zone [1.24]. Hence, the corrugation development mechanism should be governed by the vehicle-track frictional rolling contact in dynamics. According to the assumption, a model which considers both aspects will theoretically reproduce the corrugation growth and initiation. Xie and Iwnicki [1.12] made a further investigation with a three-dimensional non-Hertz and non-steady model but found the corrugation could not grow. It seems that the corrugation becomes an “enigmatic” problem [1.26].

When looking at the solution process, the possible answer to this failure in prediction corrugation growth is twofold. The first explanation to the failure in prediction corrugation development is the lack of the directly coupling between the structural dynamics and contact mechanics. This is done in two different models/steps, i.e., a vehicle-track model and a contact model. The second explanation is that for a certain kind of wheel/rail contact failures to happen, there should be an initial energy input into the system, which is given the name of “initial excitation”. With this initial excitation, dynamical wheel-rail contact forces of certain patterns and in certain frequency ranges are produced, which generate a differential wear, or plastic deformation, and after many wheel passages the corrugation are formed. The initial excitation on the rail corrugation may come from the geometrical discontinuity, e.g., corrugation-like waves following a rail squat [1.27], or from geometrical discontinuity plus the material discontinuity, e.g., rail welds, or from anomalies of the track system, when no visual discontinuity appears. Yet a major difference has been identified between the corrugation that originates from railhead irregularities and the general type. The former is caused by a dynamic force excited by known irregularities. The wavelength of the force is determined by the local track system; the phase of the force is determined by the location of the irregularities. Thus there are clear mechanisms of wavelength and phase fixing. The wavelength and phase of the force at a given irregularity are, for different wheel passages, always the same; the resulting differential wear and/or plastic deformation are always in-phase so that they accumulate. The corrugation can thus initiate and grow. The latter, that is the focus of this paper, does not have a visually known initiation source. Although the wavelength might be fixed by track structure such as the “pin-pin” resonance [1.23] or the stick-slip process [1.31], the randomness of passing wheels and of the track can lead to phase variation of the contact force so that the total effect over many wheel passages may be the cancellation of the differential wear and deformation. The second difference between the corrugations developed with/without local geometrical or material discontinuities, is that the local discontinuities inducing corrugation-like waves usually appear and develop for limited number of gradually decaying waves, while in reality the corrugation continuously appears over quite a long distance. A first question about the latter type would be: what are the causes of the dynamic force

that results in differential wear and/or differential plastic deformation that are always in-phase with themselves for the many different passing wheels so that the wear and deformation can accumulate and corrugation can initiate and grow.

Rail initial roughness was usually considered as a possible explanation of this initial excitation in some publication [1.23], [1.24] and [1.28]. However, field evidence shows that railway tracks with the similar roughness levels after grinding maintenance can develop the corrugation quite differently, at some locations with severe corrugation but at some other locations no corrugation appeared. In this sense, it could indicate that the roughness alone could not be sufficient to cause the corrugation initiation. The introduction of the concept of initial excitation may well explain the confusion that "there is inadequate knowledge of why the corrugation appears on some types of track form in some circumstances and not in others" [1.29]. There have been some studies on the initiation mechanism of the corrugation from the aspect of track parameters, e.g. railpad stiffness [1.16], [1.30], while a gap is still left that how the track parameters induce the fluctuation of wheel-rail contact forces and thus cause the differential wear which is responsible for the corrugation initiation. Therefore, the present paper attempts: on one hand, to investigate if it is possible to simulate the corrugation initiation under certain track parameters; on the other hand, to determine which parameters contribute to the initial excitation and govern the corrugation wavelength and phase.

In recent years, the finite element method was employed to investigate the development mechanism of squats in the vehicle-track system [1.32]. The modelling also provides a good explanation for the development of corrugation initiated from isolated railhead irregularities [1.33]. Because the corrugation from isolated railhead irregularities was of a short pitch type, it arouses the hope that the method could also be valid for investigating the general type of short pitch corrugation.

In an effort that is hoped to lead to an answer to the question a 3D finite element (FE) approach that combines the vehicle-track interaction model of [1.32] with the solution for transient frictional rolling of [1.31] is presented. The vehicle-track structural dynamics are directly coupled with the wheel-rail contact mechanics through the continuum treatment of the wheel and rail. The contact is treated as continuum surface-to-surface. Thus, the mechanical contact filtering effect [1.34], which determines roughness only above a certain wavelength to grow, will also be automatically taken into account. In comparisons to the Hertzian based contact assumption, there are no restrictions on the contact geometry. By keeping a sufficiently small integration time step, all the relevant vibration and wave propagation modes of both the wheel-rail contact and the wheel-track interaction system can be included up to a sufficient accuracy [1.31]. The dynamic loads, the contact pressures, the tangential stresses, the micro-slip together with the frictional work can be obtained. Subsequently, their non-steady variations in magnitude and phase can be investigated to calculate the accumulation or cancellation of periodic wear. Besides, the model can study the plastic deformation, as reported being the other damage mechanism of the corrugation, by treating the material in elasto-plasticity [1.35]. The reliability of the method of [1.32] was shown by the agreement between its predictions of squats growth process and field observations [1.36] and by comparison with measurement of axle box acceleration [1.37]. The dynamics considered is up to 2 kHz. The method of [1.31] has been verified extensively with established solutions of Hertz, Spence, Cataneo, Mindlin and Kalker [1.31], [1.38].

Besides, the model also provides a good explanation for the development of corrugation initiated from isolated railhead irregularities [1.39]. This approach was presented in [1.40] to analyse the phase relationship between given corrugation and the resulting periodic wear. Next, the transient states of the rolling contact and wear are evaluated under a variety of loading conditions in relation to the dynamic forces excited by a passing wheel over a rail with and without corrugation. Here the damage mechanism is limited to wear, as the focus of this paper is on the condition that may lead to consistent initiation and growth of the corrugation.

1.2 Bibliography

[1.1] *Rail corrugation: characteristics, causes and treatments.* **SL Grassie.** s.l. : P I MECH ENG F-J RAI, 2009, Vols. 223:581-596.

[1.2] *Rail corrugation in The Netherlands – measurements and simulations.* **M Hiensch, JCO Nielson, and E Verherjen.** s.l. : Wear, 2002, Vols. 253: 140–149.

[1.3] *Automatic Detection of Squats in Railway Infrastructure.* **M Molodova, Z Li, A Núñez, and R Dollevoet.** s.l. : IEEE T INTELL TRANSP, 2014, Vols. 15(5):1980–1990.

[1.4] Review on short pitch rail corrugation studies. **KH Oostermeijer.** s.l. : Wear 265 (2008) 1231–1237

[1.5] Surface analysis of corrugated rail treads. **HG Feller and K Waif.** s.l. : Wear, 144 (1991) 153-161.

[1.6] "Brown etching layer": A possible new insight into the crack initiation of rolling contact fatigue in rail steels? **S Li , J Wu, RH Petrov, Z Li, R Dollevoet, J Sietsma.** s.l. : Engineering Failure Analysis 66 (2016) 8–18.

[1.7] The Dynamic Response of Railway Track to High Frequency Vertical Excitation. **SL Grassie, RW Gregory, D Harrison and KL Johnson.** s.l. : Journal of Mechanical Engineering Science, 1982 24: 77. DOI: 10.1243/JMES_JOUR_1982_024_016_02.

[1.8] A linear dynamic wear model to explain the initiating mechanism of corrugation. **AR Valdivia.** s.l. : Vehicle System Dynamics, 17:sup1, 493-496, DOI:10.1080/00423118808969290.

[1.9] Evolution of rail corrugation predicted with a non-linear wear model. **JB Nielsen.** s.l. : Journal of Sound and Vibration (1999) 227(5), 915–933.

[1.10] Numerical prediction of rail roughness growth on tangent railway tracks. **JCO Nielsen.** s.l. : Journal of Sound and Vibration 267 (2003) 537–548.

[1.11] Short wavelength rail corrugation and non-steady-state contact mechanics. **K Knothe, A Groß-Thebing.** s.l. : Vehicle System Dynamics Vol. 46, Nos. 1–2, January–February 2008, 49–66.

[1.12] Simulation of wear on a rough rail using a time-domain wheel–track interaction model. **G Xie, SD Iwnicki.** s.l. : Wear 265 (2008) 1572–1583.

[1.13] Field studies of the effect of friction modifiers on short pitch corrugation generation in curves. **DT Eadie, M Santoro, K Oldknow and Y Oka.** s.l. : Wear, 2008, 265, 1212–1221.

[1.14] Surface corrugations spontaneously generated in a rolling contact disc. **RM Carson and KL Johnson.** s.l. : Wear, 1971, 17, 59–72.

[1.15] Experimental study on mechanism of rail corrugation using corrugation simulator. **Yoshihiro Suda, Hisanao Komine, Takashi Iwasa, Yoshiaki Terumichi.** s.l. : Wear 253 (2002) 162–171.

[1.16] The influence of railpad stiffness on wheelset/track interaction and corrugation growth. **Ilias H.** s.l. : J Sound Vib 227 (5) (1999) 935–948.

[1.17] Effect of discrete track support by sleepers on rail corrugation at a curved track. **Jin X, Wen Z.** s.l. : J Sound Vib 315 (2008) 279–300.

[1.18] Microstructure alterations at the surface of a heavily corrugated rail with strong ripple formation, **E Wild, L Wang, B Hasse, T Wroblewski, G Goerigk, A Pyzalla.** s.l. : Wear 254 (9) (2003) 876–883.

[1.19] Plastic deformation of corrugated rails—a numerical approach using material data of rail steel. **A Böhmer, T Klimpel.** s.l. : Wear 253 (2002) 150–161.

[1.20] Effect of a scratch on curved rail on initiation and evolution of plastic deformation induced rail corrugation. **Z Wen, X Jin, X Xiao, Z Zhou.** s.l. : International Journal of Solids and Structures, 45 (2008) 2077–2096.

[1.21] Three-Dimensional Elastic Bodies in Rolling Contact. **JJ Kalker.** s.l. : Kluwer, Dordrecht, 1990.
(1.22) A fast non-steady state creep force model based on the simplified theory. **Z Shen, Z Li.** s.l. : Wear 191 (1996) 242-244.

[1.23] An extended linear model for the prediction of short pitch corrugation. **Hempelmann K, Knothe K.** s.l. : Wear 191; (1996) 161–169.

[1.24] A linear wheel/track model to predict instability and short pitch corrugation. **Müller S.** s.l. : J Sound Vib 227; (1999) 899–913.

[1.25] An investigation of rail corrugation using friction-induced vibration theory. **Brockley CA.** s.l. : Wear 128; (1988) 99–106.

[1.26] Short-pitch rail corrugation: A possible resonance-free regime as a step forward to explain the “enigma”? **L Afferrante, M Ciavarella.** s.l. : Wear 266; (2009) 934–944.

[1.27] Squat growth—some observations and the validation of numerical predictions. **Z Li, R Dollevoet, M Molodova, X Zhao.** s.l. : Wear 271; (2011) 148–157.

[1.28] Railhead corrugation growth explained by dynamic interaction between track and bogie wheelsets. **A Igeland.** s.l. : P I Mech Eng F-J Rai 210; (1996) 11–20.

[1.29] Rail corrugation: advances in measurement, understanding and treatment. **Grassie SL.** s.l. : Wear 258; (2005) 1224–1234.

[1.30] Investigation of the influence of rail pad stiffness on rail corrugation on a transit system. **JI Egana, J Vinolas, M Seco.** s.l. : Wear 261; (2006) 216–224.

[1.31] The solution of frictional wheel-rail rolling contact with a 3D transient finite element model: Validation and error analysis. **X Zhao, Z Li.** s.l. : Wear 271 (2011) 444–452.

[1.32] An investigation into the causes of squats–Correlation analysis and numerical modelling. **Z Li, X Zhao, C Esveld, R Dollevoet, M Molodova.** s.l. : Wear 265 (2008) 1349–1355.

[1.33] Squats and squat-type defects in rails: the understanding to date. **SL Grassie.** s.l. : Proc IMechE F: J Rail Rapid Transit 226 (2012) 235–242.

[1.34] Wheel/rail noise–Parts IV: Rolling noise. **PJ Remington.** s.l. : J Sound Vib 46 (1976) 419–436.

[1.35] A 3-D finite element solution of frictional wheel–rail rolling contact in elasto-plasticity. **X Zhao, Z Li,** s.l. : P I Mech Eng J-J-Eng 229; (2015) 86–100.

[1.36] Squat growth—some observations and the validation of numerical predictions. **Z Li, R Dollevoet, M Molodova and X Zhao.** s.l. : Wear 271 (1–2) (2011) 148–157.

[1.37] Axle box acceleration: Measurement and simulation for detection of short track defects. **M Molodova, Z Li, R Dollevoet.** s.l. : Wear 271 (2011) 349–356.

[1.38] 3D FE modelling and validation of frictional contact with partial slip in compression–shift–rolling evolution. **Z Wei, Z Li, Z Qian, R Chen, R Dollevoet.** s.l. : Int J Rail Transportation 4(1) (2015) 20–36.

[1.39] Squats and squat-type defects in rails: the understanding to date. **SL Grassie.** s.l. : Proc IMechE F: J Rail Rapid Transit 226 (2012) 235–242.

[1.40] Wear study of short pitch corrugation using an integrated 3D FE train-track interaction model. **S Li, Z Li, R Dollevoet.** s.l. : The 9th International Conference on Contact Mechanics and Wear of Rail/Wheel Systems, Chengdu, China (2012) 216–222.

2 Axle-box acceleration measurement system for detection of corrugation

2.1 ABA measurement system

In the presence of the rail corrugation, the wheel/track dynamic interactions in the high frequency are excited. It is accompanied with an accelerated degradation process of the track parameters, e.g. the deterioration in fastening components [2.2] and the rail surface material structural failures in forms of WEL/BEL and cracks [2.3], [2.4]. Besides, the generated high frequency "roaring" noise due to the corrugation is a nuisance to residents living nearby the railway lines.

To avoid such problems, early stage detection of the corrugation becomes necessary. Axle box acceleration (ABA), as the technique used in this research, detects the acceleration signals of the wheel box when passing over the track structure. Theoretically, once the wheel passes over a defect, the information will be included in the acceleration signals. By a proper signal processing scheme, this defect can be identified by its signature tune (particular frequency response). Hence, the advantages of ABA measurement over for instance a video inspection are: 1) the false prediction by contaminations will be avoided; 2) invisible track structural failures can be potentially detected. This system can be easily instrumented on commercial operating trains. Thus, the inspection is carried out in a loaded condition at the normal operating speed. The loaded condition and the equivalent speed promise that the signature tunes responsible for the defects in eigen frequency ranges will be excited and picked up by the accelerometers. Thus among the other inspection methods, ABA measurement is efficient in comparison to the visual inspection or portable instruments [2.5] and economical in comparison to other testing systems which usually need a measurement train to be arranged. This system has been shown reliability in detection of rail surface single defects, e.g. rail surface defects smaller than the light squats (light squats refers to the squats in its early stage whereas small rail defects will not necessarily grow into squats but can be worn off) [2.6], damaged welds and insulated joints [2.7]. Characteristic frequency components used for detection are up to 2000 Hz. Based on the relationship of $v=\lambda f$ (v is the train speed, λ the corrugation wavelength and f the frequency), the corrugation related frequency response falls within the range. Moreover, the corrugation was reported to be potentially connected to rail squats [2.8]. Therefore, it is expected to extend the ABA measurement on detection of the corrugation.

The instrumentation of the ABA measurement system and the process of the fault diagnosis are shown in Figure 2-1. Accelerometers are installed in the wheel axles. When the wheel rolls over rail with defects, the dynamic response of the system is recorded in the vibration signals. GPS and tachometer signals are simultaneously registered to provide the position information of the ABA signals. With data processing tools, an automatic detection algorithm is developed for detection of track defects. The algorithm is validated with field monitoring. Figure 2-2 shows the present applications of the ABA measurement system. It is noted that the present applications are mainly focused on rail surface defects. In [2.9], it is also shown that ABA system can be extended to detect loosening bolts at insulated rail joints, i.e., the structural failure beyond the wheel-rail contact surfaces. Thus, the ABA system is a promising inspection tool for multiple targets of measurement integrated in one system.

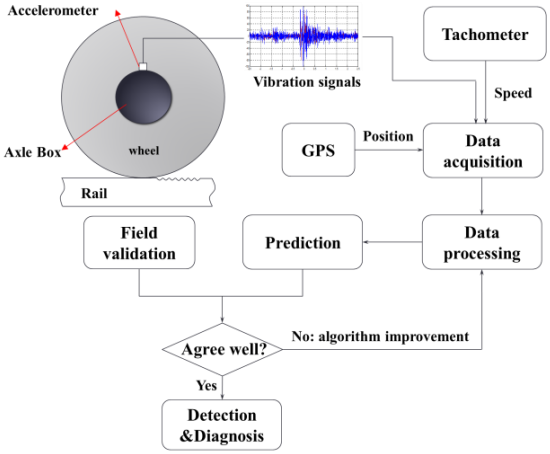

Figure 2-1. ABA measurement system and diagnosis system

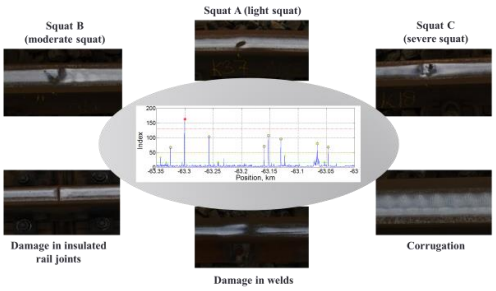

Figure 2-2. Applications of ABA measurement

2.2 Signature tunes identification with the FE model

Similar to the detection of rail single defects, a signature tune corresponding to the corrugation should be identified beforehand. This is usually done through a validated numerical simulation [2.10]. The numerical model is a three dimensional finite element track-track dynamic interaction model in frictional rolling. A schematic diagram is shown in Figure 2-3a.

As the corrugation is commonly seen in straight tracks or at gentle curves, axle loads are thought equally distributed on both rails. Only a half track of length 18 m is modelled. The length of the track is enough to avoid the wave reflections from both ends of the rail. The primary suspension isolates the high frequency vibrations of the sprung mass from transmission to the above structures. As a result, sprung mass above the primary suspension can only vibrate below 10 Hz [2.11]. This frequency is far below the corrugation related frequency range of 500-2000 Hz (based on Dutch railway network, v=140 km/h). The sprung mass is lumped into a mass of value Mc. The primary suspension, the fastening system, and the ballast are represented as spring-damper elements. The wheel, the rail and sleepers are modelled as 3D solid element (see Figure 2-3b). The geometry of the wheel is type of ICR car, with nominal radius of 0.46 mm. The wheel flange is ignored as there is no wheel flange and rail gauge corner contact. The rail is 54 E1 with 1:40 inclination. The Coulomb friction law is employed with a friction coefficient of 0.3. Other system parameters are referred to [2.12] (see Table 2-1).

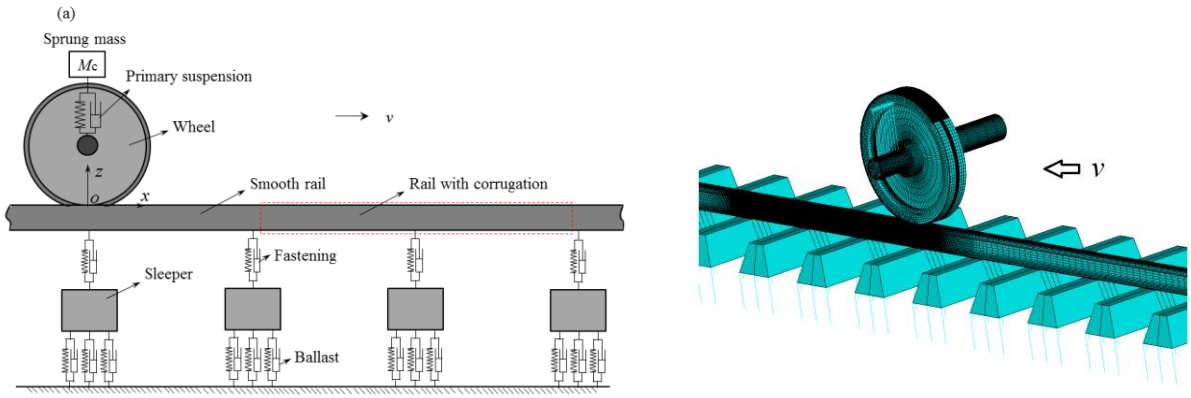

(a) Schematic diagram of the FE model (b) 3D FE model with mesh

Figure 2-3. The FE model

Table 2-1 Parameters of the model

Components	Parameters	Values
Sprung mass	Mass (kg)	10,000
1st suspension	Stiffness (MN/m)	1.15
	Damping (kNs/m)	2.5
Railpad	Stiffness (MN/m)	1,300
	Damping (kNs/m)	45
Ballast	Stiffness (MN/m)	45
	Damping (kNs/m)	32
Wheel and rail	Young's modulus (GPa)	210
	Poisson ration	0.3
	Density(kg/m3)	7,800

To simulate the wheel-track system dynamic response in the presence of the corrugation, the geometry of the corrugation was measured with the assistance of RAILPROF (see in Figure 2-4). The RAILPROF measures the vertical-longitudinal profile of rail crown center. A location with corrugation was found on Dutch railway network (see in Figure 2-5). From the measurement of the corrugation with RAILPROF, three components of 28-30 mm, 50 mm and 70 mm are identified. The 28-30 mm wavelength component is more commonly seen in the measurement, which implies a dominating wavelength.

Figure 2-4. RAILPROF measurement of rail corrugation longitudinal profile

Figure 2-5. A location with corrugation recorded on Dutch railway network

The rolling speed of the wheel is designed being 28.5 m/s, approximately equivalent to the speed of ABA measurements. Figure 2-6 shows the power spectral density distributions of the acceleration signals from the simulation. The main frequency components is around 1000 Hz, which can be found the explanation from $v=\lambda f$. Thus the 1000 Hz frequency component is the corrugation sensitive signature tune, which will be used for automatic detection of defects.

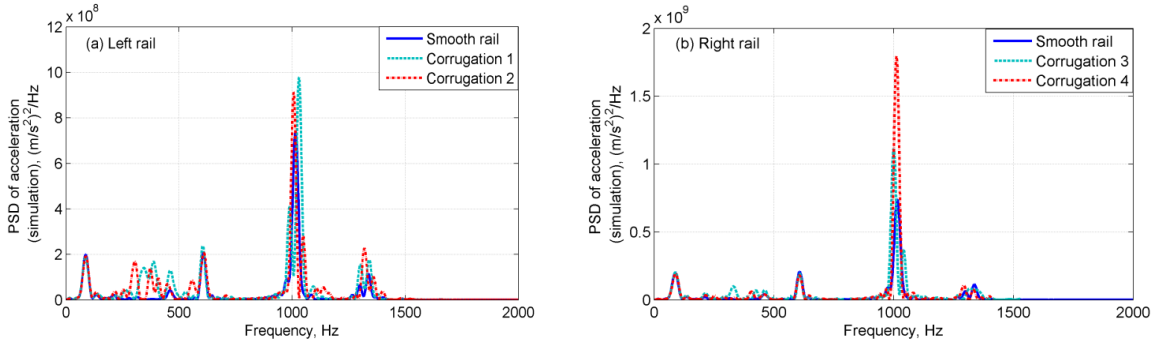

Figure 2-6. PSD of the simulated accelerations

2.3 ABA signals analysis

To validate the numerical simulation, ABA signals from detection are analysed. The measured signals with and without (or quite light) corrugation are shown in Figures 2-7 and 2-8, respectively. The distance of the signals is 200 m. The PSD of the ABA signals with corrugation shows a main frequency component of 900-1100 Hz in both rails. ABA signals without corrugation are also shown a frequency component in the range of 900-1100 Hz. However, the amplitude of the PSD is about 25% of the ABA signals with corrugation. Therefore, the signature tune found in the numerical simulation is confirmed in the ABA measurement signals.

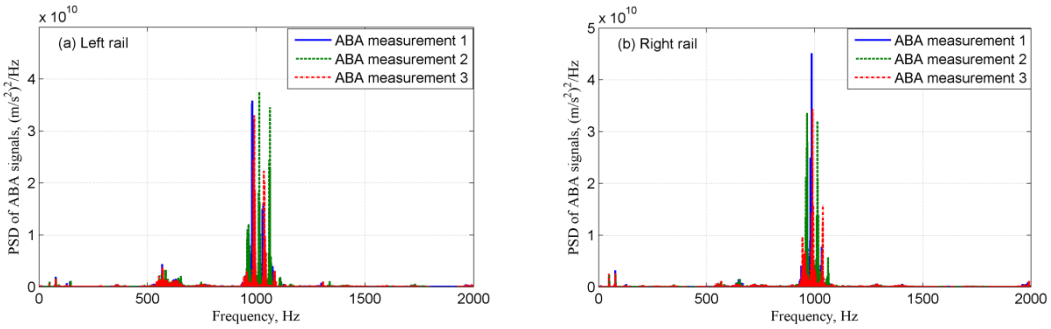

Figure 2-7. PSD of ABA signals with corrugation

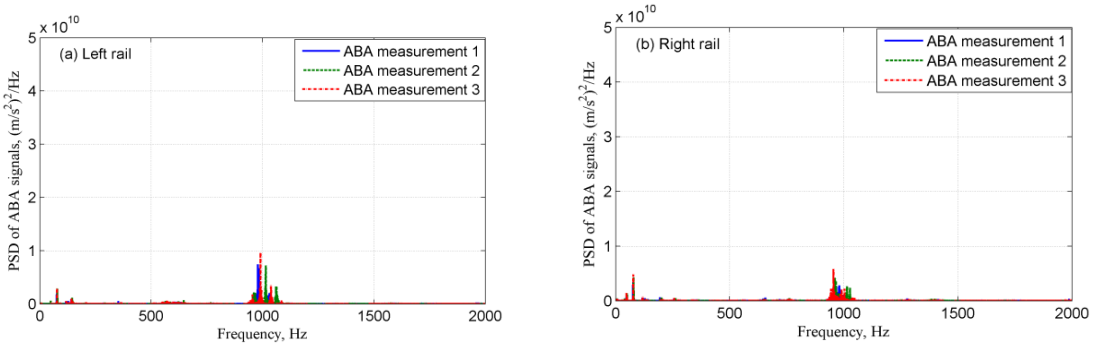

Figure 2-8. PSD of ABA signals without corrugation

2.4 Algorithm for the corrugation detection

Signal magnitude analysis and time domain analysis of the accelerations give basic information of signals and is not sufficient. Time-frequency analysis based on wavelet transform is used to study the acceleration signals. This technique has shown the advantage in fault diagnosis for the better time and frequency resolution with comparison of Fourier transform (FT) and short-time Fourier transform (STFT).

The continuous wavelet transform (CWT) is performed to analyse the time-frequency distribution of the ABA signals. CWT can be defined as [2.13]:

$$W_x(s,\tau) = \frac{1}{\sqrt{s}} \int_{-\infty}^{\infty} x(t)\psi^*\left(\frac{t-\tau}{s}\right) dt \qquad (2\text{-}1)$$

where $x(t)$ is the analysed signal, $\psi(t)$ is a mother wavelet, $\frac{1}{\sqrt{s}}\psi\left(\frac{t-\tau}{s}\right)$ is a family of wavelets from the mother wavelet by a translation of τ and a wavelet scaling of s; $W_x(s,\tau)$ are wavelet coefficients, and * indicates a complex conjugate. In this research, Morlet function is used as the mother wavelet. It is expressed as

$$\psi(\eta) = \pi^{-1/4} e^{iw_0\eta} e^{-\eta^2/2} \quad (2\text{-}2)$$

where ω_0 is a non-dimensional frequency.

The power spectrum of a wavelet transform is defined as the square of wavelet coefficients, expressed by $|W_x^2(s,\tau)|$. The wavelet power spectrum (WPS) provides information of position and frequency content of a certain defect.

In order to automatically detect the rail corrugation, a parameter should be quantized to reflect the situation of rail. To such end, a term of scale-averaged wavelet power (SAWP) is introduced to perform the automatic detection of the corrugation. The SAWP is defined as the weighted sum of the WPS over the scales s_{j1} to s_{j2} [2.14]:

$$\overline{W}_n^2 = \frac{\delta_j \delta_t}{C_\delta} \sum_{j=j_1}^{j_2} \frac{|W_n(s_j)|^2}{s_j} \quad (2\text{-}3)$$

where n is the time index, δ_j is a scale step, δ_t is the time step, and C_δ is an empirically derived constant for each wavelet function. The SAWP is calculated in the frequency range of the signature tune identified in aforementioned sections, both from the numerical investigation and ABA signals analysis. For the present case, this signature tune is 900-1100 Hz. Of course, different situations of track structure may influence the signature tune accordingly.

The time series of distribution of the SAWP has maximum values at certain locations with defects, and is used to detect local defects, such as squats [2.15]. However, corrugation appears continuously along the track. Instead of reporting the defect with a precise position, the detection of corrugation provides distance ranges of corrugation. A threshold will be defined based on levels of SAWP. Considering the overlap of signature tune of local short wave defects and the corrugation, the SAWP level of a 10 m distance will be studied to reduce the contribution by local defects. For maintenance consideration, if signals of a continuous distance longer than 100 m are above the threshold, it will be reported as corrugation, while shorter than 100 m will be not reported. Table 2-2 describes a detection of 600 m ABA measurement. Overall, there are two locations are identified as corrugation: 56.68-56.9 km and 57.05-57.17 km. Shortly after the ABA measurement, field validation was arranged to calibrate the prediction. The positions identified in the table were confirmed with corrugation. The corrugation shown in Figure 2.5 was taken during the field validation.

Table 2-2 Automatic detection of the corrugation with ABA measurement

ABA measurement	Left rail (from km to km)	Right rail (from km to km)
Measurement 1	56.68-56.9 57.05-57.16	56.67-56.9 57.05-57.17
Measurement 2	56.68-56.9 57.05-57.16	56.67-56.77 57.05-57.17
Measurement 3	56.68-56.87 57.05-57.17	57.06-57.17
Report	Corrugation: 56.68-56.9 (validated) 57.05-57.17(validated)	

2.5 Bibliography

[2.1] Automatic detection of corrugation: preliminary results in the Dutch network using axle box acceleration measurements. **S Li, A Núñez, Z Li, R Dollevoet.** s.l. : Proceedings of the ASME/ASCE/IEEE 2015 Joint Rail Conference.

[2.2] *Rail corrugation: characteristics, causes and treatments.* **SL Grassie.** s.l. : P I MECH ENG F-J RAI, 2009, Vols. 223:581-596.

[2.3] Surface analysis of corrugated rail treads**. HG Feller and K Waif**. s.l. : Wear, 144 (1991) 153-161.

[2.4] "Brown etching layer": A possible new insight into the crack initiation of rolling contact fatigue in rail steels? **S Li , J Wu, R.H. Petrov, Z Li, R Dollevoet, J Sietsma.** s.l. : Engineering Failure Analysis 66 (2016) 8–18.

[2.5] Measurement of railhead longitudinal profiles: a comparison of different Techniques. **SL Grassie.** s.l. : Wear 191 (1996) 245-251.

[2.6] Improvements in Axle Box Acceleration Measurements for the Detection of Light Squats in Railway Infrastructure. **Z Li, M Molodova, A Núñez, R Dollevoet**. s.l. : IEEE TRANSACTIONS ON INDUSTRIAL ELECTRONICS, VOL. 62, NO. 7, JULY 2015.

[2.7] Health Condition Monitoring of Insulated Joints based on Axle Box Acceleration Measurements. **M Molodova, M Oregui, A Núñez, Z Li, R Dollevoet.** s.l. : Engineering Structures, Volume 123, Issue 2016, September 2016, Pages: 225-235. DOI: 10.1016/j.engstruct.2016.05.018

[2.8] An investigation into the causes of squats—Correlation analysis and numerical modelling. **Z Li, X Zhao, C Esveld, R Dollevoet, M Molodova.** s.l. : Wear 265 (2008) 1349–1355

[2.9] Monitoring bolt tightness of rail joints using axle box acceleration measurements. **M Oregui, S Li, A Núñez, Z Li, R Carroll and R Dollevoet.** s.l. : Struct. Control Health Monit. (2016), DOI: 10.1002/stc.1848.

[2.10] Validation of a finite element model for axle box acceleration at squats in the high frequency range. **M. Molodova, Z Li, A Núñez, Rolf Dollevoet.** s.l. : Computers & Structures (2014) 141:84–93.

[2.11] Modelling of railway track and vehicle/track interaction at high frequencies. **KL Knothe, SL Grassie.** s.l. : Vehicle Syst Dyn 22; (1993) 209–262.

[2.12] *Rail corrugation in The Netherlands – measurements and simulations.* **M Hiensch, JCO Nielson, and E Verherjen.** s.l. : Wear, 2002, Vols. 253: 140–149.

[2.13] The wavelet transform, time–frequency localization and signal analysis**. I. Daubechies.** s.l. : IEEE Trans. Inf. Theory, vol. 36, no. 5, pp. 961–1005, Sep. 1990.

[2.14] "A practical guide to wavelet analysis," **C Torrence and GP Compo.** s.l. : Bull. Amer. Meteorol. Soc., vol. 79, no. 1, pp. 61–78, Jan. 1998.

[2.15] Automatic detection of squats in railway infrastructure. **M. Molodova, Z. Li, A. Núñez, R. Dollevoet.** s.l. : IEEE Transactions on Intelligent Transportation Systems 15-5 (2014) 1980-1990.

3 Sensitivity analysis of railpad and fastening parameters on vertical railway track dynamics

This chapter is based on the open access paper: M. Oregui, A. Núñez, R. Dollevoet, and Z. Li, "Sensitivity analysis of railpad parameters on vertical railway track dynamics". ASCE Journal of Engineering Mechanics, Volume 143, Issue 5, May 2017. DOI: 10.1061/(ASCE)EM.1943-7889.0001207

3.1 Introduction

In the railway system, fastenings are fundamental components of the track, mainly consisting of the railpad and clamps. The railpad is a resilient material placed between the rail and the sleeper to reduce vibration and noise by adding "flexibility" to the track. Clamps fix the rail to sleeper to ensure that it remains attached to it under train loads. Clamps have been studied rarely up to now, on the contrary, the railpad has been investigated widely, see a review in [3.1]. Results indicate that the railpad plays an important role in development of corrugation [3.2], rolling noise [3.3], load distribution to sleeper and ballast [3.4], [3.5], impact loads at switches and crossings [3.6], transition zones [3.7] and at insulated rail joints [3.8]. Although these studies gave an initial insight into the effect of the railpad stiffness on the track dynamics, a more in-depth analysis of influence of fastenings parameters on the global responses is necessary.

The properties of railpads are a key contributor to the track dynamic behaviour. Obtaining precise information of railpads is a fundamental requirement for understanding track dynamics. For this purpose, the NEN-EN 13146-9 standard was released in 2011 [3.9], and was applied to test recycled rubber railpads in [3.10]. Furthermore, many test approaches have also been developed during the past decades. For instance, in some tests, frequency-dependent stiffness of railpads is derived and static-load-deflection curves are defined [3.11]. In others, the dynamic behaviour of railpads are obtained under different frequencies and preloads and results show that railpads stiffness is more sensitive to preloads than frequency [3.11], [3.12], [3.13]. Additionally, the influence of temperature and aging on railpads mechanical performance was investigated and results indicated that comparing to longer operational life, the environmental aging has smaller effect on the dynamic properties of railpads [3.14], [3.15]. In [3.16], considering four relevant factors (frequency, preload, temperature, aging), the dynamic properties of railpads were obtained in a wide frequency range via combining dynamic mechanical analysis (DMA) with time-temperature superposition principle(TTS) [3.17]. In this section, we make use of this methodology to model the behaviour of railpads.

On the basis of obtaining accurate parameters of the fastening system, its effects on the track dynamic behaviour could be investigated. In the literature, track dynamics with different kinds of fastenings models have been developed, see [3.18] and [3.19]. The most commonly used model is a parallel of a spring and a damper, but it is not suitable for a detailed analysis of fastenings parameters. Firstly, recent studies show that the lateral and longitudinal directions of railpads have a significant influence on track global response [3.20], [3.21], [3.22]. Therefore, the rail seat area should be taken into consideration in a more detailed model. Secondly, the model should consider the non-linear behaviour

of fastening, that is, the upward load is resisted by clamps and the downward load compress the railpads. In this manner, the influence of railpads stiffness and preload (toe load) can be differentiated. Last, the model should take the dynamic behaviour of railpads into account, for instance, frequency-dependent railpads stiffness, according to measurements in [3.16].

3.2 Methodology

A 3D finite element (FE) model is developed for a railway track with monoblock sleepers in a ballast bed (see Figure 3.1). The track dynamic is studied by numerically simulating hammer test. In this model, the UIC54 rails and NS90 sleepers are modelled according to their respective nominal geometry using the elastic solid element, which is considered to be suitable material model for hammer loads [3.22], [3.23].

The ballast bed is represented as multiple linear spring and viscous damper pairs homogenously distributed under the sleeper. The upper nodes connected to the sleeper are fixed in the lateral direction of the track (i.e. *y* direction in Figure 3.1) to consider the lateral stiffness of the ballast. The lower nodes are fixed in three directions. The lower layers under ballast bed are not considered because they have ignorable influence on track response in the frequency range of interest (i.e. 300-3000Hz) [3.24].

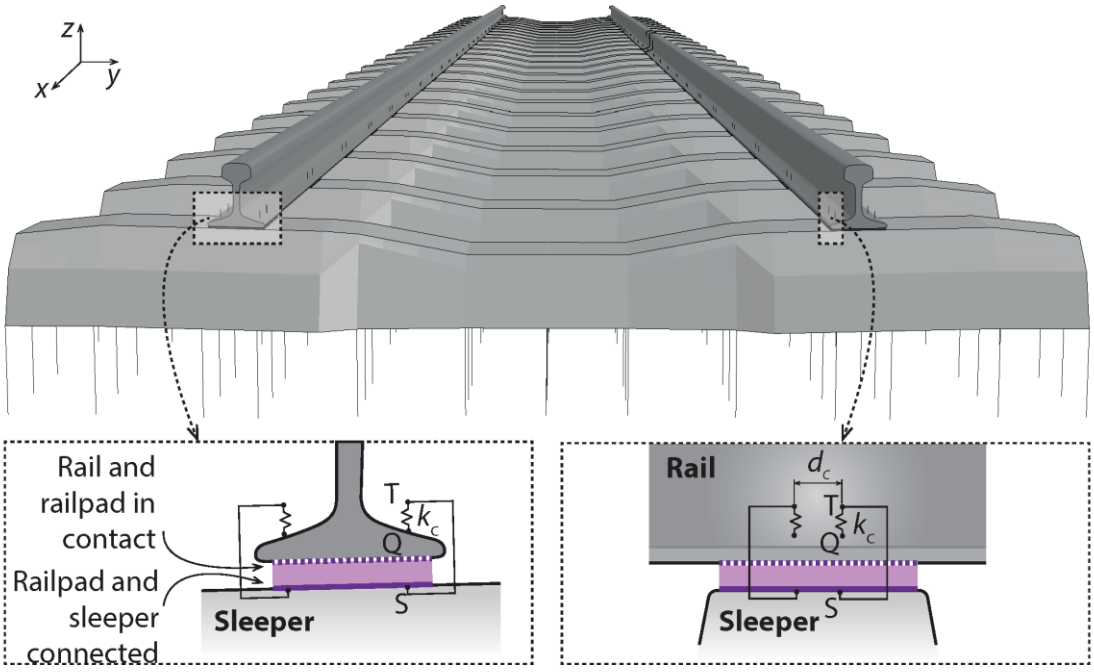

Figure 3.1: 3D FE track model with close-ups of the fastening model

The fastening is represented via its two main components: railpads and clamps. The railpad is modelled with solid element covering the entire rail seat. Its upper surface is in frictional contact with the rail (see left close-up in Figure 3.1), so that the relative movement between the railpad and rail and the non-linear behaviour of fastening can be considered. Its lower surface is connected to the sleeper. FC9 railpads, commonly used in the mainline in the Netherlands, are modelled. The Prony series is used as material model (see Figure 3.2) so that frequency-dependent stiffness and damping are considered. The Prony series is defined in time domain as [3.25]:

$$E(t)=\frac{\sigma(t)}{\varepsilon_0}=E_\infty+\sum_{j=1}^{n}E_j e^{-t/\tau_j} \tag{3.1}$$

where E_∞ is the stiffness of the spring in parallel, E_j is the stiffness of the spring *j*, τ_j is the ratio η_j / E_j known as the relaxation time constant of the term *j*, η_j is the viscosity of the damper *j*, and *n* is the number of terms. The number of terms required to accurately model a given material response is determined based on the quality of the fitting of the measured response data. The frequency-dependent behaviour of FC9 railpads under different preloads and temperatures is obtained by combining the DMA and TTS principle. The measured dynamic behaviour can be displayed as complex dynamic modulus E^* (viscoelastic behaviour), loss modulus E'' (viscous behaviour) or storage modulus E' (elastic behaviour). The three entities are related as follows:

$$E^*(\omega)=E'(\omega)+\mathrm{i}E''(\omega) \tag{3.2}$$

$$\left|E^*(\omega)\right|=\sqrt{\left(E'(\omega)\right)^2+\left(E''(\omega)\right)^2} \tag{3.3}$$

where $\omega=2\pi f$ and f is the frequency.

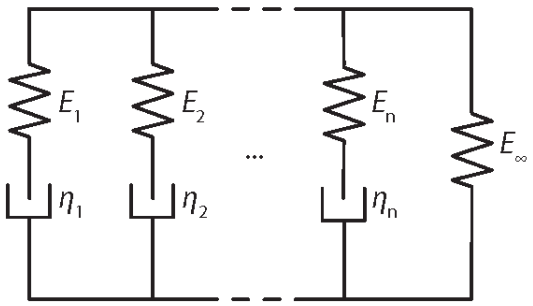

Figure 3.2: Prony series railpad model

By fitting the measured storage and loss moduli, the values of the stiffness E_j and viscosity η_j of the Prony series are derived. The fitting between the measurements and numerical material model is performed in the frequency domain by minimizing the error between the measured storage modulus E' and the loss modulus E'' and the modelled storage modulus E'_{prony} and loss modulus E''_{prony}, respectively:

$$\min\left[\left(E'-E'_{\text{prony}}\right)^2+\left(E''-E''_{\text{prony}}\right)^2\right]=$$
$$\min\left[\left(E'-\left(E_\infty+\sum_{j=1}^{n}\frac{E_j\omega^2\tau_j^2}{1+\omega^2\tau_j^2}\right)\right)^2+\left(E''-\left(\sum_{j=1}^{n}\frac{E_j\omega\tau_j}{1+\omega^2\tau_j^2}\right)\right)^2\right] \quad (3.4)$$

The clamp is represented as two springs on each side of the rail to fix the rail to the support. In each side, two springs are separated a distance of d_c which is a distance between the acting points of a clamp on the rail in the longitudinal direction. The fixing of the clamp to the sleeper is represented by coupling in the *x*, *y* and *z* directions to the upper node of the spring (T) and its vertical projection on the sleeper (S) (see close-ups in Figure 3.1). Moreover, the lateral constraint that the base plate of the fastening system applies on the rail and railpad is represented by coupling the upper and lower nodes of the spring (T and Q, respectively) in the *y* direction of the rail. The springs are preloaded to consider the toe load F_{TL} that clamps apply on the rail in the field. In the model, the toe load is considered by defining an initial displacement of the springs Δl as follows:

$$\Delta l=\frac{F_{\text{TL}}}{k_{\text{c}}} \quad (3.5)$$

where k_{c} is the stiffness of the clamp. The toe load is divided equally between the two springs of a clamp.

The impact of a hammer is represented as a triangle force applied on the top of a rail (i.e. on support) to simplify the simulation [3.26]. The starting time t_0 , maximum force time t_1, finishing time t_2 and maximum force F_{max} can be derived from the field hammer measurements. Employing the Implicit-Explicit FE approach, the response of the track to hammer impact is simulated in the time domain. In order to extract information from the numerically simulation, the input force $F(t)$ and output acceleration $a(t)$ are transformed into the frequency domain by Fast Fourier Transform (FFT), and then the receptance function $H(f)$ is calculated as follows:

$$H(f)=\frac{1}{(2\pi f)^2}\frac{S_{aF}(f)}{S_{FF}(f)}=\frac{1}{(2\pi f)^2}\frac{\sum_{n=1}^{N}\sum_{m=1}^{N-m-1}a[m+n]F[m]e^{-i2\pi fn}}{\sum_{n=1}^{N}\sum_{m-1}^{N-m-1}F[m+n]F[m]e^{-i2\pi fn}} \quad (3.6)$$

where f is frequency, S_{aF} is the cross-spectrum between the force and the acceleration, and S_{FF} the autospectrum of the force.

3.3 Sensitivity Analysis

Firstly, the influence of frequency-dependent parameters of railpads on track dynamic response is studied. Secondly, the effects on track vibration of properties of FC9 railpads at several temperatures, toe loads, ages are investigated. Additionally, track dynamic behaviour using different types of railpads is studied.

a. Frequency dependency

Figure 3.3a displays the Prony series model fitted to measured dynamic parameters of new FC9 railpad at a toe load of 18kN and a temperature of 26 ° C and the frequency-independent model (i.e. elastic model) whose Young's modulus E' corresponds to the storage modulus of the Prony series model at 1000Hz (i.e. E'_{1000Hz}). Figure 3.3b shows simulated track receptance function using the frequency-dependent and frequency-independent railpad models. Results indicate that except for the small difference of receptance magnitude in low frequency range of interest, the track dynamic response using elastic model of railpad is in good agreement with that of Prony series model. Thus, the frequency-dependent parameters of railpads can be considered in the frequency range 300-3000Hz by defining a young's modulus E equivalent to storage modulus E' at 1000Hz (i.e. E'_{1000Hz}) to reduce the simulation time caused by non-linear material model.

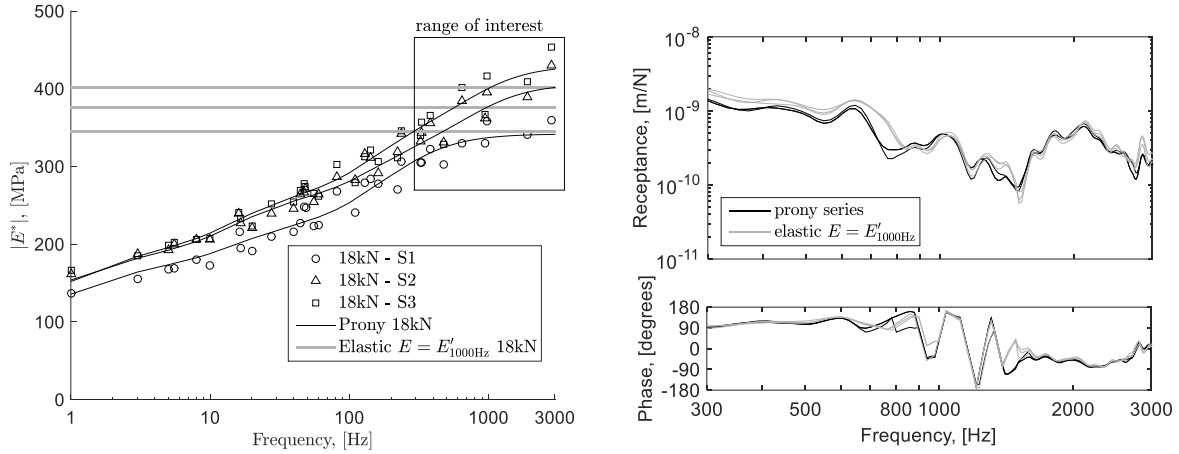

(a) (b)

Figure 3.3: New FC9 railpads at a toe load of 18 kN and a temperature of 26 ° C (a) measured railpad dynamic properties (S: sample), and elastic and Prony series models and, (b) simulated vertical track response

b. Temperature

Figure 3.4a shows the dynamic performance of new FC9 railpads at 26 ° C, 10 ° C and 0 ° C at a toe load of 18kN. Figure 3.4b displays the receptance functions of the track at the three different temperatures. It should be pointed out that the changes in the rail and clamps because of the temperature variation was not considered. Figure 3.4b indicates that although the resulting phase angles are dispersed between 600 and 900Hz, the receptance functions are almost identical, except for the two curves

which respond to the railpad with significant smaller stiffness than the others at 10 °C and 0 °C. Therefore, the track dynamic behaviour is not significantly influenced by the change in railpad properties caused by temperature.

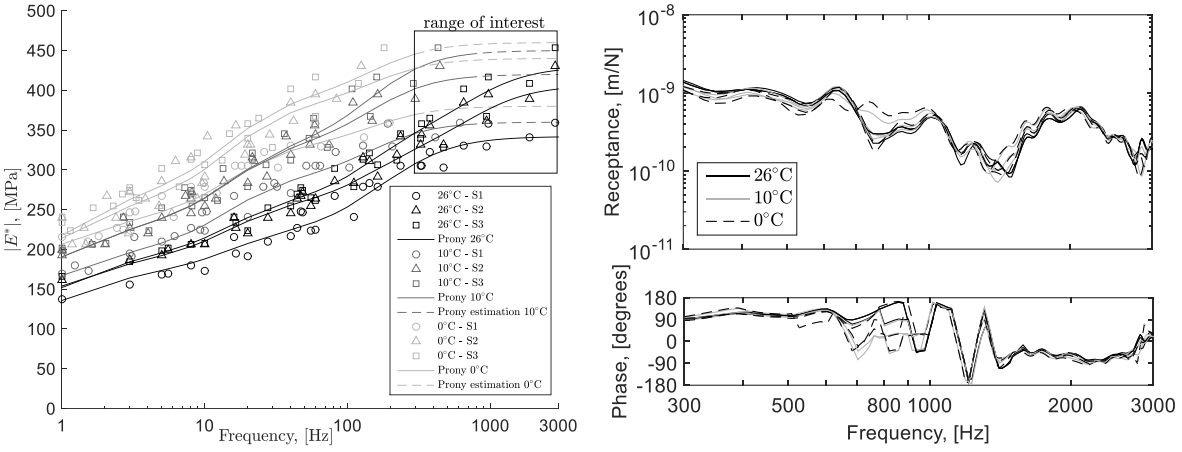

(a) (b)

Figure 3.4: New FC9 railpads for a toe load of 18 kN at different temperatures: 26 °C, 10 °C and 0 °C: (a) measured railpad dynamic properties (S:sample) and Prony series models, and (b) simulated vertical track response

c. Toe load

Figure 3.5a shows the dynamic behaviour of new FC9 railpads at toe loads of 18kN,12kN and 6kN at 26 °C. The corresponding simulation track dynamic responses at different toe loads are displayed in Figure 3.5b. Results indicate that if the toe load decreases from 18kN to 12kN, the main difference of the receptance functions is the shift to lower frequencies of the antiphase rail resonance (peak at 900-1000Hz) and the fourth bending mode of the sleeper (deep at 1300-1500Hz). when toe loads goes down to 6kN, the track dynamic behaviour changes significantly because the connection between the rail and sleeper is so loose that the rail-sleeper interaction changes. This change of track receptance functions is expected as the fastening is one of the dominant components that define the track dynamic behaviour in these frequencies [3.22].

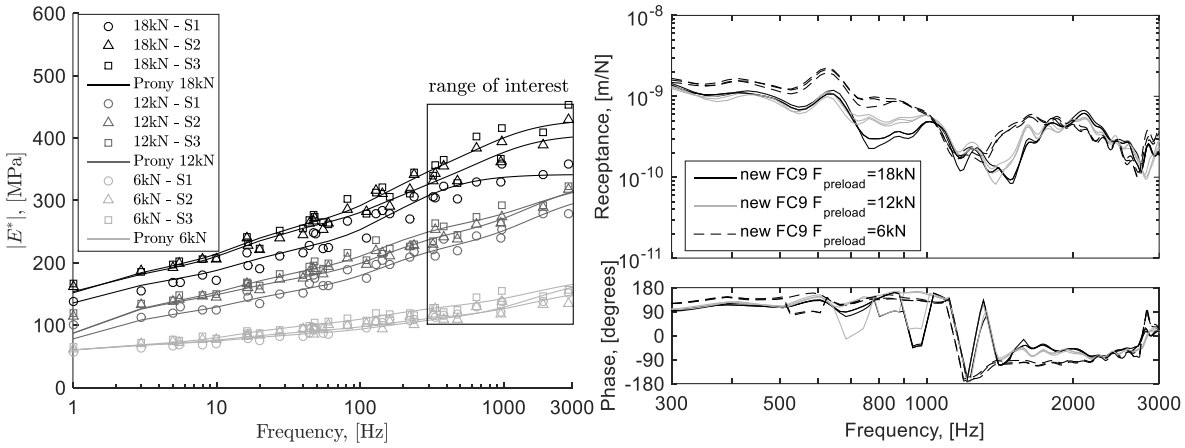

(a) (b)

Figure 3.5: New FC9 railpads at a temperature of 26 °C for different toe loads: 18 kN, 12 kN and 6 kN: (a) measured railpad dynamic properties (S: sample) and Prony series models, and (b) simulated vertical track response.

d. Aging

Worn railpads used for 10 years were removed from the Woerden-Utrecht line in the Netherlands, in which they withstood 60 Million Gross Tons. Figure 3.6a shows their measured dynamic behaviour for the toe loads of 18kN, 12kN and 6kN at 26 °C. The dynamic parameters of worn railpads are weakly temperature-dependent [3.16] and thus weakly frequency-dependent by applying time-temperature superposition principle [3.27]. Therefore, the stiffness of worn railpads in the frequency range of 300-3000Hz is suitable to be defined as a constant stiffness. The Young's modulus *E* assumed was the largest measured storage modulus (i.e.E'_{200Hz}). Figures 3.6b, 3.6c, 3.6d show vertical track dynamics with worn and new FC9 railpads for toe loads of 18kN, 12kN and 6kN respectively. For the three preloads, the same trend is observed: when worn FC9 railpads are defined instead of new FC9 railpads, some characteristics of the track response function shift to lower frequencies, for instance, the antiphase rail resonance (900-1000Hz), the fourth bending mode of sleeper (1300-1500Hz). In addition, the track receptance function increases for frequencies below 1000Hz when employing worn railpads, which means that the displacement is larger and therefore , more energy concentrated at these frequencies.

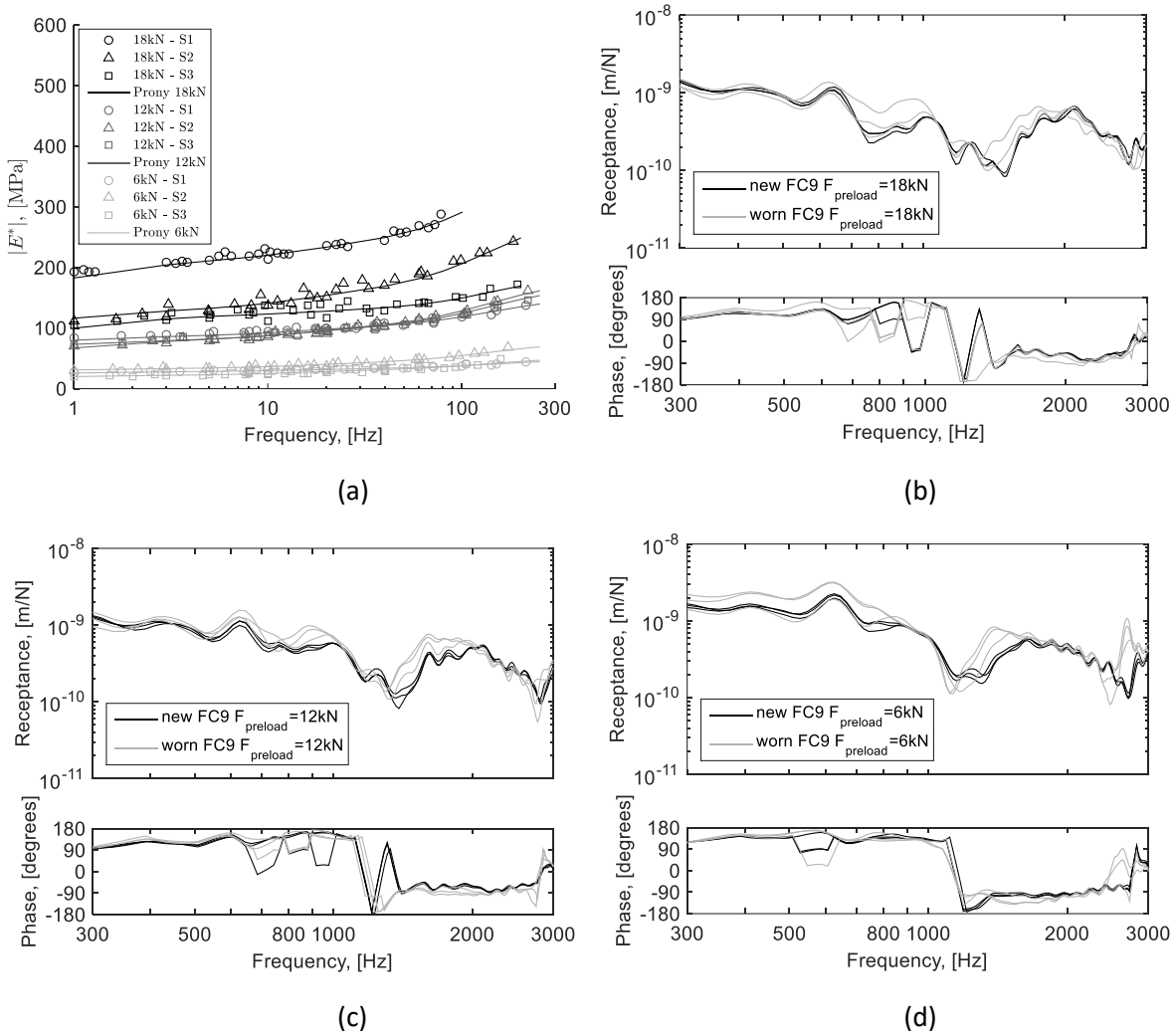

Figure 3.6: Worn FC9 railpads at 26 ° C for different toe loads: 18 kN, 12 kN and 6 kN: (a) Prony series and, simulated vertical track response: (b) 18 kN, (c) 12 kN, and (d) 6 kN.

e. Railpad types

Besides FC9 railpads, FC1950 and Orange railpads are investigated. Both FC1950 and FC9 are made of polyurethane cork rubber, but the cork content in FC1950 railpads is higher than in FC9 railpads. Orange is recently developed material designed for the absorption of short, intensive dynamic loads and vibrations.

Figure 3.7a and 3.8a show the measured dynamic behaviour of FC1950 and Orange railpads for toe loads of 18kN, 12kN and 6kN at 26 ° C respectively. Figure 3.7b and 3.8b display the resulting track global responses of FC1950 and Orange railpads respectively. At a toe load of 18kN, the track receptance functions of FC1950 and Orange railpads are significantly different from that of FC9

railpads because of the big difference in stiffness: FC1950 and Orange railpads are at least four times softer than FC9 railpads. As the FC9 railpads, the dynamic behaviour of track with FC1950 and Orange railpads changes when toe load is 6kN. The variation in behaviour is not caused by the downward force compressing the railpad but the upward force resisting by the clamps.

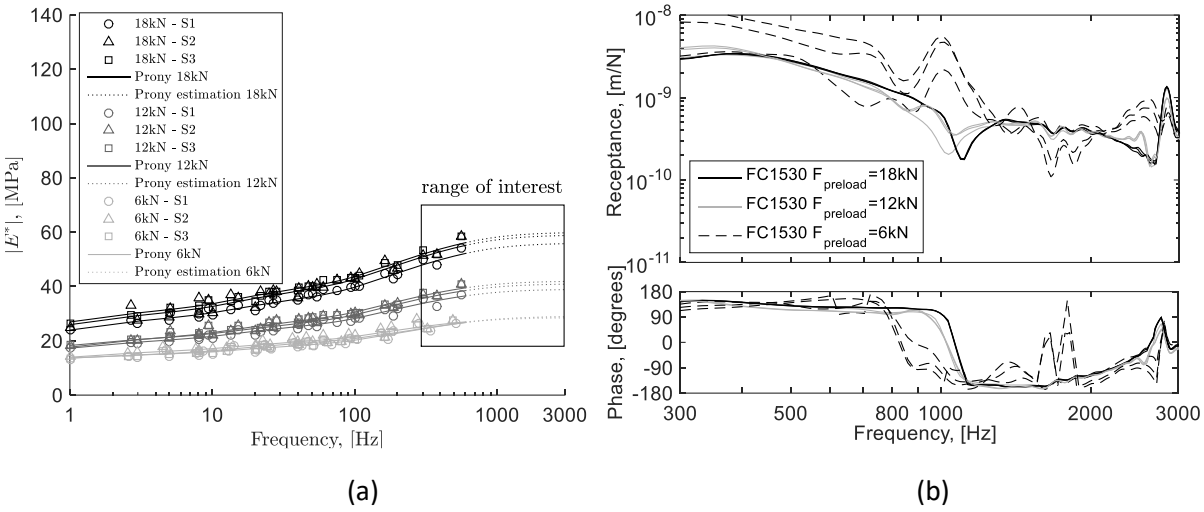

(a) (b)

Figure 3.7: FC1530 railpads at 26 °C for different toe loads: 18 kN, 12 kN and 6 kN: (a) Prony series and, (b) simulated vertical track response

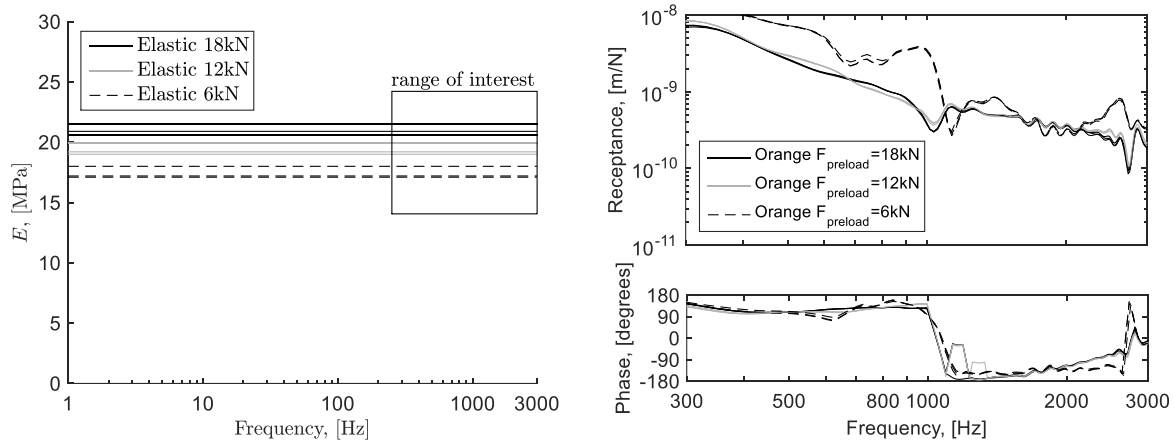

(a) (b)

Figure 3.8: Orange railpads at 26 °C for different toe loads: 18 kN, 12 kN and 6 kN: (a) Young's modulus and, (b) simulated vertical track response

3.4 Monitoring of the Fastening Condition

The information obtained from the sensitivity analysis could be applied to monitor the condition of fastening with FC9 railpads. Under service and environmental conditions, railpads worn and clamps loosen. What is more, these two processes of railpad aging and toe load decrease are closely related, that is, railpad aging feeds back to toe load decrease, and vice versa, and therefore, fastening deterioration accelerates.

In the sensitivity analysis, the same trends were observed on the vertical track dynamics for both railpad aging and toe load decrease. Figure 3.9 shows the case closest to the nominal condition (i.e. new FC9 for a toe load of 18 kN), the most deteriorated case (i.e. worn FC9 for a toe load of 6kN) and an intermediate case (i.e. worn FC9 for a toe load of 18 kN). According to the study presented in Section 3.3, if rails wear and/of clamps loosen [3.31]:

- The frequencies of the antiphase rail resonance f_{M3}, the second bending mode of the sleeper f_{M5} and, the maximum at 2000 Hz f_{M7} shift to lower frequencies;
- and the receptance function for frequencies lower than 1000 Hz increases significantly.

This information could be used to monitor the condition of fastening systems by dynamic-response-based train-borne measurements systems such as axle box acceleration systems [3.28], [3.29] and strain-gauge-instrumented wheelsets systems [3.30].

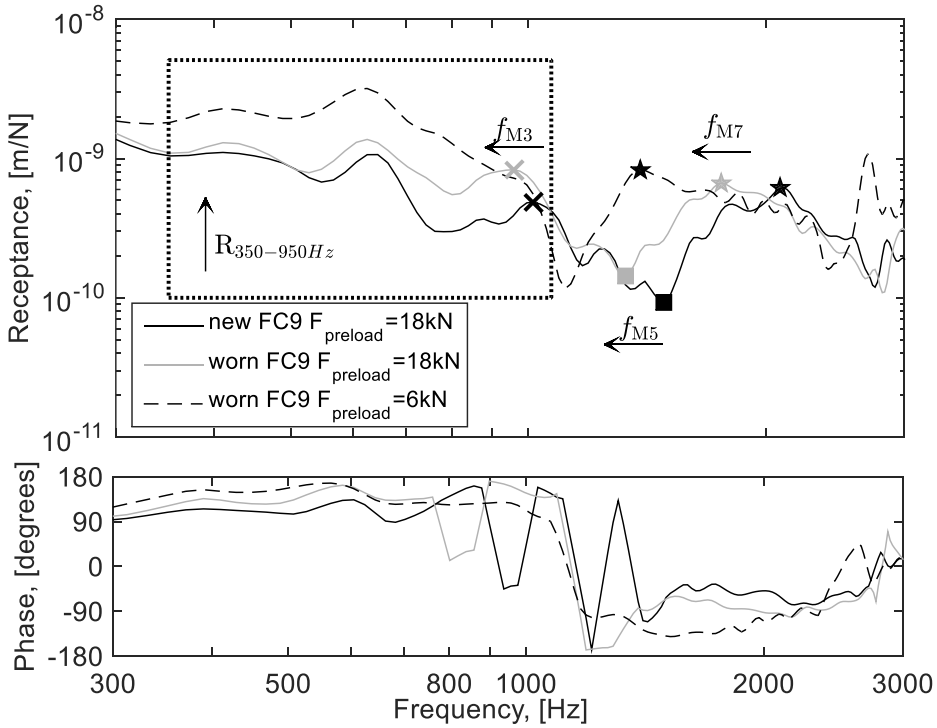

Figure 3.9: Effect of fastening deterioration on vertical track dynamics

3.5 Conclusions

The influence of railpad parameters on the railway track response is investigated by numerically reproducing vertical track dynamics via a 3D finite element (FE) model. The advanced fastening model defined includes solid frequency-dependent railpads in contact with the rail and clamps as preloaded springs. By introducing in the 3D FE model measured dynamic railpad properties, five main parameters of the fastening have been studied: frequency-dependency of railpads, temperature, toe load (i.e. clamping force), aging and railpad type. According to the results [3.31]:

- Variations in railpad properties due to temperature lead to negligible changes on the vertical track dynamics.
- The frequency-dependent properties of FC9 railpads can also be neglected if the railpads are defined with a Young's modulus corresponding to the storage modulus at 1000 Hz.
- Toe load, aging, and railpad type affect significantly vertical track vibrations.
- Loosened clamps (i.e. $F_{\mathrm{TL}} \leq 6kN$) drastically change the global track response, whereas with tighter clamps (i.e. $F_{\mathrm{TL}} \geq 12kN$) the railpad type and wear contribute to determine to a large extend the track dynamics.

3.6 References

[3.1] The use of elastic elements in railway tracks: A state of the art review. **Sol-Sánchez, M., Moreno-Navarro, F., and Rubio-Gámez, M.** s.l. : Construction and Building Materials, 75:293-305, 2015.

[3.2] The influence of railpad stiffness on wheelset/track interaction and corrugation growth. **Ilias, H.** s.l.: Journal of Sound and Vibration, 227(5):935-948, 1999.

[3.3] Track dynamic behaviour at high frequencies, part 1: theoretical models and laboratory measurements. **Thompson, D. J. and Vincent, N.** s.l: Vehicle System Dynamics, 24(Suppl):86-99, 1995.

[3.4] Vertical interaction between train and track with soft and stiff railpads - full-scale experiments and theory. **Fermer, M. and Nielsen, J.C.O.** s.l.: Proceedings of the Institution of Mechanical Engineers, Part F: Journal of Rail and Rapid Transit, 209(1):39-47, 1995.

[3.5] Sensitivity analysis of track parameters on train-track dynamic interaction. **Zakeri, J. A. and Xia, H.** s.l.: Journal of Mechanical Science and Technology 22(7): 1299-1304, 2008.

[3.6] Dynamic vehicle-track interaction in switches and crossings and the influence of rail pad stiffness field measurements and validation of a simulation model. **Palsson, B. and Nielsen, J.** s.l.: Vehicle System Dynamics 53(6): 734-755, 2015.

[3.7] Investigation on dynamic behavior of railway track in transition zone. **Zakeri, J.A. and Ghorbani, V.** s.l.: Journal of Mechanical Science and Technology, 25(2):287-292, 2011.

[3.8] Impact forces at dipped rail joints. **Mandal, N. K., Dhanasekar, M., and Sun, Y. Q.** s.l.: Proceedings of the Institution of Mechanical Engineers, Part F: Journal of Rail and Rapid Transit, 230(1):271-282, 2016.

[3.9] EN 13146-9+A1:2011, Railway applications - Track - Test methods for fastening systems - Part 9: Determination of stiffness. **European Committee for Standardization**, s.l.: European Standard, 2012.

[3.10] Viability analysis of deconstructed tires as material for rail pads in high-speed railways. **Sol-Sánchez, M., Moreno-Navarro, F., and Rubio-Gámez, M.** s.l.: Materials and Design 64:407-414, 2014.

[3.11] Developments of the indirect method for measuring the high frequency dynamic stiffness of resilient elements. **Thompson, D. J., Van Vliet, W. J., and Verheij, J. W.** s.l.: Journal of Sound and Vibration 213(1): 169-188, 1998.

[3.12] Static and dynamic properties of rubber rail pads [statische und dynamische eigenschaften von gummi-zwischenlagen fr eisenbahnschienen]. **Knothe, K. and Yu, M.** s.l.: Forschung im Ingenieurwesen/Engineering Research 66(6): 247-259, 2001.

[3.13] Measurements of the dynamic railpad properties. **Maes, J., Sol, H., and Guillaume, P.** s.l.: Journal of Sound and Vibration 293(3-5): 557-565, 2006.

[3.14] Dynamic behaviour of railway fastening setting pads. **Carrascal, I. A., Casado, J. A., Polanco, J. A., and Gutierrez-Solana, F.** s.l.: Engineering Failure Analysis 14(2): 364-373, 2007.

[3.15] Investigation and prediction of stiffness increase of resilient rail pad due to train and environmental load in high-speed railway. **Kim, E., Yang, S., and Jang, S.** s.l.: 2015 Joint Rail Conference, 2015.

[3.16] Obtaining railpad properties via dynamic mechanical analysis. **Oregui, M., de Man, A., Woldekidan, M., Li, Z., and Dollevoet, R.** s.l.: Journal of Sound and Vibration 363: 460-472 (2016).

[3.17] The temperature dependence of relaxation mechanisms in amorphous polymers and other glass-forming liquids. **Williams, M. L., Landel, R. F., and Ferry, J. D.** s.l.: Journal of the American Chemical Society 77(14): 3701-3707, 1955.

[3.18] Elastomeric materials used for vibration isolation of railway lines. **Castellani, A., Kajon, G., Panzeri, P., and Pezzoli, P.** s.l.: Journal of Engineering Mechanics 124(6): 614-621, 1998.

[3.19] Dynamic characteristics of infinite and finite railways to moving loads. **Chen, Y. and Huang, Y.** s.l.: Journal of Engineering Mechanics, 129(9): 987-995, 2003.

[3.20] A contact-area model for rail-pads connections in 2-d simulations: Sensitivity analysis of train-induced vibrations. **Ferrara, R., Leonardi, G., and Jourdan, F.** s.l.: Vehicle System Dynamics 51(9): 1342-1362, 2013.

[3.21] Influence of the fastening modeling on the vehicle-track interaction at singular rail surface defects. **Zhao, X., Li, Z., and Dollevoet, R.** s.l.: Journal of Computational and Nonlinear Dynamics, 9(3), 031002, 2014.

[3.22] An investigation into the modeling of railway fastening. **Oregui, M., Li, Z., and Dollevoet, R.** s.l.: International Journal of Mechanical Sciences 92: 1-11, 2015.

[3.23] Influence of cracked sleepers on the global track response: Coupling of a linear track model and non-linear finite element analyses. **Gustavson, R. and Gylltoft, K.** s.l.: Proceedings of the Institution of Mechanical Engineers, Part F: Journal of Rail and Rapid Transit 216(1): 41-51, 2002.

[3.24] Receptance behaviour of railway track and subgrade. **Knothe, K. and Wu, Y.** s.l.: Archive of Applied Mechanics 68(7-8): 457-470, 1998.

[3.25] Theory of stress-strain relations in anisotropic viscoelasticity and relaxation phenomena. **Biot, M. A.** s.l.: Journal of Applied Physics 25(11): 1385-1391, 1954.

[3.26] Experimental investigation into the condition of insulated rail joints by impact excitation. **Oregui, M., Molodova, M., Nunez, A., Dollevoet, R., and Li, Z.** s.l.: Experimental Mechanics 55(9): 1597-1612, 2015.

[3.27] Theory of viscoelasticity: An introduction. **Christensen, R.** s.l.: Academic press, New York, 1982.

[3.28] Automatic detection of squats in railway infrastructure. **Molodova, M., Li, Z., Nunez, A., and Dollevoet, R.** s.l.: IEEE Transactions on Intelligent Transportation Systems, 15(5): 1980-1990, 2014.

[3.29] Improvements in axle box acceleration measurements for the detection of light squats in railway infrastructure. **Li, Z., Molodova, M., Nunez, A., and Dollevoet, R.** s.l.: IEEE Transactions on Industrial Electronics 62(7): 4385-4397, 2015.

[3.30] Dynamic interaction between train and railway turnout: Full-scale field test and validation of simulation models. **Kassa, E. and Nielsen, J.** s.l: Vehicle System Dynamics 46(SUPPL.1): 521-534, 2008.

[3.31] Sensitivity analysis of railpad parameters on vertical railway track dynamics. **Oregui, M., Núñez, A., Dollevoet, R., and Li, Z.** s.l: ASCE Journal of Engineering Mechanics 143(5), DOI: 10.1061/(ASCE)EM.1943-7889.0001207

4 Effect of grinding

4.1 Introduction

Rail grinding was first used for the purpose of the removal of rail corrugations. The technique developed from the 1960s onwards, initially tackling corrugations to depths of 2-3mm, at that time a 2 inch wide grinding pattern was applied at the centre of the corrugated rail. The early fixed orientation of the grinding motors, although effective at removing corrugation peaks resulted in the flattening the railhead and did not correct plastic flow or remove cracks propagating in the corrugation troughs, also the root causes of corrugation formation were not addressed [4.1]. Grinding has since been developed with current grinding machines able to grind as much as 70° to the gauge side of the rail in different orientations to maintain the profile of the rail and remove plastic deformations, and the purposes of grinding now includes the removal of rolling contact fatigue cracks as well as the maintenance of the rail head profile. Improved technology also allows for various grinding patterns to be implemented with precise control over the power consumption of the individual wheels resulting in a capacity to precisely position the grinding motors with greater accuracy.

To fully understand the benefits of effectiveness of rail grinding it is important to look at the root causes of corrugation, grinding will generally have a positive effect on mitigating the impact of corrugation [4.2] , but only for certain types of corrugation will it be able to remove the root causes and the particular grinding strategy can have a large impact on the total effectiveness of the grinding solution.

Corrugation formation and growth can be understood in terms of a feedback loop, first summarised by Grassie [4.3]; where initial profiles of wheels and rails excites a “wavelength fixing mechanism” which sets the wavelength and position of the eventual corrugation. Other important parameters include the tangential forces between the wheel and the rail which can be dependent upon traction, curvature of track and friction at the wheel rail interface, as well as other factors such as track stiffness, and rail and wheel surface conditions or irregularities. The resulting periodic variation in the normal forces to wheel-rail contact result in uneven wear and then the consequential uneven profile [4.3].

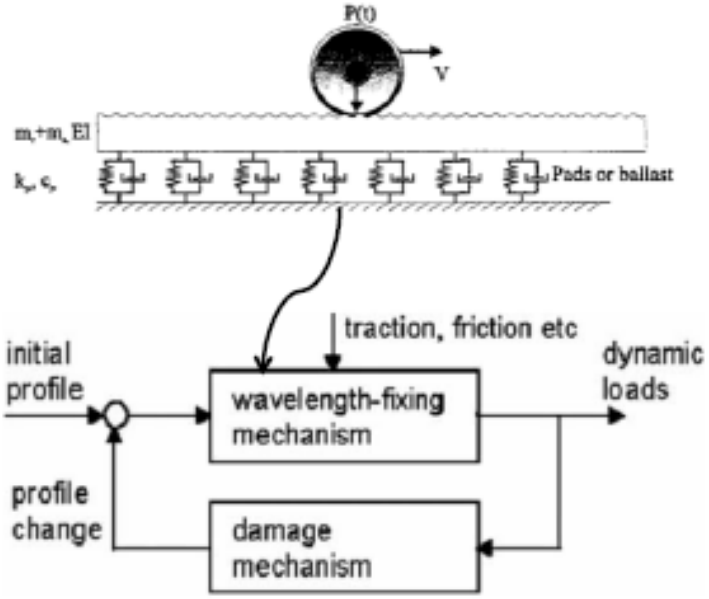

Figure 4-1 Feedback loop demonstrating the initiation and growth of corrugations [4.3]

Grassie also categorised corrugations depending upon the mechanisms which causes the corrugation and the corrugation pitch and frequency [4.1] [4.3].

The **pinned-pinned resonance** corrugation is perhaps the most common type of corrugation, particularly for mixed traffic, tangential or long radius curved lines. The corrugation is caused by the resonance of the rail as if was a beam, pinned at the sleepers, therefore the wavelength of the corrugations is twice the sleeper pitch. Grinding is not able to have any impact on the initiators of this type of corrugation, and it will be fixed by the track design, so grinding will not be able to eliminate the corrugations. However, grinding will mitigate these types of corrugations and as corrugations generally grow at exponential rates [4.4] regular grinding will slow the growth rate the corrugations.

Rutting corrugation occurs in severe, small radius, curves or in tangential track when braking or traction is severe. Rutting corrugation tends to be initiated by discrete irregularities in the track such as welds and joints, these then fix the position of the corrugation along the track. In this case grinding can be used in some cases to remove the discrete irregularity to prevent the initiation of the corrugation as well as mitigate and slow the growth of these corrugations. The wavelength fixing mechanism in rutting corrugation is the torsional resonance of the wheelsets resulting in a roll-slip oscillation between the wheel and the rail. For this type of corrugation the main cures include the control of friction, hard rail and improved steering including reduced cant and also modifications to the rail pads and rail system to disrupt the wavelength fixing mechanism [4.5] [4.3].

The wheel shape can also be a cause of rail corrugation and hollow wheels and asymmetric wheel profiles can have also have an impact on corrugation [4.1].

Name	Cause	Frequencies / Hz
P2 resonance	Vertical resonance of vehicle's unsprung mass on the track stiffness	50-100
"Pinned-pinned resonance" or "Roaring rails"	Rail vertical vibration – as if a beam pinned at the sleepers and/or other fixings	400-1200
Second torsional resonance of driven wheelsets or "Rutting"	Longitudinal variation in slip and wear at the wheel-rail contact due to resonance	250-400

Table 4.1 Types of corrugation and causes [4.6] [4.7]

There are number of reasons why it is important to treat corrugations, and grinding is the primary method for the treatment of corrugations, these are:

- Risk of derailment
- Noise and vibration
- Passenger comfort
- Wear of rail reducing rail life
- Increase risks of rail breakage
- Damage to track components, eg in some cases cracking concrete sleepers [4.5] [4.8]

Today grinding is the main treatment for restoring rail profile for the treatment of:

- Corrugations
- Lateral excursions of the running band on the rail
- Vertical and lateral excursions of contact over welded joints
- Rail profile management
- Surface fatigue damage elimination/management [4.9]

Most modern rail grinders use stones that rotate about an axis normal to the rail. A result of the grinding is a characteristic signature on the rail head, this signature will have a wavelength equal to the distance the grinder moves in one revolution of the grinding of the grinding stone. It is therefore essential that the characteristic signature should have a different frequency to the corrugations in order to prevent it propagating future corrugation. It is possible to impose grinding regimes which leave very little signature, this is to be recommended where possible, not only to prevent corrugation, but it also provides benefits for immediate noise reduction [4.1] [4.3] [4.10] [4.11] [4.12].

Grinding has been found to provide benefits when carried out after the installation of new rail, as well as on existing rail. Studies by PKP in Poland found that grinding new rails provided benefits with respect to corrugation formation were still visible after 4.5years [4.13].

Another major issue with grinding is that of capacity constraints. Typical grinding trains run at between 15-30km/h, significantly slower that the in service vehicles, this makes them difficult to schedule into the normal timetable and therefore grinding may only be carried out during night time possessions or with large slots scheduled in the timetable. High speed grinding methods have been developed and tested by Deutsche Bahn these high speed grinding trains developed by Vossloh can operate at between 60 and 100km/h, although their normal operation in Europe has been at about 80km/h, this allows for them to operate between service trains much more easily and not add to the capacity constraints within the network [4.14] [4.15].

4.2 Grinding costs

Grinding is an expensive operation and in the early 1980's grinding costs worldwide were estimated at over $100m per annum [4.3]. Maintenance costs were also studied in the within the InnoTrack FP6 project which found, though workshops carried out in 2009 with infrastructure managers across Europe including ADIF, CD, RFF, Banverket (now Trafikverket), DB, ProRail, ÖBB, Network Rail the highest ranking railway problems and approximate proportion of the infrastructure maintenance budget which was spent on the particular maintenance activities [4.16] .

In ranked order biggest problems found within the InnoTrack project were:

1. Track: bad track geometry
2. Rail: cracks and fatigue
3. S+C: switch wear
4. Substructure: unstable ground
5. Joints: isolation joint failure
6. Rail: corrugations
7. Rail: wear
8. Structures: major line closures
9. Fasteners: worn/missing pads
10. Sleepers: renewal optimisation
11. Culverts/pipes: flooding
12. Ballast: stone spray
13. Ballast: ballast wear
14. Rail: low friction/adhesion
15. Joints: weld quality
16. S+C: common crossings
17. S+C: Manganese crossings
18. S+C: geometry maintenance
19. S+C: loss of detection

Rail corrugations were 6th highest ranking problems identified by the infrastructure maintenance teams across the InnoTrack partners.

InnoTrack also found the cost of grinding as proportion of overall maintenance costs to be between 2-7%, depending upon the infrastructure manager.

Many studies have been carried out to investigate the cost effectiveness of rail grinding for example in 1991 a study carried out for British Rail into the cost/benefit analysis of grinding short wavelength corrugations on concrete sleepers found that the economic benefits of grinding to save on rail and sleeper life far outweighed the costs. This 1991 found that for all growth rate of corrugations of less than 80mm wavelengths there was a cost benefit, and that for some corrugation types grinding costs would need to rise by a factor of 25 times for the grinding operations to longer be economically viable [4.17]. For the optimal cost-benefits an appropriate grinding strategy should be selected.

4.3 Grinding strategies

In theory an optimal Corrugation Grinding Maintenance Strategy requires information on:

- Rail Grinding Resources – types and numbers of grinding trains available – grinding train cost and performance of the grinding train
- Corrugation Geometry – depth of corrugation
- Operational constraints [4.18]

Ideally the measurement systems should identify the mean peak-to-trough height of the rail corrugations and the pitch of the corrugations before and after grinding [4.8] and high speed rail profile measurement is possible with an accuracy better than 0.1mm [4.19]. And a maximum acceptable mean peak-to-trough height should also be defined [4.4]. Advanced grinding machines can control the grinding wheel motors to particularly target greater energy at the peaks of the corrugations (oscillating or offset grinding) and has been shown to be quite effective [4.2].

An example of recommended maximum corrugation depths after grinding is given by Sinclair, 1994 [4.20]. The maximum corrugation depths are dependent upon the corrugation wavelength, the longer the wavelength the greater the acceptable depths, this is due to the resultant forces at the wheel rail interface being smaller for the same depth of corrugation on a long wavelength compared to a short wavelength.

Corrugation Wavelength	**Maximum corrugation depth after grinding**
Between 500mm and 750mm	0.10mm
Between 750mm and 1050mm	0.16mm
Between 1050mm and 1400mm	0.21mm
Between 1400mm and 1700mm	0.27mm

Table 4.2 Recommended maximum corrugation depths after grinding [4.20].

However, if regular measurement is not possible then an alternative grinding strategy is to grind at regular intervals and to over grind. As corrugations generally grow exponentially the number of grinding passes required to control corrugations during the life of the rail should be lower if grinding

is carried out before the corrugations have reached a damage level, and therefore over grinding may not necessarily shorten the life of the rail. However, it is still recommended that a strategy based on measurements will be optimal. Whichever strategy is adopted the grinding strategy should ensure that corrugations are not allowed to grow to a level where unacceptable damage is being caused, and that sufficient material is ground from the rail to prevent rapid regrowth of the corrugations [4.4].

Since grinding is now carried out for a range of different defects most railway infrastructure managers adopt a frequency based strategy for grinding based on equivalent million gross tonnes of traffic (EMGT), this allows for easier planning of grinding. For example the Network Rail grinding strategy for profile management is primarily for in-traffic, single pass grinding, with frequencies given in the table below. However, these frequencies should also be increased or supplemented with additional in-possession grinding where this preventative grinding regime is not sufficient to maintain the rail profile [4.21] or the risk of rolling contact fatigue is high. Also coorective grinding is carried out if the result of inspection or measurement is the detection of severe corrugation or other track geometry defects.

Geometry	**Radius**	**Frequency**
Curve	≤ 2500m	Every 15 EMGT
Curve	> 2500m	Every 45 EMGT
Straight		Every 45 EMGT

Table 4.3 Network Rail In-traffic rail grinding frequencies for plain line single pass grinding for lines with >5 EMGT per year [4.21]

The Network grinding strategy also specifies that the principal objectives of grinding rail are as follows:

a) to achieve the required transverse profile and produce a regular and consistent running band towards the crown of the rail to manage conicity and reduce forces at the wheel rail interface;
b) to correct and impose a transverse profile that reduces contact stresses on the gauge corner and shoulder of the rail;
c) to remove localised misalignment at welds and other track features;
d) to remove the fatigue damaged surface of the rail, which has or is likely to initiate rolling contact fatigue cracks.
e) to control the longitudinal profile of the rail to control the formation and growth of corrugation.

Where grinding is carried out using smaller machines operating in possessions the priorities shall be as follows:

a) rails with light or moderate RCF;
b) rail in a curve that has been previously rerailed due to rolling contact fatigue;
c) rails with heavy or severe RCF;
d) rails with severe corrugation.

Track location	Target Profile (Profile definition angle range)	Tolerances for: (Tolerance angle range)	Minimum metal removal (MMR to be achieved in the angle range)
High Rail	NR HR 1 (-5° to 50°)	+0.3 to -0.3mm (-5° to 50°)	0.2mm (0° to 45°)
Low Rail	NR 113A (-5° to 50°)	+0.3 to -0.3mm (-5° to 50°)	0.1mm (0° to 45°)
Straight Track – Both Rail	NR 113A (-5° to 50°)	+0.3 to -0.3mm (-5° to 50°)	0.1mm (0° to 45°)
Corrugated Track – Both Rails	NR HR1 or NR 113A (-5° to 50°)	+0.3 to -0.3mm (-5° to 50°)	0.2mm (0° to 45°)

Table 4.4 Network Rail target rail profiles [4.22]

High speed rail grinding also offers potential for introducing new grinding strategies, allowing grinding to be carried out in traffic with less interruption to the time table. The metal removal rates are lower than conventional grinding trains, but the benefits of not interrupting traffic allow for grinding to be time tabled more frequently and fits well with preventative grinding strategies. High speed grinding has been demonstrated successfully on the DB network and the particular grinding pattern used in high speed grinding has also been beneficial in reducing noise [4.14] [4.15].

Working speed	60-100 km/h
Current working speed in Europe	80 km/h
Metal removal per pass (Single train) Metal removal per pass (Twin train)	0.05mm 0.1mm
Roughness after grinding	<8 µm
Required traction	1,500 kW (2,000 hp)
Operational range w/o stop	About 50 km

Table 4.5 High speed grinding facts and figures [4.14] [4.15]

4.4 References

[4.1] E. Magel, "The Blending of Theory and Practice in Modern Rail Grinding," Fatigue & Fracture of Engineering Materials & Structures 26, 921-929, 2003.

[4.2] S. L. Grassie, "Rail irregularities, corrugation and acoustic roughness: characteristics, significance and effects of reprofiling," Proc IMechE Part F: J Rail and Rapid Transit 226(5) 542–557, 2012.

[4.3] S. L. Grassie, "Wheel-rail interface handbook," R. Lewis and U. Olofsson, Eds., Elsevier, 2009, pp. 349-376.

[4.4] G. Durbin, "A rail corrugation grinding strategy for the Kowloon Canton Railway Corporation light rail transit system (RR-MF-007)," 1991.

[4.5] R. Clark, "AN INVESTIGATION INTO THE DYNAMIC EFFECTS OF RAILWAY VEHICLES RUNNING ON CORRUGATED RAILS," Journal of Mechanical Engineering Science, Vol 24 No2, 1982.

[4.6] D.I.Fletcher, "MEC6429 Mechanical Engineering of Railways Lecture 11 Wear of Overhead Lines and Track Damage - Corrugation," in University of Sheffield, 2014.

[4.7] Y. Sato, A. Matsumoto and K. Knothe, "Review on rail corrugation studies," Wear , vol. 253, pp. 130-139, 2002.

[4.8] H. Tanaka, "Development and verification of monitoring tools for realizing effective maintenance of rail corrugation," in 6th IET conference on Railway Condition Monitoring, 17-18th September 2014, University of Birmingham, 2014.

[4.9] "A survey of current wheel and rail interface design and management pratices," 2015.

[4.10] S. L. Grassie, "Wheel-rail best practice handbook," F. Schmid, Ed., A & N Harris, London, 2010, pp. 4-30 - 4-40.

[4.11] S. L. GRASSIE, M. J. SAXON and J. D. SMITH, "MEASUREMENT OF LONGITUDINAL RAIL IRREGULARITIES AND CRITERIA FOR ACCEPTABLE GRINDING," Journal of Sound and Vibration, vol. 227, pp. 949-964, 1999.

[4.12] P. Sroba, "RAIL GRINDING BEST PRACTICES".

[4.13] B. Bozyslaw, "Effectiveness of rail grinding," in Railway Engineering 1999 - 2nd International Conference & Exhibition – London 25 - 26 May 1999, 1999.

[4.14] M. Hartenstein, "Preventive High Speed Grinding - six years of successful rail maintenance," in Railway Engineering 2013 - 12th International Conference & Exhibition – London 10th - 11th July 2013, 2013.

[4.15] "HSG High Speed Grinding, Preventative Rail Grinding in Sync with your Timetable," 2016.

[4.16] "D1.4.6 - A report providing detailed analysis of the key railway infrastructure problems and recommendation as to how appropriate existing cost categories are for future data collection," 2009.

[4.17] A. J. Keens, "Cost/benefit analysis of short wavelength corrugation grinding on concrete sleeper track (LR-MF-010)," 1991.

[4.18] J. C. Sinclair, "Rail corrugation management systems - part 1: Opportunities for BR research (RR-TCE-072)," 1996.

[4.19] E. Magel and J. Kalousek, "The application of contact mechanics to rail profile design and rail grinding," Wear , vol. 253, pp. 308-316, 2002.

[4.20] C. Sinclair J, "Preliminary rail grinding strategy for railtrack (RR-STR-94-087)," 1994.

[4.21] "Rail profile management, NR/L2/TRK/001/mod10," 2012.

[4.22] "Inspection and maintenance of permanent way – Rail management, NR/L2/TRK/001/B01," 2009.

[4.23] B. King, "Some Thoughts Regarding Railhead Damage with Particular Attention to Corrugation," The Journal of the Permanent Way institute, January 2016, Volume 134, 2016.

[4.24] "Rail Grinding Best Practice," 2012.

[4.25] "Inspection and Maintenance of Permanent Way, NR/L2/TRK/001," 2014.

5 Assessment of corrugation in Turkey

Corrugation is reported to occur in the Turkish railway. The defect occurs as a result of the combination of various types of damage such as wear, fatigue, and it starts on the rail surface running band. Corrugation appears as periodic irregularities on the rail surface, undulating or bright-dark colour variations of wavy wearing. In Turkey, there are no reports relating corrugation to derailments, but the phenomenon is related somehow to loosening of small fastenings, disturbance of the ballast, increase in noise and decrease in travelling comfort due to increase of the track vibrations. Rail grinding at an early stage eliminates such defect. In Turkey, the two most important types of corrugation are:

• Short Pitch Corrugation (Figure 5.1): This is the type of undulation with a wavelength of 3cm to 8cm.

• Long Pitch Corrugation (Figure 5.2): This is the type of undulation with a wavelength of 8 cm to 30 cm generally related to heavy traffic and high speed conditions.

In the case of short or long pitch corrugation, the actions to be taken: Grinding. In case of late stage, perform track repair and VT (visual inspection).

Figure 5.1: Short pitch corrugation

Figure 5.2: Long pitch corrugation

The aim is to check rail corrugation on TCDD's conventional and HST lines by using track inspection machines, to determine frequency of measurements, and to interpret the results obtained. In Table 5.1 is the description of task and the responsible personnel.

The machinery and tools used in measurement of rail corrugation includes:

- Roger 800 Track And Catenary Inspection Machine (Figure 5.3).
- Piri Reis.
- Rail Grinding Machine.

Figure 5.3: Roger 800, TCDD.

No	Task Description	List of Responsible Personnel									
		Track Maintenance and Repair Officer	Track Surveyor	Chief of Track Maintenance and Repair	Technical Office	Track Maintenance Manager	Track Supervisor	Assistant Track Manager	Track Manager	Assistant Regional Director	Regional Director
1	Deciding on performing machine work on the line			R,A,S,C,I	R,A	R,A,S,C,I	S		R,A,S,C,I		
2	Inspection of machine works (according to grinding and milling tolerances)	R,A	R, A	R,A,S,C,I	R, A	R,A,S,C,I	S		A,S,C,I		
3	Carrying out preparations prior to machine work (Inspection of the machine or the tool, ensuring availability of oil, fuel, water, etc., as required, taking safety precautions, etc.)	R, A	R, A	R,A,S,C,I	R,A	R,A,S,C,I	S				
4	Reporting of the result	R,A	R,A	R,A,S,C,I		R,A,S,C,I	S,I	I	R,A,S,C,I	I	I

Abbreviations are defined below:

- R: Person carrying out the work.
- A: Personnel who is responsible for performance and supervision of the work.
- S: The individual who is ultimately accountable for supervision.
- C: Personnel who is referred to for his opinion and approval during the course of performance of the work - bilateral communication.
- I: Personnel who is informed during the course of performance of the work - unilateral communication

Table 5.1: Tasks and personnel, TCDD.

5.1 Roger 800 Track And Catenary Inspection Machine

Regarding the braking system, the main components of the disk brake and automatic retrieval system due to wear are: Sustained and automatic braking in accordance with UIC540; Direct braking; Parking brake; Emergency control braking; Total capacity of fuel reservoir: 510 litres; Compressor system Min: 400 liter and Max: 900 liter. The main components of the braking system are: Distributor Dako CV1 nd 7B 848; Manettino Direct Braking: Knorr Bremse ZB11; Manettino Indirect Braking: Knorr Bremse FB11; Brake cylinder: POLI11; Braking base : Tipo codis558 UIC541-3 compliant; Compressor: Wabco.

There are 2 encoders within train and related positioning system provides information for latitude-longitude and altitude including cycle of wheel.

The corrugation measurement system used has a significant importance for planning grinding and quality check of bearing surface. The wave length 20-1000mm and the amplitude is <20mm.

5.2 Piri Reis measurement train

Piri Reis (see Figure 5.4) was created by integrating the equipment which provide data to measure track, rail and catenary parameters on HST set bought from CAF company. The measurement systems were installed by Italian Mermec company. The features of Piri Reis include:

- Measurement Speed: 275 km/h.
- Number of Measurement Parameters: 247.
- Number of Coaches: 6.
- Coach 6: For hardware and working place.
- Coach 1: For providing two way measurement.
- Coach 2,5: For cameras on the roof.

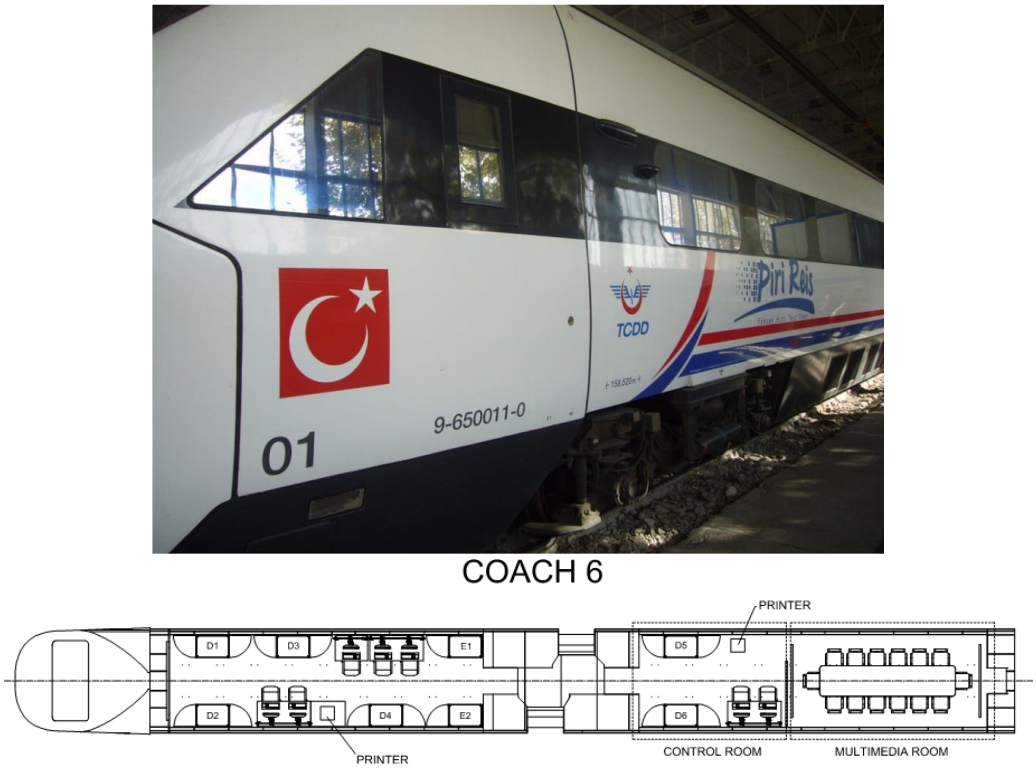

Figure 5.4: Piri Reis train.

The components of the Piri Reis measurement system are the following:

- **The localization system (TLS)**: Consisting of GPS Synchronization of distance and time, Speed measurement, Localizations of data, Determines line name, Kilometre information Hardware of TLS, Uses 2 encoders, 2 odometer interface cards : Create distance/time signals, 2 PC CTLU(function interface) : Interface of hardware and sensors, 2 passive milestone sensors, 2 GPS antennas, 2 signal boosters.
- **The Track Geometry Measurement System (TGMS)** is used for: Measurement of track geometry parameters and determination of train body position.
- **Rail Profile Measurement System (RPMS)** is used for: Determination of wear on rail profile and collapse fault on rail.
- **Rail Corrugation Measurement System (RCMS)** is used for determination of corrugation in different wave bands.
- **Vehicle Dynamic Measurement System (VDMS)** is used for: Measurement of transverse and longitudinal acceleration, driving quality measurement system, Track Vision System (VCUBE) is used for visual inspection of the track.
- **Pantograph / Catenary Measurement System** is used for determining: Interaction pantograph/catenary and catenary dynamic measurement system (PI), Electrical Parameters Measurement (EP), Electric Arcs Detection (PU).
- **Video Control System (TVIS)** is used for: View of Train Surroundings, View of Pantograph – Catenary, View of Wheel – Rail Contact.

The technique used by the Rail Corrugation Measurement System (RPMS) consists of a sensor placed in a dumped box and a target fixed to the axle box (Figure 5.5). The parameters measured by RPMS include right-left corrugation value for different wavelengths (40-100mm, 100-300mm, 300-1000mm).

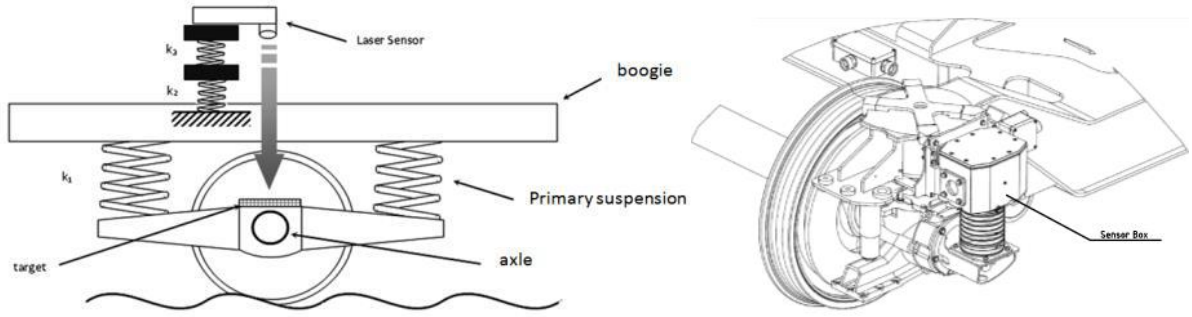

Figure 5.5: Rail corrugation measurement system.

5.3 Making use of the RPMS information

In order to verify the results obtained by the RPMS, the defect reports are verified manually on the line. Manually verification is carried out visually and by using measurement gauges. Regular inspection

of main lines is conducted as indicated below in Table 5.2. Stabling tracks outside of the main lines, station lines, sub tracks, etc. are inspected as required provided that potential changes arising from operation are taken into consideration.

V<120km/h	120km/h<=V<160km/h	160km/h<=V<220km/h	V>=220km/h
Every 12 months (as an exception, every 24 months)	Every 12 months (as an exception, every 18 months)	Every 8 months (as an exception, every 12 months)	Every 6 months (as an exception, every 9 months)

Table 5.2: Time intervals for regular inspection of rail corrugation on railway mainlines, V= Maximum operating speed on the line.

In case where the time interval foreseen for regular inspection cannot be met due to malfunctioning or unavailability of the track inspection machine, the track manager checks whether the inspection can be carried out by using another appropriate measurement tool (RGI 20 rail grinding machine with RCA measurement system), or whether exception rule is applied, or not. If neither option is available, speed restriction is applied as per the speed group with an appropriate measurement period. However, if no defect at IL level has been found according to the result of the previous measurement, no speed restriction is applied until the next regular measurement.

Regarding planning and implementation of inspection, TCDD is responsible for ensuring that track measurement machines are inspected. Track inspection machines located at directorate of track mechanical workshop or at directorates of track maintenance and repair is assigned by the track manager to perform planning and implementation of inspection of rail corrugation.

Results of the measurement is evaluated by specialized staff (personnel who possess certificate with respect to such evaluation), and the report to be prepared as a result of the evaluation is delivered to the relevant track manager, track maintenance manager and chief of track maintenance and repair within 15 calendar days as of the measurement date.

Results of the measurement is verified in-situ by the relevant chief of track maintenance and repair, or the track surveyor, or the track maintenance and repair officer or track maintenance and repair foreman appointed by him, and the defects determined is remedied within the program to be prepared.

The chief of track maintenance and repair is report the defects which have been remedied in his area of responsibility, to the track maintenance and repair manager and the track manager on a monthly basis.

5.4 Remedying of defects

Decisions as to how the defects detected on the rail is remedied, are taken by the track maintenance and repair manager and the chief of track maintenance and repair based on the works to be performed by the engineers of the technical office. Rail corrugation defects detected on the line shall be remedied by grinding or machining rail in areas with corrugation, or by replacing such rails.

Before determining the action to be taken, the remaining life span of the rail must be calculated and compared against the cost of grinding and machining. In cases where the detected value of corrugation is remedied by grinding or machining the condition of wear on the existing rail status is taken into consideration. Grinding or machining is permitted if rail wear values are to remain within limit values following grinding or machining.

Some or all of the following tools and equipment may be used during rail grinding and milling works as appropriate:

- Rail grinding machine.
- Rail milling machine.
- Manual rail grinder.
- Transverse rail profile measuring tool.
- Longitudinal rail profile (corrugation) measuring tool.
- Roughness measuring tool.
- Tool for measuring the removed material.
- Control form.

Rail maintenance methods are as follows:

- Preventive grinding.
- Re-profiling (corrective) grinding.
- Grinding after laying, repair or replacement of rails.
- Milling.

Rail profile influences the dynamic forces which are created during movement of the vehicle and has a major influence on the forces applied to the track and the vehicle. Sudden changes which occur in the profile due to defects, and large deviations from the optimum (ideal) profile, significantly increase the rate at which the rails and the track superstructure are damaged, and also reduce vehicle ride quality.

Although both grinding and milling processes involve removal of material from the rail surface, they extend the safe operational life of rails by controlling the forces applied on rails and by reducing the extent of damage. The rails stay in service for longer periods of time if rail profiles are up to the standards. If managed carefully, the rails can remain in service longer and a greater return on the investment in rails can be achieved in terms of the traffic cried by the rail during its life and the maintenance investment in the rail.

Grinding removes material from the rail surface, eliminating or slowing the development of rail surface defects, and equalizing the wear around or along the rail to restore the transverse and/or longitudinal rail profile up to the standard rail profile. Grinding is used:

- Within a regular maintenance program to maintain the existing rail condition (preventive grinding). Periodic grinding operations are planned to counteract the predicted degradation of the rails condition due to surface defects arising from production of the new rails installed on the line following relaying or construction of new tracks, or due to rail vehicle traffic, both in terms of the profile of the rail and the damage to the surface and structure of the rail. Maintaining the rails within the required specifications reduces the rate of degradation and helps protect rails against developing of defects which could threaten the integrity of the rails.
- On an as-required basis to correct issues with the rail condition (corrective grinding), additional maintenance is required to correct sections of rail which are found to be approaching or exceeding defect size limit or target profile deviation limits. Such a reactive maintenance used to restore the rails to within specified defect sizes and profile limits, when routine or post-incident inspection identifies issues with the rail.
- During installation and repair of rails (profile alignment grinding). Grinding is carried out as part of rail installation, repair or replacement works. Grinding is used ensure that any variation in alignment or profile where rails have been joined, particularly where the rails joined are of different sections (i.e., rail profile) or have different amounts of wear, forms gradually. Additionally, where the joint is formed by welding, grinding is used to grind back the excess weld at the joint to the profile of the rails. Where the surface of the rails has been repaired by welding, grinding is used to make the profile of the repaired rail the same as the parent rail.

Rail Milling is used when it is necessary to remove larger amounts of material from the rail, compared to grinding. Milling is used:

- To restore the profile of a worn rail up to the standard profile.
- To eliminate severe rail surface defects.

Rail milling must be preferred in cases where a number of grinding procedures are required to be performed in order to correct the defect, by taking into account the time and the costs involved. Rail milling can be significantly more efficient, and in some cases milling can be used to maintain a rail that would otherwise have been discarded because of the high cost of grinding.

In summary, the benefits of performing maintenance of the rail via grinding and milling are as follows:

- To achieve the required transverse profile and to ensure a regular and consistent distribution of forces towards the crown of the rail in order to manage conicity and reduce forces at the wheel-rail interface.
- To impose a transverse profile that reduces contact stresses on the gauge corner and shoulder of the rail.

- To remove excess material from welds so that the profile at the weld matches the parent rail, or the profile through a weld transitions gradually between the profile of rails of different profiles which have been joined.
- To remove the fatigue damaged surface of the rail, which has or is likely to initiate rolling contact fatigue cracks.
- To control the longitudinal profile of the rail in order to control the formation and growth of corrugation.

5.5 Grinding

5.5.1 Track sections which can be subject to grinding

For the purposes of grinding, the track can be divided into two main categories, these are

- Plain line
- Switches and crossings

Plain line and switches and crossings have different grinding requirements, and not all of the types of grinding equipment are suitable for usage at each track section.

Plain line grinding machines are programmable automated machines built into special machinery. These machines have varying numbers of grinding heads which use an electrical or hydraulic motor to rotate a grinding stone against the rail and to remove material from the surface of the rail.

Rail grinding heads rotate the grinding stones about an axis normal to the longitudinal axis of the rail, the angle of rotation of each grinding stone around the circumference of the rail head can be controlled independently. This allows for arrangement of the grinding stones in various ways to control the amount of material to be removed from each location around the rail; in order to achieve the required profile. However, more than one pass of the machine might be required in order to achieve the final profile required.

The capacity of each machine to remove material from the rail and to reshape the rail profile depends on the number of the grinding stones and the power applied. These machines have built in rail profile measurement equipment for measuring the rail profile before and after the grinding work.

Switch and crossing grinding machines are similar to, and can perform the same functions as plain line grinding machines. In addition, they are capable of accommodating additional rail components of switches and crossings. They tend not to be able to grind as much metal off the surface of the rail in a single pass, when compared to plain line grinding machines with more grinding stones. Specific and complex areas of switches and crossings (the nose and the blade parts) cannot be ground using switch and crossing grinding machines – these areas must be ground using manual grinders.

The application of the grinding stones to the rail is less flexible compared to that of conventional grinding machines, and the amount of material removed per pass is significantly less. Therefore, high-speed rail grinding trains are only suited for profile maintenance and defect prevention, not for correction of the profile or elimination of defects. They are intended as a preventative maintenance measure to be applied more frequently than conventional grinding. Due to their capability to perform grinding at higher speeds, they present relatively little obstruction and disruption to traffic whilst doing so.

5.5.2 Preventive rail grinding

Benefits of performing preventive grinding on the rail are as follows:

- It helps prevent development of critical RCF (Rolling Contact Fatigue) cracks on the rail, prevents formation and further development of other rail defects.
- It keeps the transverse profile of the rail within specified limits.
- It helps prevent formation of longitudinal irregularities such as corrugations, and maintains the rail's longitudinal profile within limits.
- Maintenance of the rail profile reduces wear, slows the growth of defects on both the rails and on rolling stock wheels, and maintains vehicle ride quality.

The aim of preventative grinding is to extend the life of the rail by reducing the rate at which the rail defects progress, and controlling the sizes of defects on the rail surface, within safe limits. This prolongs the rail's service life.

An effective preventative grinding programme extends the life of the rail, improves the condition of the rail throughout its life, and provides a balance between extending the life of the rail by treating rail defects which would limit rail life, the wear produced by rail grinding activities and the cost of rail grinding and other maintenance activities. The target here, is to obtain the maximum economic life from the rail while maintaining safety.

Where preventative grinding at the frequencies shown above is insufficient to maintain rail profile or defects within acceptable limits; more frequent grinding must be performed.

In Table 5.4 are the limit values for selection of grinding and milling.

Table 5.3: Preventive grinding frequency.

Tracks	Track Geometry	Frequency
Conventional lines	Curve radius ≤ 2500 m	At every 15-20 million tons
	Curve radius > 2500 m	At every 40-60 million tons

	Tangent/Straight	At every 40-60 million tons
High Speed Train lines	Curve radius ≤ 2500 m	At every 10-15 million tons
	Curve radius > 2500 m	At every 15-20 million tons
	Tangent/Straight	At every 20-30 million tons
NOTE 1: Minimum metal removal for each grinding operation is 0.1mm. NOTE 2: The above specified frequencies shall be extended or shortened depending on rail surface defects and corrugation values.		

Table 5.4: Table for selection of grinding and milling.

Amount of metal to be removed	Grinding	Grinding or milling	Milling
Up to 1 mm.	**Applicable**	**Not applicable**	**Not applicable**
Between 1mm. - 1,5mm.	**Not applicable**	**Applicable**	**Not applicable**
Between 1.5mm. - 3mm.	**Not applicable**	**Not applicable**	**Applicable**

5.5.3 Corrective (reactive) rail grinding

Corrective (reactive) grinding works are grinding operations which are not a part of the scheduled preventive grinding activities. This method is usually utilized in elimination of rail defects which are detected during inspections and which require immediate action. The grinding procedure carried out within the scope of a corrective rail maintenance program should aim to eliminate all rail surface defects. If this is not possible, the size of the defects should be reduced, and further grinding should be planned to maintain the rail condition within limits. Alternatively, the rail may require replacement. If the rail condition has deteriorated to the extent that the profile or defects are no longer tolerable, yet there is still significant wear life (that is residual rail height) remaining, then rail milling is a potentially viable alternative to rail replacement.

Where the rail requires removing more than 1.5mm of material from any location around the transverse profile in order to achieve the specified rail profile, it is unlikely that restoration of the profile by grinding would be economically viable. That is, the cost of removing the required amount of material would be greater than the value of the residual life of the rail gained by restoring the profile by grinding to allow the rail to continue to be in service. In this case, either the rail should be monitored until it requires replacement, or rail milling should be considered as an alternative treatment.

5.5.4 Grinding of switches and crossings

Grinding of switches and crossings must be considered in two parts:

1) grinding of the plain rails of switches and crossings, and,

2) grinding of other running surface components such as the switch blades, movable frogs, and stock rails adjacent to switch blades and the crossings.

The primary method for managing profiles of switches and crossings is to utilize manual grinders at locations on switches and crossings where the grinding stones of grinding machines are unable to reach.

It is essential that the profiles of switch blades and crossings are carefully maintained. When grinding switches blades and crossings the following need to be considered:

- Correct position of switch blade when switch blade is open and closed.
- Variations in height of switch blade due to sliding plates.
- Correct opening and closing of switch blade after grinding.
- Ensuring wheel load transfer when switch rail is closed.
- The ground rail must not interfere with the rolling profile of the vehicle wheels.

The effective guidance and support of the wheels provided by the design profile should not be interfered with by the grinding operations.

5.6 Milling

The equipment, tools and machines to be used are:

- Rail milling machine.
- Transverse rail profile measuring tool.
- Longitudinal rail profile (corrugation) measuring tool.
- Roughness measuring tool.
- Tool for measuring the removed material.
- Control form.

Rail milling involves use of a cutting tool rotated against the surface of the rail to remove metal. The process is capable of removing significantly more material from the surface of the rail compared to grinding within the same time period. Rail milling is generally more economical than rail grinding when 1.5mm or more of material is required to be removed. Rail milling is suited for situations where multiple passes with a rail grinding machine would be necessary to correct the rail profile or to remove the defects, whereby rail grinding is uneconomical.

Rail grinding or milling machines are precision machines. Their accuracy can be influenced by variations in the track alignment and in the original profile which the machines take their reference data from. Therefore, the tolerances which should be specified for acceptance of grinding works have been prepared by taking into account the following factors:

- The precision which can be achieved in the field.
- The cost of achieving precision.
- Having the finished work conform to the specified profile as closely as possible.

5.7 Participation in the inspection

The track maintenance and repair manager, or personnel to be appointed by the track maintenance and repair manager (chief of track maintenance and repair, or track surveyor or track maintenance and repair officer or track maintenance and repair foreman) participate in regular inspection rail rides to be performed in their areas of responsibility.

Table 5.5: Limit values.

TYPE	**Vmax Km/h**	**Wave Length Mm**	**AL warning mm**	**IL Maintenance mm**
Short Wave	V<160	30<ʎ<100	0,030	0,070
	V>= 160		0,020	0,030
Moderate Wave	V<160	100<ʎ<300	0,100	0,200
	V>= 160		0,040	0,100
Long Wave	V<160	300<ʎ<1000	Not applicable	Not applicable
	V>= 160		0,400	0,500

5.8 Evaluation and documentation

The result of the measurement is evaluated by specialized staff (personnel who possess certification for such evaluation) and a report is prepared with respect to the evaluation. The below specified information is provided in the report to be prepared.

- Person in charge of the measurement train
- Line section on which measurements are conducted
- Date of measurement
- Measurement criteria
- Scaled graphic printout
- Defect report printout

5.9 Measures to be taken

Check with limits the rail corrugation detected on the line fall within among the limit values (AL or IL) and take necessary precautions as specified in the table below.

Table 5.6: Table for evaluating rail corrugation.

Limit Value Condition	Measured Value	Observations And The Measures/ Precautions To Be Taken
AL warning level	Higher than AL level Lower than IL level	Acceptable track quality, but needs to be kept under observation. Continue normal operation monitor the line.
IL maintenance level	Higher than IL Level	Determine the period of replacement or planning, determine the estimated time period for replacement according to values obtained as a result of regular inspection carried out on the line, and develop a rail replacement or grinding plan accordingly. Monitor the line. Include in maintenance schedule.

5.10 Track inspection machines

Track inspection machines are important for inspecting and observing the existing track condition, planning maintenance works to be performed on the track and operating the line so as to ensure safety and comfort.

Inspection and observation can be made by walking along the line, in the driver's cab (inspections in the train, locomotive, track machine, work machinery or similar cabins), by using manual tools, track maintenance machines and track inspection machines. However, inspection and observation with Track Inspection Machines allow measurements of several track parameters at track speed, without obstructing normal operations.

Track inspection machines should comply with the standard EN 13848-1 with respect to precision and with the standard EN13848-2 with respect to calibration. The scope of this standard is to specify the requirements for measuring systems mounted on machine or train whose purpose is to make measurements on the track. The specification of these requirements makes the measurement results provided by any measurement machine or train comparable with each other.

5.10.1 Purpose of track inspection machine

Track inspection machines are inspection and observation vehicles. Use these machines for the following purposes:

- Superstructure status check to provide foundation for maintenance planning,
- Analysis of the measured data,
- Testing of dynamic interaction between pantograph and overhead contact line,
- Testing of dynamic interaction between rail and wheel profile
- Acceptance tests for new superstructure,
- Video inspection of track surface.

Make sure that the following parameters are measured with the systems installed on the Track Inspection Machine:

1. Track geometry measurement: Track gauge, Cant, Levelling (at wavelength D1 and D2), Alignment (at wavelength D1 and D2), Twist.

2. Rail profile measurement: Rail profile, Rail wear, Rail profile loss.

3. Rail corrugation measurement: Short-, moderate-, long-wave corrugations.

4. Vehicle acceleration measurements: Vertical accelerations on the axle box, Horizontal acceleration on the bogie, Vertical and transverse accelerations on the vehicle.

5. Track surface measurement system: Fastenings with deficient or incorrect installation and their condition, Loose fastenings, Deficiencies of the ballast bed.

6. Track surface inspection system: Missing rail fasteners or their condition, Sleeper faults, Rail surface faults, Deficiencies of the ballast bed, Trackside signal systems.

7. Fishplate Control system: Missing fishplate bolts, Fishplate cracks.

8. Overhead contact line measurement and inspection: Inspection of contact wire position and wear, Contact wires and insulators.

9. Tunnel inspection systems: Tunnel gauge, Platform gauge, Comparison of the existing gauge and actual gauge on the track.

10. Video inspection (overview video from the perspective of a locomotive driver): Track, Signal visibility, Vegetation check.

11. GPS Positioning

5.10.2 Measuring equipment

Perform operation, maintenance and calibration works of the Measuring Machine according to the manufacturer's manuals.

Specification and precision of the measuring systems must meet the requirements specified in Section 1 in EN 13848.

Figure 5.5: Line geometry measuring system on the track inspection machine.

5.10.3 Calibration requirements

Calibrate the measuring devices to ensure the continued accuracy of measurements.

If any one of the following occurs, check the calibration:

a) after the measuring equipment has been installed in the vehicle;

b) after changes (new or maintained state) to the software or hardware systems or to the measuring equipment or to the vehicle which may affect the track geometry recording system;

c) After periodic maintenance and repair works of the machine or line geometry recording systems.

Validation by field tests requirements

In addition to a static verification of the accuracy of the track geometry recording system, a method based on comparison between different measurements of the same section (repeatability and reproducibility) shall be used to assess a measuring system.

5.10.4 Measurement requirements

Measurements made with the Track Inspection Machine shall be subject to repeatability and reproducibility tests as described in EN 13848-2. As a result, values obtained shall be consistent irrespective of the measuring speed and direction of travel, and shall be precise as required.

The track geometry recording system shall meet the requirements of EN 13848-1.

5.10.5 Track geometry measurement

This is used to determine the actual geometrical parameters of the track.

Minimum measuring speed:

- 10 km/h for D1 Wave Band.
- 30 km/h for D2 Wave Band.
- 40 km/h for D3 Wave Band.
- 5 km/h for track gauge and cant parameters.

Maximum measuring speed

- Roger 800: 120 km/h for all parameters (or maximum measuring speeds of measurement machines).
- Piri Reis Measurement Train: 275 km/h for all parameters (or maximum measuring speeds of the measurement train).

5.10.6 Rail profile measurement

This is used for determination and evaluation of the rail profile and rail wear.

Minimum measuring speed: 5 km/h for all parameters.

Maximum measuring speed

Roger 800: 120 km/h for all parameters (or maximum measuring speeds of measurement machines),

Piri Reis Measurement Train: 275 km/h for all parameters (or maximum measuring speeds of the measurement train).

By means of the analysis software, it compares the worn profile to the original, allowing the maintenance team to detect areas with problem.

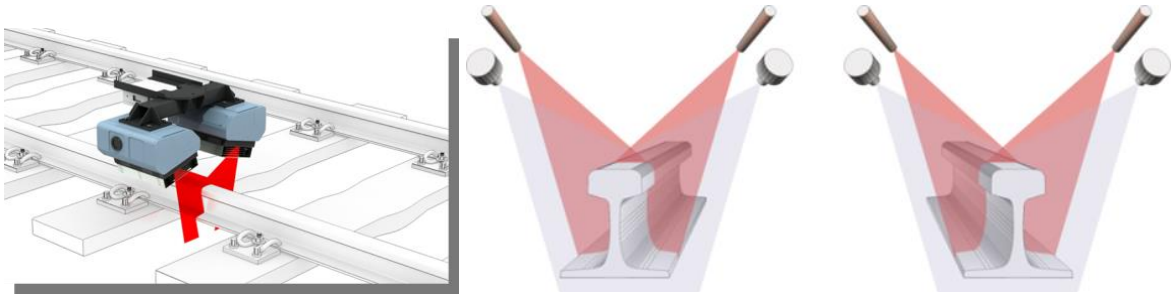

Figure 5.6: Rail profile measurement system.

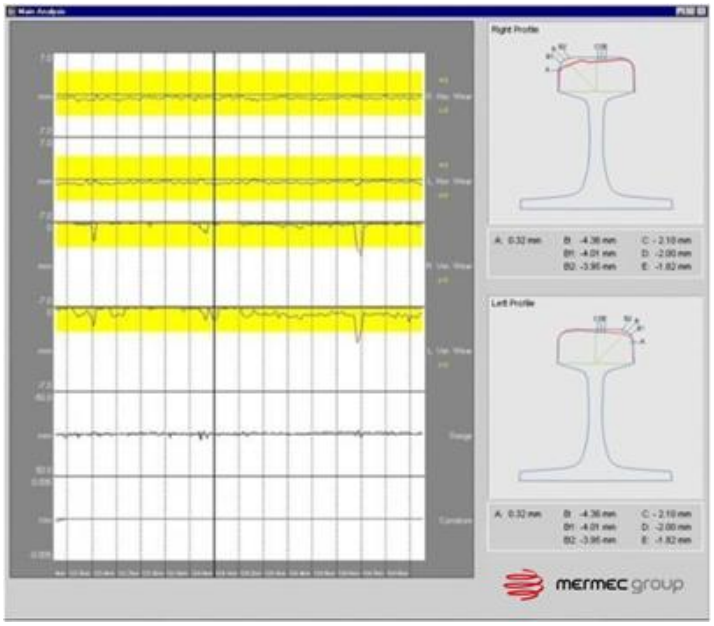

Figure 5.6: Rail profile measurement interface.

Rail corrugation measurement

This is the system used for measurement of rail corrugation.

Minimum measuring speed:

- 60 km/h for all parameters,

Maximum measuring speed

- Roger 800: 120 km/h for all parameters (or maximum measuring speeds of measurement machines),

- Piri Reis Measurement Train: 275 km/h for all parameters (or maximum measuring speeds of the measurement train).

Rail Grinding Machines

Rail grinding machines enable re-profiling of the rail head by means of circular grinding stones, on one rail or two rails at a time, on railway lines, switches and crossings. Defects such as corrugation, burrs, welding residues, etc. on rails shall be eliminated to ensure that the track complies with the tolerances specified in EN 13231-3.

The machine is capable of grinding the entire top surface of the rail head, i.e. from 70 degrees on the inner lateral surface to 5 degrees on the outer lateral surface.

Figure 5.7: Rail grinding machine.

Make a prior planning for the mechanized works.

Check the following conditions are ensured for the machine and line prior to the commencement of works with machines:

- At least three licensed operators on the machine;
- Transverse and longitudinal profile measurements on the track before the inspection,
- Choosing the appropriate grinding profile based on the measurement results,
- Necessary safety precautions prior to grinding and a full cooling water tank and good operating condition of fire water pump,

Record the works conducted with machine and save in the model 1529 and KKY/AVYS module.

(Recording process is carried out by the Track Maintenance and Repair Foreman, Track Maintenance and Repair Officer, Track Surveyor or Chief of Track Maintenance and Repair that superintends the work)

5.10.7 Roger800 principle

The amplitude of RMS of signal is evaluated for different wavelengths and all wave lengths

Defined wave length: 20-1000mm

Amplitude <0.2mm

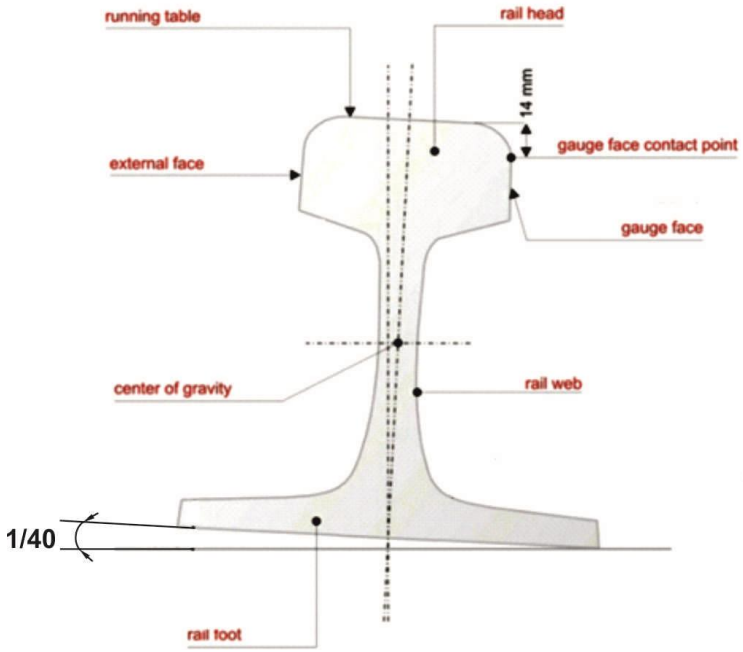

The measured parameters are the following:

- Filtered profile amplitude.
- The moving average of Root mean square value of amplitude.
- The moving average of the amplitude from crest to crest .

The principle of measurement consists of the filtered profile amplitude (1/13)- EN 13231-3

Filtered Profile: this is the profile which is gained by applying a new filter on main profile.

Main Profile: this is the profile before a filter.

Profile Filter: electronic device or signal processing that is used for differentiating long wave constituents from short wave constituents or differentiating constituents for special wave lengths.

Filtered Profile Amplitude (2 /13)- Main Profile

Sinusoids

$$x(t) = A\sin(\omega t + \phi)$$

$$\begin{aligned} A &= \text{peak amplitude (nonnegative)} \\ \omega &= \text{radian frequency (rad/sec)} \\ &= 2\pi f \ (f \text{ in Hz}) \\ t &= \text{time (sec)} \\ f &= \text{frequency (Hz)} \\ \phi &= \text{initial phase (radians)} \\ \omega t + \phi &= \text{instantaneous phase (radians)} \end{aligned}$$

For example:

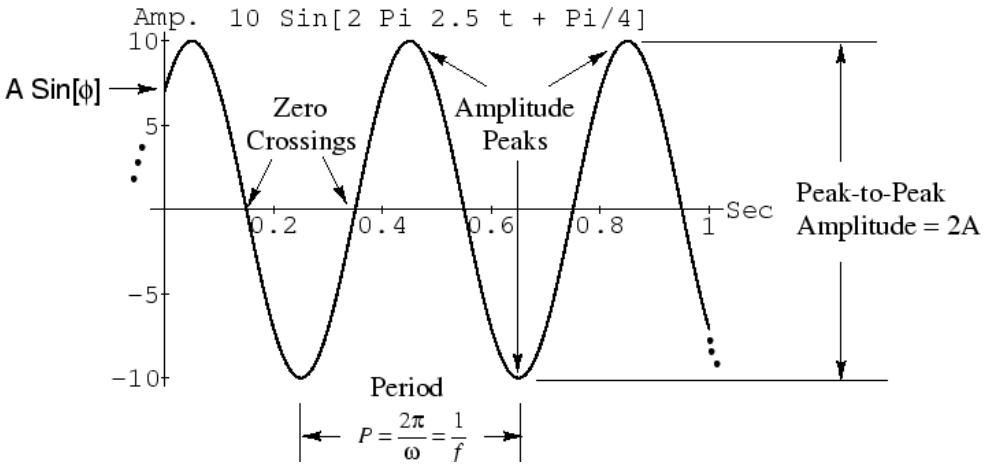

A=10, F=2.5, Φ= pi/4**,** t ∈[0,1].

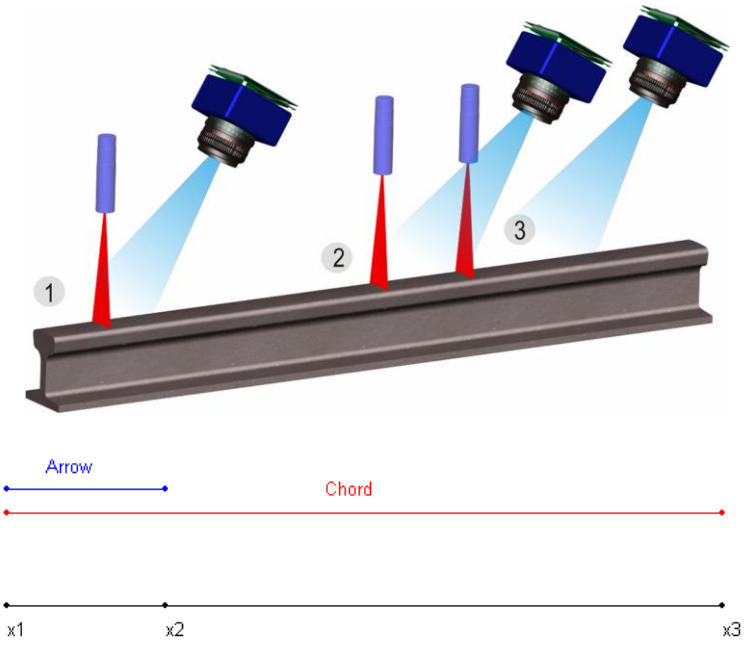

Figure 5.7: 3 Point Measurement (Inverse Sinus) System.

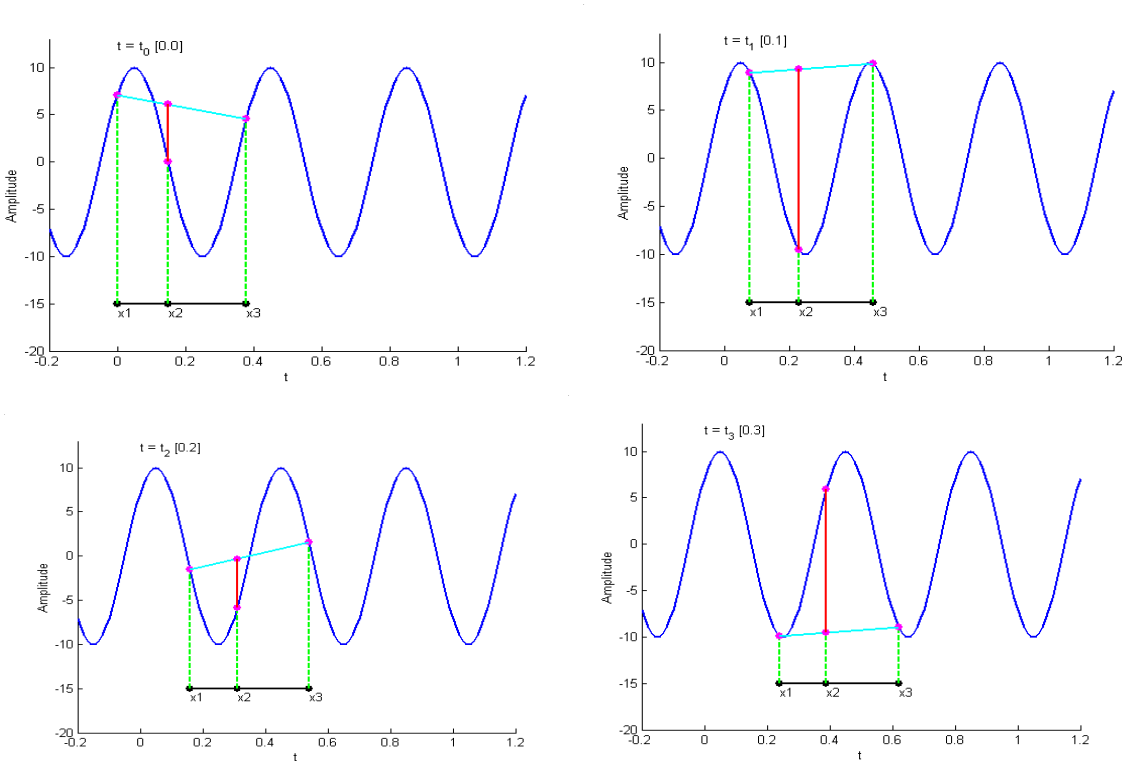

Figure 5.8: Example of measurement with 3 Point Measurement (Inverse Sinus) System.

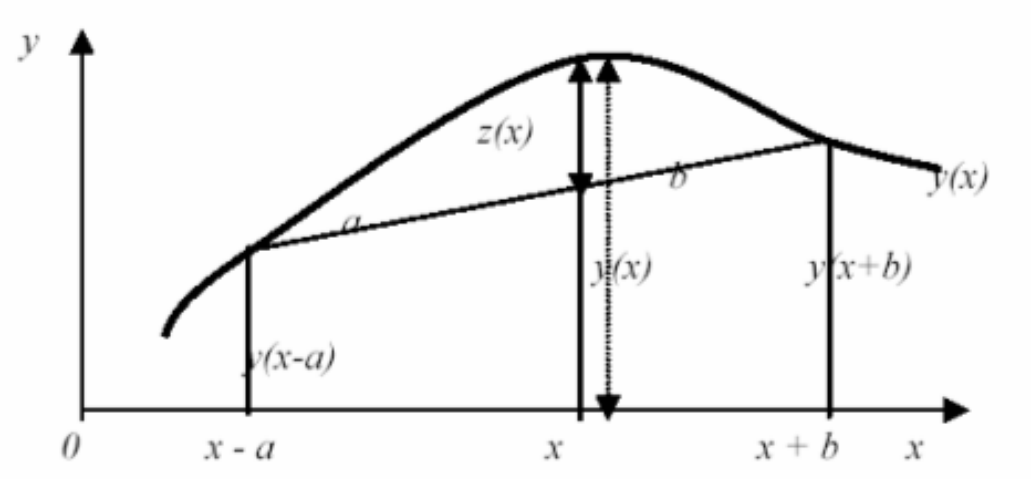

Figure 5.9: Inverse Sınus Transfer Function.

The formula used for estimating the inverse sinus transfer function are the following:

$$z(x) = y(x) - \left[\frac{b}{a+b} y(x+a) + \frac{a}{a+b} y(x+b) \right]$$

$$Z\left(j\frac{2\pi}{\lambda} \right) = Y\left(j\frac{2\pi}{\lambda} \right) \left[1 - \frac{b}{a+b} e^{-j\frac{2\pi a}{\lambda}} - \frac{a}{a+b} e^{-j\frac{2\pi b}{\lambda}} \right]$$

For passing from time zone to frequency zone, Fast Fourier Transformation is used. Inverse Transfer Function of Inverse Sınus Function on 3 point asymmetric beam is as follows

$$H^{-1}\left(j\frac{2\pi}{\lambda} \right) = 1 - \frac{b}{a+b} e^{-j\frac{2\pi a}{\lambda}} - \frac{a}{a+b} e^{-j\frac{2\pi b}{\lambda}}$$

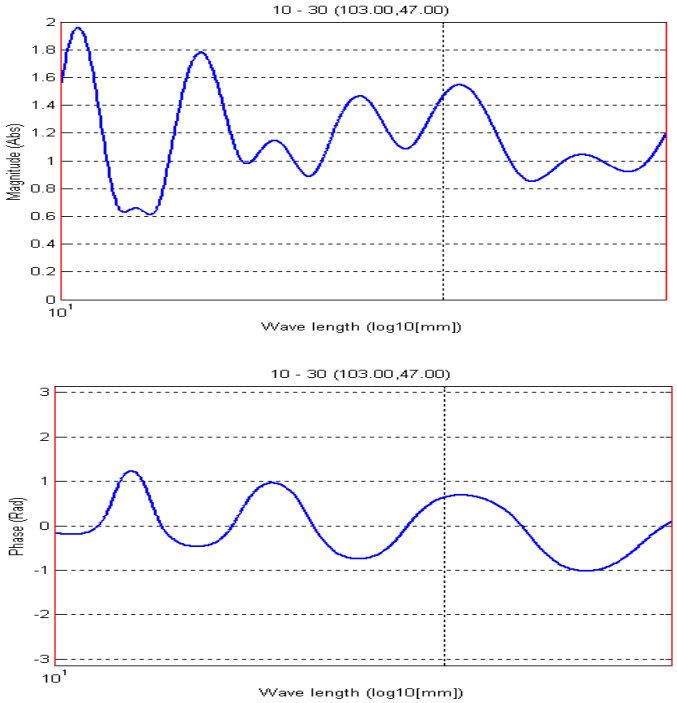

Figure 5.10: Transfer Function 10-30 mm.

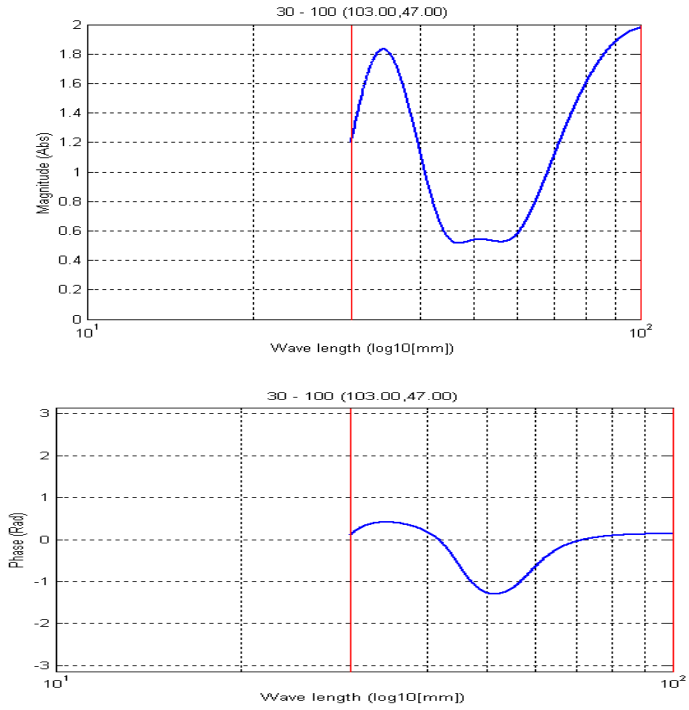

Figure 5.11: Transfer Function 30-100 mm.

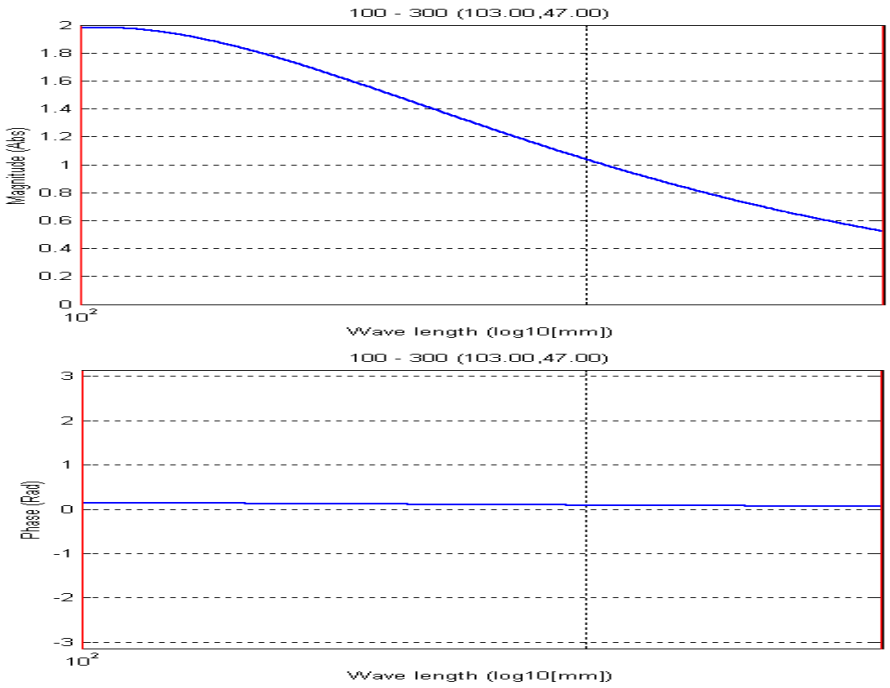

Figure 5.12: Transfer Function 100-300 mm.

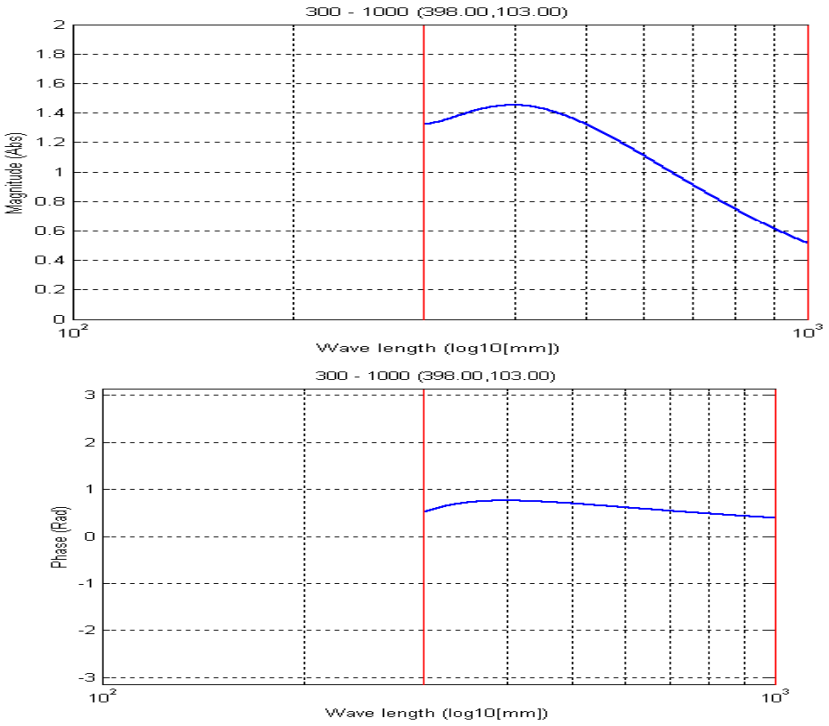

Figure 5.13: Transfer Function 300-1000 mm.

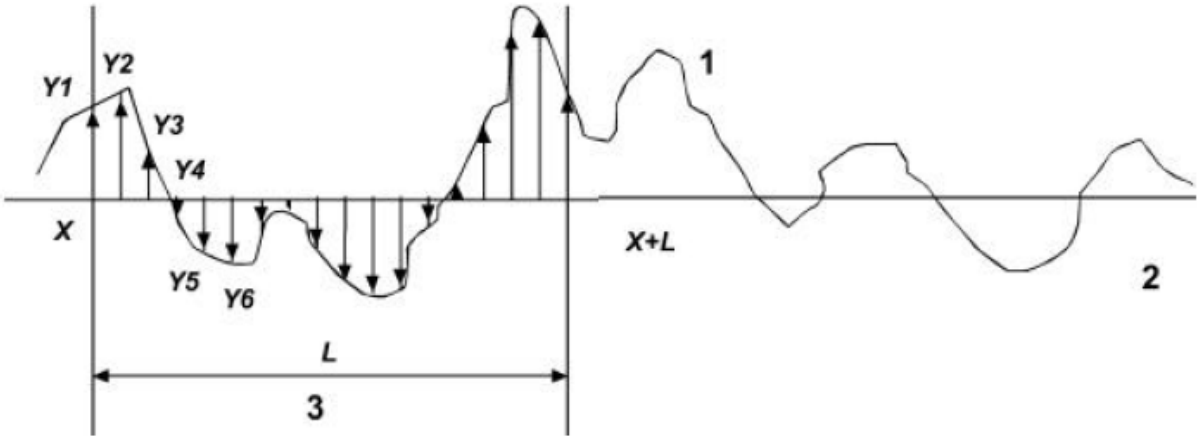

Figure 5.14: Moving average of root mean square amplitude.

Root mean square (RMS) amplitude of a profile is calculated as semi-perminent function of road distance. Average is calculated a profile section which is inside a distance , distance function is calculated increasingly on sampling intervals. The moving average of RMS of y(x) inside the distance L, is given by:

$$RMS(x,L)=\left(\frac{1}{L}\int_{x}^{x+L} y^2(x)\,dx\right)^{1/2}$$

If y(x), y(x+Δx), y(x+2Δx) etc. uses digitized description, RMS amplitude of digitized profiles:

$$RMS(x,L)=\left(\frac{1}{n-1}\sum_{i=1}^{n} y_i^{\,2}\right)^{1/2}$$

Distance *L* (EN13231-3 standard). Next the window lenghts:

Wavelength range (mm)	10 - 30	30 - 100	100 - 300	300 - 1 000
Window length (m)	0,15	0,5	1,5	5

Moving average of crest to crest is also estimated, given by:

$$PP(x,L)=(a1+a2+....+an)/n$$

Distance *L* length(EN13231-3 standard). Next the window lenghts:

Wavelength range (mm)	10 - 30	30 - 100	100 - 300	300 - 1 000
Window length (m)	0,15	0,5	1,5	5

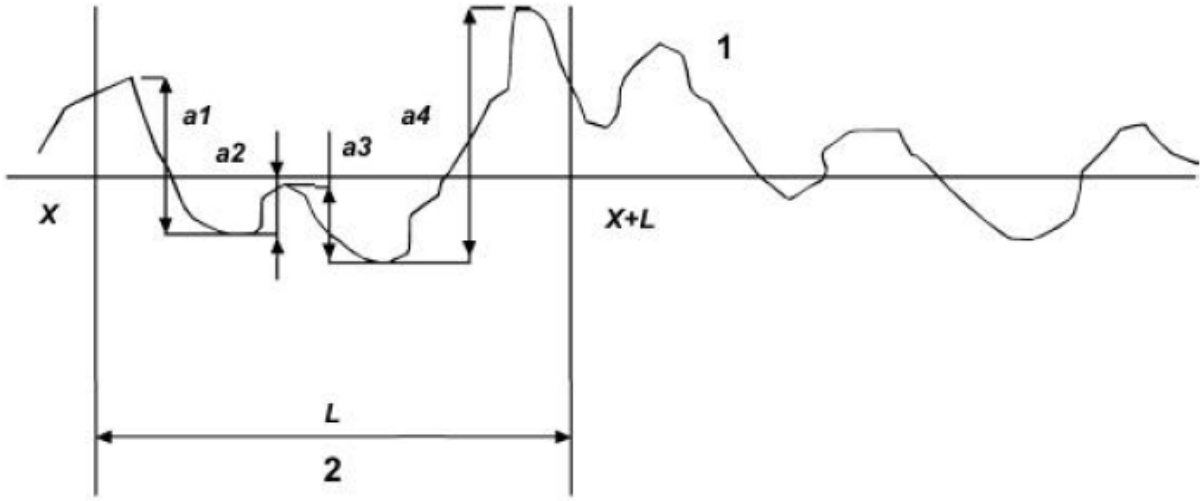

Figure 5.15: The moving average of a length L from crest to crest.

Next, some examples of the rail corrugation measurement system:

Data collection for 10 mm sampling interval.

Filtering for different bands [30-100]mm, [100-300]mm, [300-1000]mm.

Calculation of parameters.

Review of graphics.

Storing and printing of all data and reports .

Starting and stopping data collection.

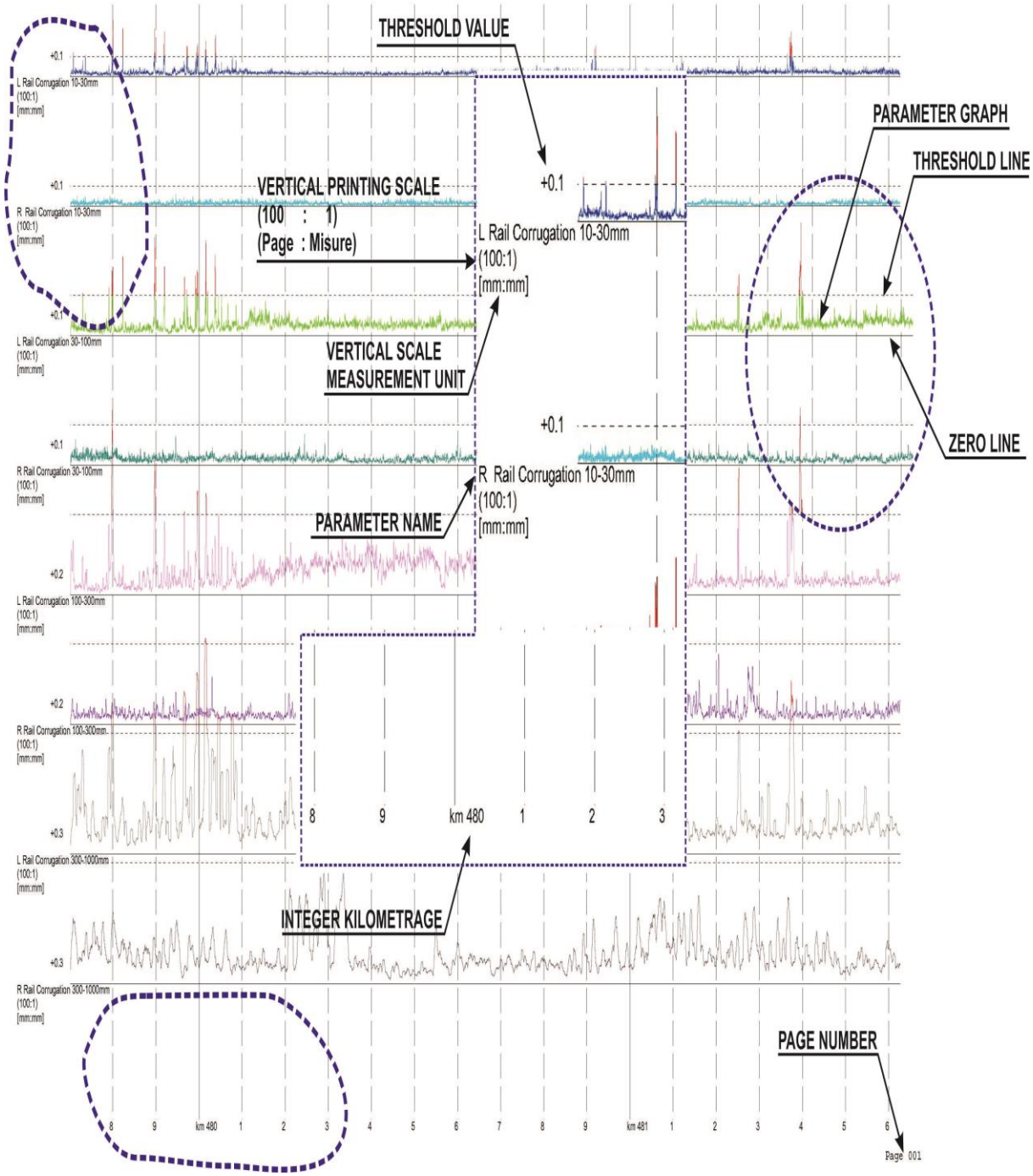

Figure 5.16: Example of the data.

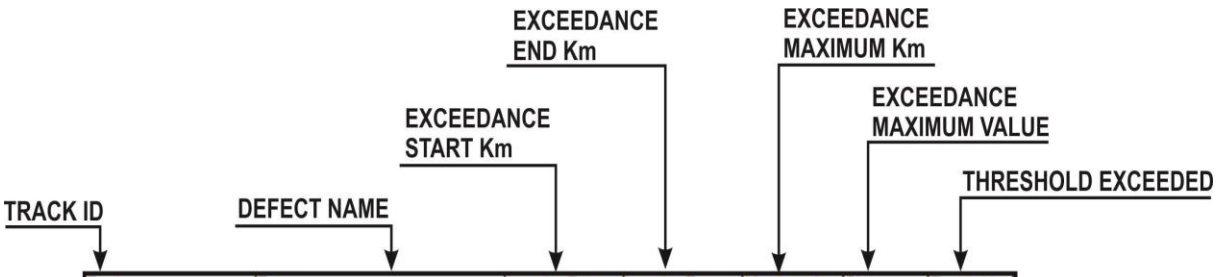

Track	Type	Location From	Location To	Max Location	Size	Threshold
*	*	*[Km]	*[Km]	[Km]	[um]	[um]
Skopje - Gevgelija						
Skopje - Gevgelija	RMS.Right Filtered Profile 100-300	482,1995	482,2035	482,2017	248	240
Skopje - Gevgelija	RMS.Right Filtered Profile 100-300	482,2145	482,219	482,2157	272	240
Skopje - Gevgelija	RMS.Right Filtered Profile 100-300	482,2312	482,2352	482,2335	212	200
Skopje - Gevgelija	RMS.Right Filtered Profile 100-300	482,2527	482,2572	482,2567	223	200
Skopje - Gevgelija	RMS.Right Filtered Profile 300-1000	483,2902	483,3025	483,2985	350	300
Skopje - Gevgelija	RMS.Right Filtered Profile 30-100	488,662	488,6637	488,6627	122	120
Skopje - Gevgelija	RMS.Right Filtered Profile 300-1000	490,7172	490,7462	490,7217	437	400
Skopje - Gevgelija	RMS.Right Filtered Profile 300-1000	494,7992	494,8175	494,8085	483	400
Skopje - Gevgelija	RMS.Right Filtered Profile 30-100	497,2387	497,2405	497,2402	142	120
Skopje - Gevgelija	RMS.Right Filtered Profile 10-30	497,239	497,2422	497,2407	72	60
Skopje - Gevgelija	RMS.Left Filtered Profile 10-30	499,7652	499,767	499,7667	92	60
Skopje - Gevgelija	RMS.Right Filtered Profile 30-100	499,8897	499,8917	499,8905	275	120
Skopje - Gevgelija	RMS.Right Filtered Profile 300-1000	499,91	499,9247	499,9142	382	300
Skopje - Gevgelija	RMS.Left Filtered Profile 30-100	500,5711	500,5728	500,5723	244	120
Skopje - Gevgelija	RMS.Left Filtered Profile 300-1000	500,6641	500,6976	500,6901	535	400
Skopje - Gevgelija	RMS.Right Filtered Profile 300-1000	500,8002	500,8135	500,809	347	300
Skopje - Gevgelija	RMS.Right Filtered Profile 30-100	500,8062	500,809	500,8067	193	120
Skopje - Gevgelija	RMS.Left Filtered Profile 300-1000	502,0446	502,0553	502,0491	430	400
Skopje - Gevgelija	RMS.Left Filtered Profile 30-100	502,0466	502,0493	502,0488	279	120
Skopje - Gevgelija	RMS.Left Filtered Profile 100-300	502,0506	502,0548	502,0516	238	200
Skopje - Gevgelija	RMS.Right Filtered Profile 300-1000	502,4027	502,419	502,4072	523	400
Skopje - Gevgelija	RMS.Right Filtered Profile 100-300	502,404	502,413	502,4095	504	240
Skopje - Gevgelija	RMS.Right Filtered Profile 30-100	502,4082	502,4122	502,4117	256	120
Skopje - Gevgelija	RMS.Left Filtered Profile 300-1000	502,4576	502,4731	502,4621	443	400
Skopje - Gevgelija	RMS.Left Filtered Profile 100-300	502,4591	502,4631	502,4603	415	240
Skopje - Gevgelija	RMS.Left Filtered Profile 10-30	502,4671	502,4688	502,4681	79	60
Skopje - Gevgelija	RMS.Right Filtered Profile 100-300	503,6002	503,604	503,6012	247	240
Skopje - Gevgelija	RMS.Right Filtered Profile 100-300	503,6205	503,6257	503,6217	243	240
Skopje - Gevgelija	RMS.Right Filtered Profile 100-300	503,6562	503,662	503,6575	273	240
Skopje - Gevgelija	RMS.Right Filtered Profile 100-300	503,6902	503,6945	503,6922	223	200
Skopje - Gevgelija	RMS.Right Filtered Profile 100-300	503,7262	503,7505	503,7387	245	240
Skopje - Gevgelija	RMS.Right Filtered Profile 100-300	503,7815	503,7877	503,7852	250	240
Skopje - Gevgelija	RMS.Right Filtered Profile 100-300	503,7972	503,8127	503,81	513	240
Skopje - Gevgelija	RMS.Right Filtered Profile 30-100	503,8082	503,811	503,8085	235	120
Skopje - Gevgelija	RMS.Right Filtered Profile 100-300	503,8225	503,8522	503,851	282	240
Skopje - Gevgelija	RMS.Left Filtered Profile 300-1000	503,8623	503,8743	503,8703	492	400
Skopje - Gevgelija	RMS.Right Filtered Profile 100-300	503,8945	503,9517	503,9347	339	240
Skopje - Gevgelija	RMS.Right Filtered Profile 100-300	503,9717	503,9997	503,977	296	240
Skopje - Gevgelija	RMS.Right Filtered Profile 100-300	504,034	504,0377	504,035	227	200

Figure 5.17: Example of the report.

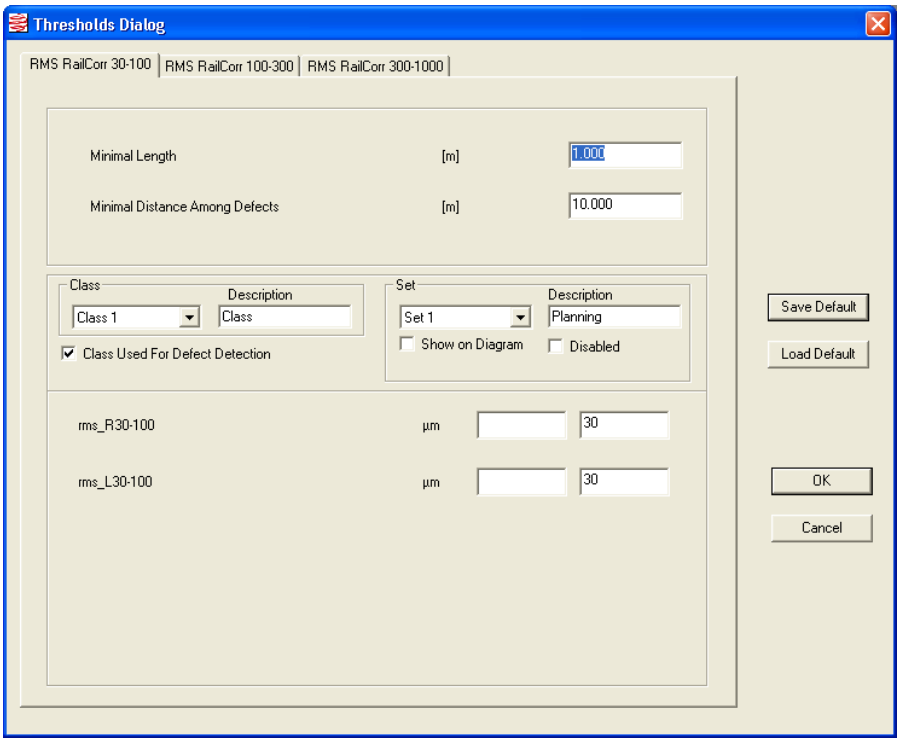

Figure 5.18: Example of the interface, threshold dialog box.

6 Assessment of corrugation in Slovenia (SZ)

The dynamic force, which occurs between the wave corrugation on the tread of the rail and the wheels, causes serious stress both for the vehicle and the track. For the planning of rail treatment works (grinding, whetting, planning) needed for the elimination of them, it is indispensable to survey the corrugation extent.

In Slovenia, we are measuring the corrugation with measuring car MAV "AB25-SDS-AB35" (MAV Central Rail Inspection). Beside rail corrugation we are at the same time measuring ultrasonic measurements of the rails and the rail profile (rail wear). On the map are presented the location where the corrugation was found on the main lines in 2016.

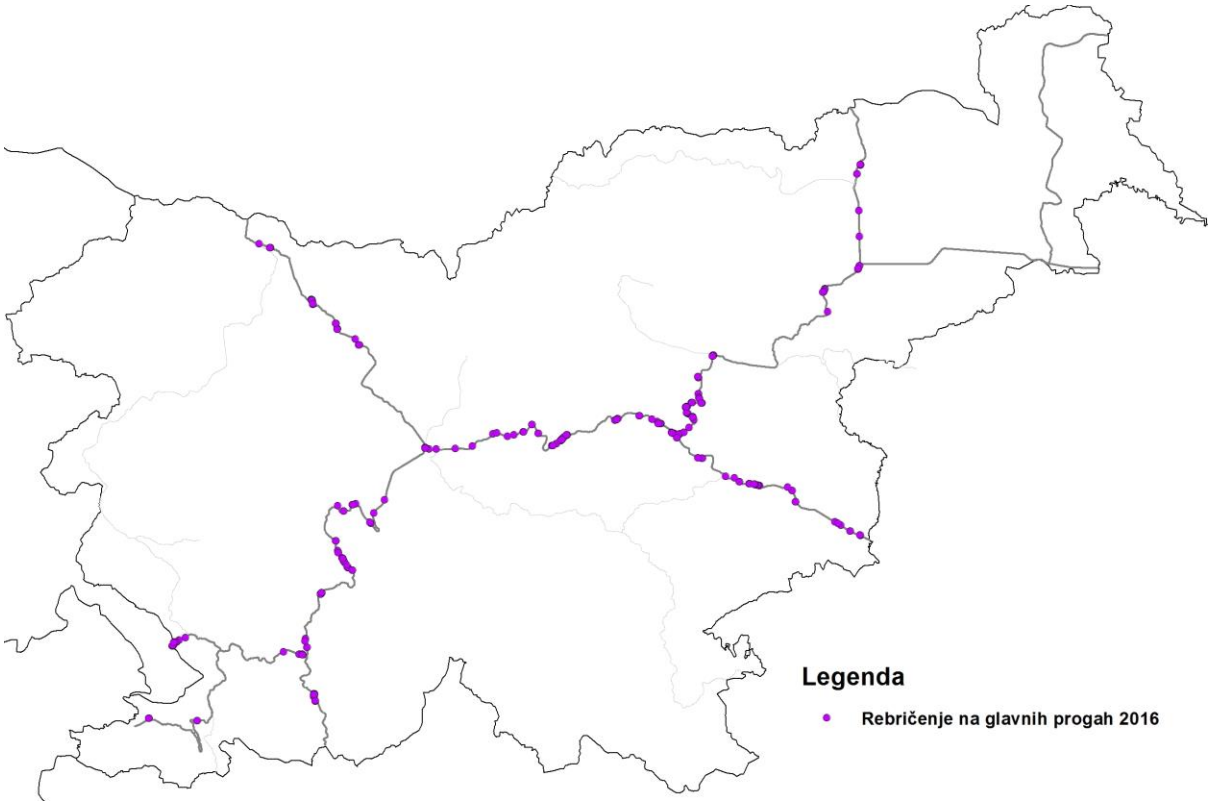

Figure 6.1: Karta-rebricenje_2016 – Rail corrugations map 2016

Thematic map of rail corrugation shows local poor places (locations), where the corrugation of rails is greater than the tolerance (violet points).

There are many methods for measuring the corrugation.

In the case of direct method, the sensor measures the distance from the rail surface, which means the depth of the corrugation. The sensor moves along a straight line and samples point by point according to 2 mm distance signals.

On the MÁV Central Rail and Track Inspection Ltd's Rail Diagnostic Train (SDS) there are two contactless inductive sensors (one for each rail) to measure the size of the corrugation.

For the characterisation of rail corrugation, the amplitude (A) and the wavelength is specified for each evaluation phase.

The evaluation can be done in various wavelength ranges. In the current system the 30-300 mm range is divided for a 30-100mm and a 100-300mm sub-range for the evaluation. We use 60dB/decade convolution filters with brake points according to the sub-ranges. The filters remove the slow-varying signal components, so the result signal's average, (the base line) is equal to 0.

The size of the evaluation phase is one meter for the 100-300mm, and 50cm for the 30-100mm range.

There are two current methods for calculating the amplitude values corresponding to an evaluation phase.

- The first is the peak to peak method, which calculates the mean value of the difference of adjacent „hills" and „valleys".
- The second is the energy-related RMS value, which calculates the root mean square of the samples in the evaluation phase.

To evaluate the measurement result we determine the RMS amplitude.

Determination of the typical wavelength is done by using an auto correction function. This function shows, how a series of signals similar to itself shifted with a given number of samples.

The program's aim is to display the results of the evaluated wave corrugation, and to list the rail faults exceeding a given dimension range.

6.1 Data of corrugation in Slovenia

Measurement of corrugation of rails on main lines on the network of public railway infrastructure in Slovenia is carried out in autumn. Measuring train (MAV-SDS-AB25 AB35) calculates the following parameters:

- size of corrugation,
- the wavelength of corrugation.

Measuring train MAV AB25-SDS-AB35 [6.2] is shown on two pictures below.

Figure 6.2: Measuring train MAV AB25-SDS-AB35

https://www.google.si/search?q=MAV+AB25-SDS-AB35&biw=1837&bih=974&source=lnms&tbm=isch&sa=X&ved=0ahUKEwj4mvb8yOnRAhUCPRQKHRKdB44Q_AUIBygC#imgrc=Y794v3m80SCynM%

Figure 6.3: Measuring train MAV AB25-SDS-AB35

https://www.google.si/search?q=MAV+AB25-SDS-AB35&biw=1837&bih=974&source=lnms&tbm=isch&sa=X&ved=0ahUKEwj4mvb8yOnRAhUCPRQKHRKdB44Q_AUIBygC#imgrc=RxF3tiBEJuc3BM%3A

The measurement results are shown in the following forms:

- diagrams of rail corrugation with the permissible limits;
- thematic map of exceeding the limits of permissible size of rail corrugation;
- a list of local poor places where excessive rail corrugation on tracks (fault list).

On the diagram of rail corrugation the following parameters and limits are marked:

- size of corrugation in the wavelength range from 30 to 100 mm,
- size of corrugation for a wavelength of 100 to 300 mm,
- the wavelength of corrugation.

In Slovenia there are no regulations for permissible size of corrugation. To determine the local poor places on the track are used tolerances which are in use on the Hungarian rail network MAV. Tolerances are established for the two speed grade.

Table 6.1: Speed ≥ 120km/h.

RMS amplitude	30-100 mm wavelength µm	100-300 mm wavelength µm
A (new construction)	15	15
B (maintenance)	25	25
C (intervention)	50	50

Table 6.2: Speed < 120km/h.

RMS amplitude	30-100 mm wave lenght µm	100-300 mm wave lenght µm
A (new construction)	25	25
B (maintenance)	50	50
C (intervention)	100	100

6.1.1 Diagrams of rail corrugation

After starting the program, the measurement to be displayed is selected. After the program loading three diagrams are displayed. They show the RMS amplitude for the 30-100mm sub-range (up), for the 100-300mm sub-range (in the middle), and the typical wavelength (down). Each diagram shows two curves. A red one is for the left rail and a green one for the right rail (Left rail / Right rail).

On the next diagrams is shown the corrugation for some lines in Slovenia. Along the diagram is below the km position of the track. The diagram above is representing the corrugation value (RMS amplitude 30-100 mm (micro-m) for the left and right rail). The second diagram is representing the corrugation value (RMS amplitude 100-300 mm (micro-m) for the left and right rail). The third diagram is representing the basic curve elements of the actual line. Further is shown the maintenance work with the comment (black line and the year when the section was grinded). The lower diagram is representing the wavelength (mm).

The following diagrams are the results of measurements of rail corrugation in the last three years on the NeTIRail case study lines: Divača-cepišče (junction) Prešnica-Koper, Pivka-Ilirska Bistrica. Two case study lines are main Slovenian lines where corrugation is measured. On the route Ljubljana-Kamnik corrugation is not measured. The total length of the local poor places excessive corrugation in 2016 has decreased in comparison with year 2015. Data are presented in reports on measurements of corrugation for the years 2014, 2015, 2016 [6.1].

60E Divača – cepišče (junction) Prešnica / single line

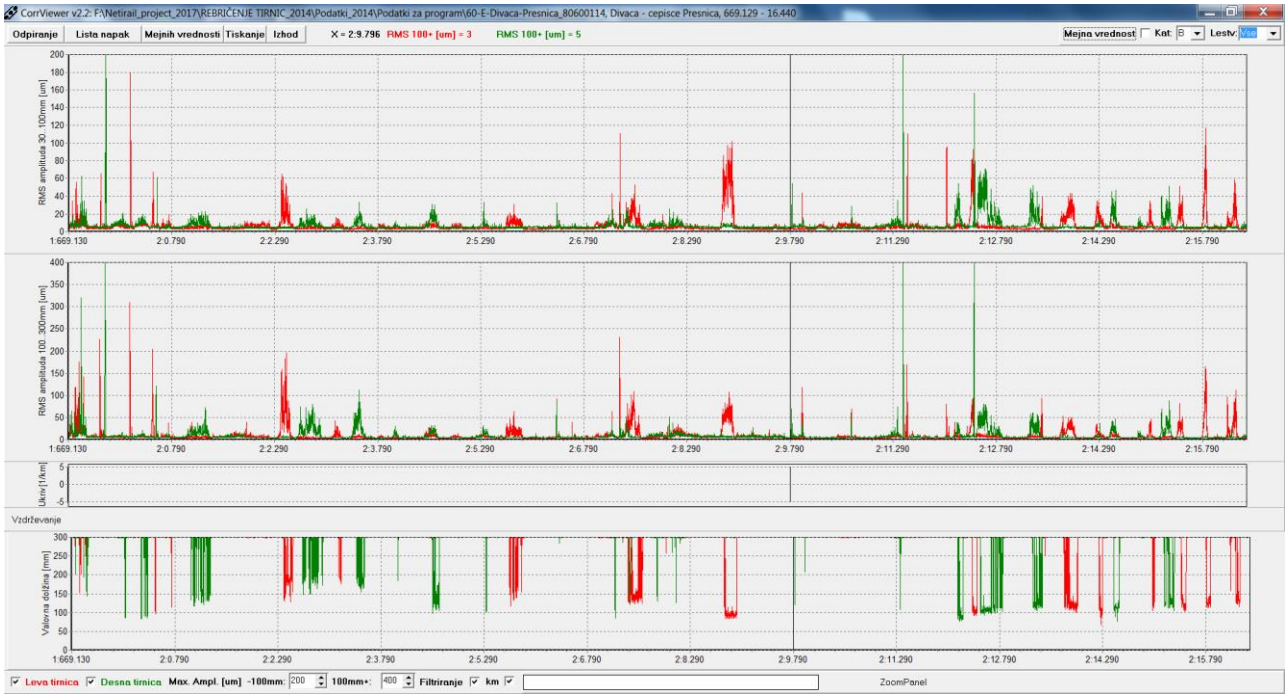

Figure 6.4: Corrugation diagram for line 60E Divača-cepišče Prešnica in 2014.

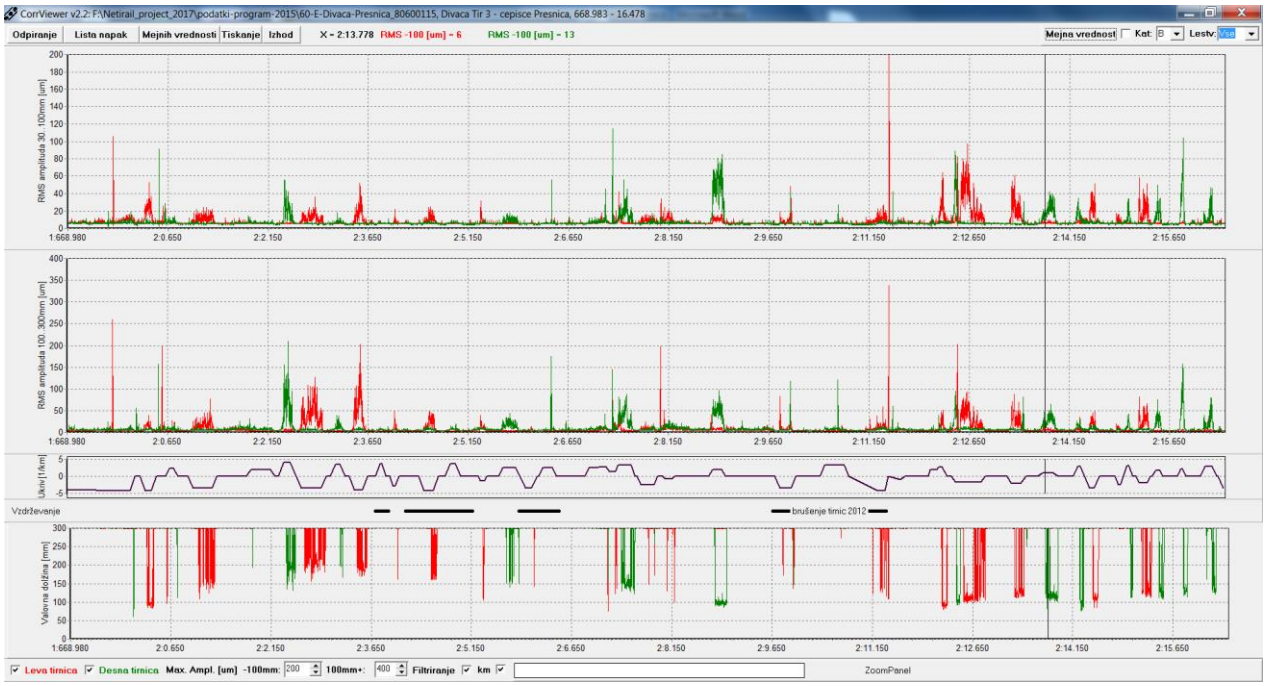

Figure 6.5: Corrugation diagram for line 60E Divača-cepišče Prešnica in 2015.

No data recorded for line 60E Divača-cepišče Prešnica in 2016.

62E cepišče (junction) Prešnica – Koper / single line

Figure 6.6: Corrugation diagram for line 62E cepišče Prešnica-Koper in 2014.

Figure 6.7: Corrugation diagram for line 62E cepišče Prešnica-Koper in 2015.

Figure 6.8: Corrugation diagram for line 62E cepišče Prešnica-Koper in 2016.

64E Pivka – Ilirska Bistrica – d.m. (state border) / single line

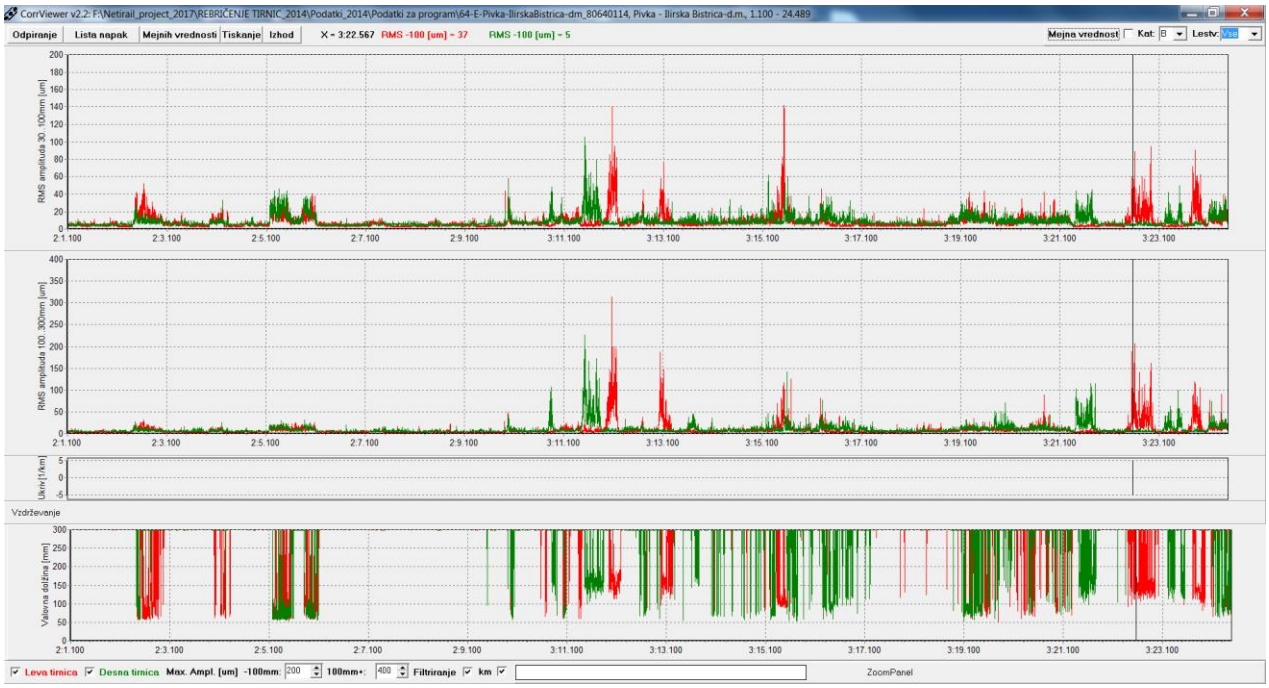

Figure 6.9: Corrugation diagram for line 64E Pivka-Ilirska Bistrica in 2014.

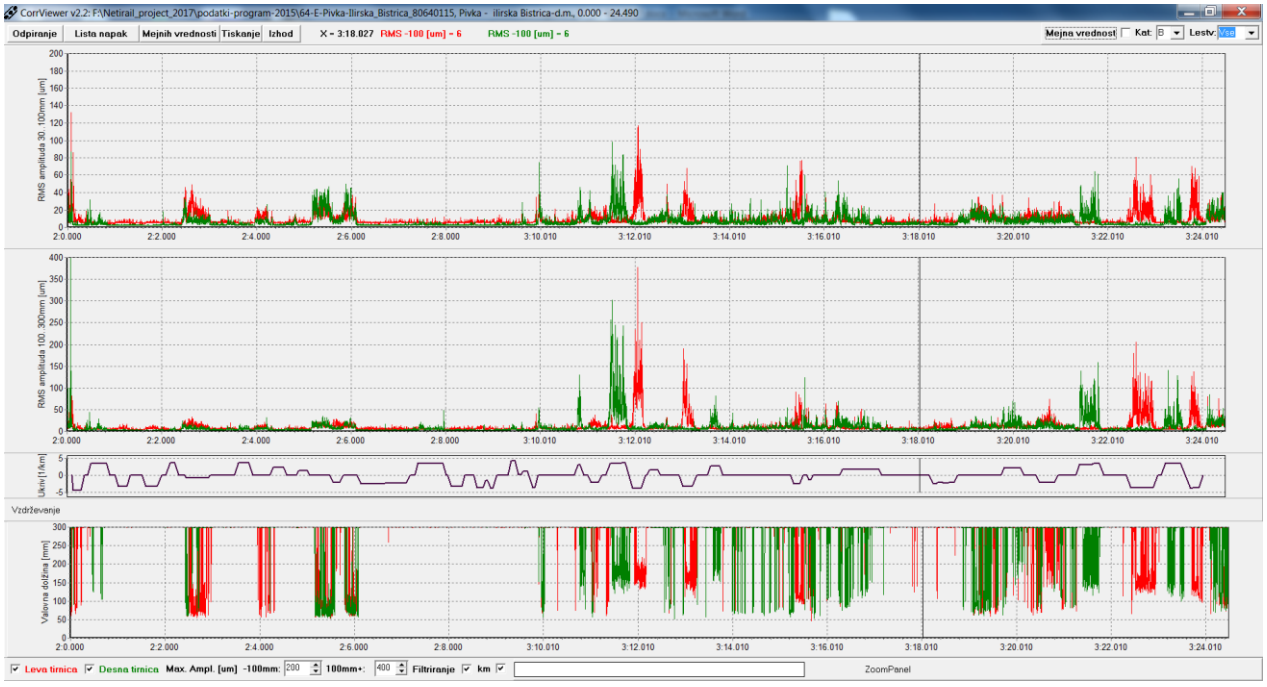

Figure 6.10: Corrugation diagram for line 64E Pivka-Ilirska Bistrica in 2015.

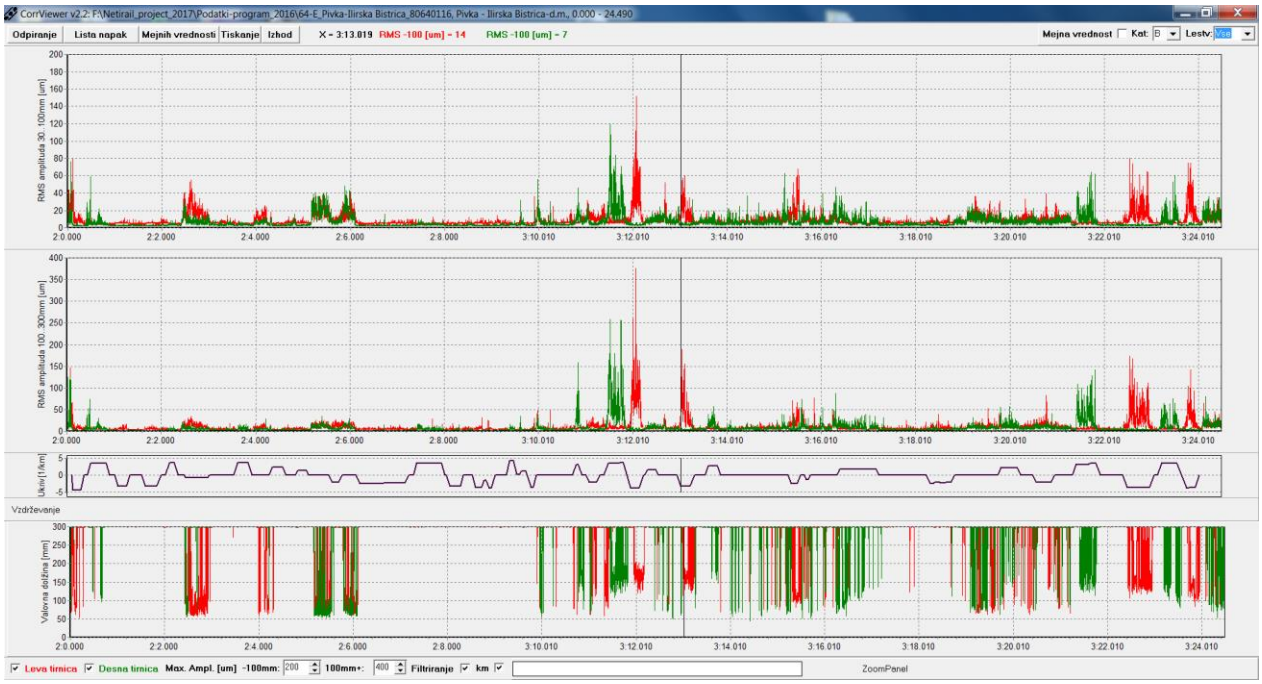

Figure 6.11: Corrugation diagram for line 64E Pivka-Ilirska Bistrica in 2016.

6.1.2 Corrugation fault list

The fault list consists of the zones which exceed the size limit for the rails. The size limit is given by the selected category, and the actual maximal speed for the track. The category can be selected at the upper right corner. The loaded measurement contains the actual maximal speed for the track. If it is not available then 120km/h is set for the entire line.

Fault list can be made from filtered, or non-filtered measurement, depending on the state of the „filter" (szűrés) switch.

The completed list is saved into the parent folder, from which the measurement has been opened. The program loads the fault list into Excel file if it is needed.

The columns of the fault list contain next attributes:

1. Rail (left or right)
2. Fault beginning, zone
3. Fault beginning, section (from km)
4. Fault ending, zone
5. Fault ending, section (to km)
6. The biggest amplitude place, zone
7. The biggest amplitude place, section (max. profile km)
8. Value of the biggest amplitude in 0.01mm
9. Wavelength at the biggest amplitude in mm
10. Wavelength area in mm

The following table contains local poor places with failures (faults) of excessive rail corrugation on tracks on Slovenian case study lines in last three years (2014-2016).

Table 6.3: Fault list of corrugation on main rail lines 60, 62 and 64 in 2014, 2015 and 2016.

Line no.	1	2	3	4	5	6	7	8	9	10
2014										
60	L	2	2387	2	2397	2	2394	15,8	170	100-300mm
60	L	2	2412	2	2418	2	2412	12,2	187	100-300mm
60	L	2	2440	2	2451	2	2446	18,2	181	100-300mm
60	L	2	2456	2	2463	2	2460	19,6	191	100-300mm
60	L	2	15833	2	15852	2	15836	16,4	141	100-300mm
60	L	1	669588	1	669594	1	669588	22,7	400	100-300mm
60	D	1	669662	1	669668	1	669664	34,1	299	30-100mm
60	D	1	669662	1	669668	1	669665	53,4	400	100-300mm
62	L	1	5981	1	5989	1	5985	33,6	185	100-300mm
62	D	2	14533	2	14542	2	14539	15,1	299	30-100mm
62	D	2	14486	2	14558	2	14539	53	183	100-300mm
62	D	2	14569	2	14583	2	14577	41	194	100-300mm
62	D	2	14589	2	14607	2	14597	41,6	196	100-300mm
62	L	2	14853	2	14906	2	14901	30,7	208	100-300mm
62	L	2	14923	2	14971	2	14950	36,9	193	100-300mm
62	L	2	14995	2	15007	2	15004	22,6	202	100-300mm
62	L	2	15011	2	15029	2	15019	25,8	210	100-300mm
62	L	2	17523	2	17536	2	17528	13,5	299	30-100mm
62	L	2	17541	2	17559	2	17552	15	299	30-100mm
62	L	2	17516	2	17567	2	17555	91,5	217	100-300mm
62	L	2	17573	2	17705	2	17609	85,6	227	100-300mm
62	L	2	17582	2	17612	2	17611	14,7	299	30-100mm
62	L	2	17623	2	17630	2	17626	13,1	299	30-100mm
62	L	2	17635	2	17643	2	17641	13	299	30-100mm
62	L	2	17712	2	17762	2	17738	52,9	217	100-300mm
62	D	2	18039	2	18060	2	18052	17,7	299	30-100mm
62	D	2	18010	2	18167	2	18052	106,6	219	100-300mm
62	D	2	18067	2	18079	2	18075	13,6	299	30-100mm
62	D	2	18085	2	18092	2	18087	10,8	299	30-100mm
62	L	2	18505	2	18524	2	18514	15,4	299	30-100mm
62	L	2	18420	2	18602	2	18518	89,2	229	100-300mm
62	L	2	18556	2	18562	2	18556	12,8	299	30-100mm

Line no.	1	2	3	4	5	6	7	8	9	10
62	L	2	18876	2	18999	2	18921	36,1	210	100-300mm
62	D	2	19261	2	19281	2	19265	24,5	221	100-300mm
62	D	2	19313	2	19321	2	19316	14,1	149	100-300mm
62	D	2	30936	2	30942	2	30940	30,4	400	100-300mm
62	D	2	31046	2	31057	2	31052	27,2	400	100-300mm
64	D	3	11510	3	11538	3	11525	22,7	139	100-300mm
64	D	3	11748	3	11755	3	11751	14,1	170	100-300mm
64	L	3	12066	3	12080	3	12075	31,4	166	100-300mm
64	L	3	12105	3	12117	3	12117	20	156	100-300mm
64	L	3	12133	3	12139	3	12139	13,8	219	100-300mm
64	L	3	12147	3	12166	3	12162	19,4	187	100-300mm
64	L	3	13104	3	13114	3	13110	14,7	151	100-300mm
64	D	3	21722	3	21729	3	21722	11,4	164	100-300mm
64	L	3	22600	3	22609	3	22605	20,7	156	100-300mm
2015										
60	L	2	2851	2	2858	2	2858	12,7	221	100-300mm
60	L	2	3525	2	3539	2	3529	20,2	193	100-300mm
60	L	2	3543	2	3549	2	3549	13,6	189	100-300mm
60	L	2	12467	2	12473	2	12470	20,3	400	100-300mm
60	D	2	2408	2	2418	2	2418	13,1	191	100-300mm
60	D	2	2441	2	2451	2	2448	21	191	100-300mm
60	D	2	15836	2	15853	2	15841	15,7	147	100-300mm
62	L	3	14927	3	14938	3	14934	12,2	299	30-100mm
62	L	3	14948	3	14961	3	14951	12,8	299	30-100mm
62	D	3	14503	3	14513	3	14504	14,1	299	30-100mm
62	D	3	14528	3	14548	3	14535	16,5	299	30-100mm
62	D	3	14570	3	14577	3	14577	14,4	299	30-100mm
62	L	3	14854	3	14907	3	14894	27,9	181	100-300mm
62	L	3	14912	3	14973	3	14952	52,8	202	100-300mm
62	L	3	14980	3	15009	3	14998	24,4	210	100-300mm
62	L	3	15013	3	15029	3	15026	37,2	189	100-300mm
62	D	2	8548	2	8568	2	8563	45,6	235	100-300mm
62	D	3	14485	3	14583	3	14542	69,7	196	100-300mm
62	D	3	14588	3	14604	3	14598	45,3	200	100-300mm
62	D	3	19259	3	19287	3	19270	41,4	235	100-300mm
62	D	3	19299	3	19309	3	19305	21,3	210	100-300mm
62	D	3	19313	3	19332	3	19318	25	187	100-300mm

Line no.	1	2	3	4	5	6	7	8	9	10
62	D	3	19342	3	19349	3	19349	11,9	175	100-300mm
64	L	3	11982	3	11988	3	11987	12,7	189	100-300mm
64	L	3	11997	3	12003	3	11999	13,7	170	100-300mm
64	L	3	12010	3	12025	3	12014	23,4	179	100-300mm
64	L	3	12031	3	12047	3	12042	20,7	175	100-300mm
64	L	3	12063	3	12083	3	12069	37,8	200	100-300mm
64	L	3	12090	3	12126	3	12113	21	162	100-300mm
64	L	3	12130	3	12137	3	12132	14,2	164	100-300mm
64	L	3	12142	3	12163	3	12148	25	193	100-300mm
64	L	3	13043	3	13050	3	13045	19	187	100-300mm
64	L	3	13098	3	13108	3	13105	15,5	164	100-300mm
64	L	3	22565	3	22575	3	22572	12,1	160	100-300mm
64	L	3	22603	3	22611	3	22608	20,5	168	100-300mm
64	L	3	22930	3	22938	3	22936	11,6	153	100-300mm
64	L	3	23818	3	23824	3	23821	13,7	154	100-300mm
64	D	3	11505	3	11535	3	11529	30,2	206	100-300mm
64	D	3	11542	3	11549	3	11546	22,3	170	100-300mm
64	D	3	11592	3	11600	3	11598	24,5	193	100-300mm
64	D	3	11622	3	11639	3	11637	21,6	204	100-300mm
64	D	3	11743	3	11769	3	11759	24,3	196	100-300mm
2016										
62	L	3	28341	3	28351	3	28350	12,6	170	100-300mm
62	L	3	28429	3	28438	3	28430	13,7	153	100-300mm
62	L	3	28455	3	28464	3	28459	21	189	100-300mm
62	L	3	29440	3	29453	3	29446	13,4	191	100-300mm
62	D	1	4184	1	4205	1	4197	22,6	202	100-300mm
62	D	1	4233	1	4250	1	4240	19,6	158	100-300mm
64	L	3	11983	3	11989	3	11988	13,9	191	100-300mm
64	L	3	11997	3	12003	3	12000	11,9	170	100-300mm
64	L	3	12010	3	12026	3	12015	25,9	181	100-300mm
64	L	3	12032	3	12046	3	12043	17,1	160	100-300mm
64	L	3	12066	3	12085	3	12069	37,6	198	100-300mm
64	L	3	12104	3	12115	3	12113	16,4	160	100-300mm
64	L	3	12144	3	12152	3	12149	16,3	189	100-300mm
64	L	3	13046	3	13052	3	13047	18,8	183	100-300mm
64	L	3	13101	3	13110	3	13110	15,5	160	100-300mm
64	D	3	11503	3	11535	3	11531	25,8	210	100-300mm

Line no.	1	2	3	4	5	6	7	8	9	10
64	D	3	11544	3	11554	3	11554	11,2	193	100-300mm
64	D	3	11594	3	11601	3	11597	14,7	181	100-300mm
64	D	3	11623	3	11640	3	11625	18	227	100-300mm
64	D	3	11746	3	11763	3	11758	25,7	187	100-300mm

Local poor places are resolved in accordance with the annual plan of grinding the rails. The regular cycle of grinding rails or replacing rails in combination with a strong wear is carried out.

The long-standing practice is to plan rail grinding and thus the elimination of corrugation on the main routes, especially in the sharp curves where the occurrence of corrugation is the most remarkable and on new lines or after performing overhaul of the superstructure in order to eliminate failures of new rails and reduce the impact of termite contacts.

In the case of changed rails, where the limit values of rail corrugation have been exceeded, there are always replaced longer sections of tracks (arc, transition curve, etc.). The same applies to the grinding of the rails.

6.2 References

[6.1] Report on measurements of corrugation of rails in the area of the Republic of Slovenia with a measuring train MAV SDS-AB25-AB35; October/November 2014, October 2015, August/September 2016. **MÁV Központi Felépítményvizsgáló Kft., Prometni institut Ljubljana d.o.o.**, 2014, 2015, 2016.

[6.2] Measuring train MAV AB25-SDS-AB35: https://www.google.si/search?q=MAV+AB25-SDS-AB35&biw=1837&bih=974&source=lnms&tbm=isch&sa=X&ved=0ahUKEwj4mvb8yOnRAhUCPRQKHRKdB44Q_AUIBygC#imgrc=Y794v3m80SCynM%3A; https://www.google.si/search?q=MAV+AB25-SDS-AB35&biw=1837&bih=974&source=lnms&tbm=isch&sa=X&ved=0ahUKEwj4mvb8yOnRAhUCPRQKHRKdB44Q_AUIBygC#imgrc=RxF3tiBEJuc3BM%3A.

7 Final remarks

In the Section 1 of this deliverable, the literature review is presented and main challenges in terms of the physical understanding the origin of the phenomenon are discussed. Section 2 describes how the use of axle box acceleration measurement can support the detection of already existing short pitch corrugation. In Section 3, due to the fastening system is believed to importantly contribute to the phenomenon, a parametric study is presented. In the railway industry so far, the only corrective measure for delaying the growth of corrugation is grinding; thus, in Section 4 a review of the effects of grinding operations is discussed. Finally in Sections 5 and 6, the current situation of corrugation in Turkey and Slovenia are discussed.

The next steps of the research efforts are focus on the further development of the 3D-FE model, to better reproduce the dynamics of corrugation. Also a better use of the available information about corrugation will be evaluated by the design of a business case.